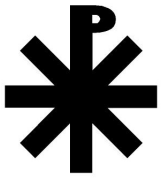

P E TECHNIKON

ANALYSIS OF MATERIAL FLOW AROUND A RETRACTABLE PIN IN A FRICTION STIR WELD

ZACHARIAS GEORGEOU

ANALYSIS OF MATERIAL FLOW AROUND A RETRACTABLE PIN IN A FRICTION STIR WELD

By

Zacharias Georgeou

A dissertation submitted in compliance with the full requirements for the degree of

Magister Technologiae: Engineering: Mechanical

in the

Faculty of Engineering

Port Elizabeth Technikon

December 2003

Promoter: Dr. D.G. Hattingh

Co-Promoter: Prof. T.I. van Niekerk

Submitted on.....

Signed.....

I **Zacharias Georgeou**,

hereby declare that this work is my original work and all sources used or referred to have been documented and recognized.

Further this work has not been submitted in full or partial fulfillment of the requirements for any degree at another recognized educational institute.

Date..... .....

Zacharias Georgeou

Abstract

Friction Stir Welding (FSW) has been researched for a number of years since its inception in 1991. The work thus far has been based on understanding the material and thermal flow using the standard fixed pin tool. The *keyhole* resulting during tool extraction in a FSW weld, is a disadvantage and a current limiting factor. Eliminating this effect from a weld using a movable pin tools would make FSW more commercially viable.

This dissertation focuses on the design of a novel retractable pin tool, and highlights the problems encountered during the welding of Aluminum plates, Al2024 and Al5083. Previously studied techniques of material and thermal flow were used, to investigate the effect of the tool during extraction in a FSW weld. A prototype retractable tool was designed using parametric and axiomatic design theory, and implementing a pneumatic muscle actuation system.

The resulting problems in the calibration of the retractable pin tool and the resulting welds are presented, these results confirming previous studies. The movable pin produced discrepancies the heat generation around the shoulder during a FSW weld. The failure of this tool to produce a reasonable weld showed that previous ideas into the workings of a retractable pin tool requires further investigation, furthermore a fresh approach to the interpretation and understanding of the FSW weld process needs consideration.

ACKNOWLEDGMENTS

Firstly, I must of course begin with my promoter, Dr. Danie G. Hattingh, for giving me this opportunity and without whose help I would never have written this dissertation. He always gave me enough direction and advice to keep me going, and knew when to let go, which made my research and introduction into academia, fun and rewarding. I have to thank Professor Theo van Niekerk, my co-promoter for this opportunity and for his advice from a different perspective.

Ian Clark, who gave me that inspirational edge, during the lows and taught me there was more to research than just research. For the many discussions on many varied topics and helping in getting my dissertation in its present form.

The following from the Automotive Components Technology Station (ACTS), a special thanks to Lucinda Lindsay, for her help. Andrew Young who with his probing questions taught me to see the simple side of a problem and life, "keep it simple". William Rall with his systematic approach to CAD and FEA. Ian Wedderburn, for the intuitive and balance in our discussions in the ACTS office.

Hannalie Lombard for the many enjoyable and intense discussions on trying to explain the physics behind Friction Stir Welding, I hope that our ideas one day bear fruit, in her research.

My fellow researchers and cubicle mates, Basil Esterhuysen, the unintentional comic, making each day different and funny. Calvin Blignault and Grant Kruger, for their help in introducing the FSW process to me. Tao Hua, who enlightening me on the Chinese culture and language in the many discussions during the long late nights. Riaan Kritzinger for the help in the metallurgy lab.

The staff of the Port Elizabeth Tecknikon, especially Annelize Els-Botes, Gideon Gouws, Clive Hands, Mervin Knoesen and Joe Maczeck for all their help and readiness to give that bit extra when asked.

This research was funded by the National Research Foundation, whom I thank for giving me this opportunity.

Finally to those who had to endure my highs and lows, Antje Goessmann, for inspiring me to carry on with my studies, without her pushing me I would not have embarked on this journey. I could not have asked for more from my brothers, Pano and Andrew, who with their enduring support and advice in all aspects of my life, I would not have completed this task.

Lastly to my parents, George (1934-1978) and Eve (1940-1998), they are my greatest inspiration and from whom I was taught the virtues of patience, perseverance and respect and most importantly that we have to fulfill our dreams, as our time is limited.

Contents

List of Figures

List of Tables

GLOSSARY OF TERMS

A

alloy - A substance having metallic properties and being composed of two or more chemical elements of which at least one is a metal.

B

butt weld - A welded joint formed between the squared ends of two joining pieces, which do not overlap.

C

capillary action - This when a fluid rises or falls within a narrow tube.

Computational Fluid Dynamics (CFD) - This is the analysis of fluid dynamics and flow dynamics using computational means.

conventional friction welding - Is the process where two materials are welded together by the friction generated when they are forced together under load.

D

deformation - Is a change in the form of a body due to stress, thermal, or other causes.

die - A shaped block of hard material used to form metal with the use of heat and pressure.

E

extrusion - The process where a material is shaped by force or squeezed through die or nozzle.

F

Finite Element Analysis (FEA) - The analysis of statics and dynamical systems using computational methods such as the finite difference method.

flow dynamics - The analysis of the motion of material objects in relation to physical factors affecting them: force, mass, momentum and energy.

fusion welding - Is the process where materials are liquefied or melted together by the application of heat to form a bond.

H

hydrodynamics - The study of motion and the forces acting on solid bodies immersed in fluids and in motion relative to them.

M

mechanical properties - The properties of a material that reveal its elastic or inelastic behavior when force is applied, indicates the suitable mechanical applications.

N

non-fusion - Is the process where the materials are not liquefied or melted, to form a bond, however with heat applied to reduce the energy required to caused plastic deformation.

P

plastic deformation - Is the distortion of material continuously and permanently in any direction.

S

stiction - The force required to cause one body in contact with another to begin to move.

V

viscosity - can be described as the measure of a fluids resistance to the shearing forces acting on the fluid.

NOMENCLATURE

Latin Letters

A – Surface area, axiom,constant of integration

B – Constant of integration

C – End condition constant

DP – Design parameter factor

E – Modulus of Elasticity

F – Force

FR – Functional requirement factor

I – Moment of inertia of cross sectional area

K – Viscosity factor, end condition constant

L – Length

M – Moment

N – Integer

Q – Power

P – Pressure, force

R – Distance

S – Distance

T – Temperature

b – Parabola intersection tangent

c – Specific heat, distance from neutral plane

d – Diameter, plate thickness

e – Eccentricity

k – Thermal conductivity, radius of gyration

l – Length

q – Heat input, heat flux

$\dot{q}$ – Rate of heat generation

q_0 – Net power

v – Velocity, welding speed

x, y, z – Coordinate, distance

Greek Letters

α – Thermal diffusivity ; $k/\rho c$

η – Dynamic viscosity

λ – Constant $= KL/k\pi(\sigma/E)^2$

μ – Coefficient of friction

ξ – Distance

ρ – Density

σ – Stress

ϕ – Constant $= \sigma/C\pi^2 E$

Subscripts

0 – Zero, initial

CR – Critical ratio

i – Cartesian coordinates, (x, y, z)

t – Time

x – Distance, coordinates

y – Distance, coordinates, yield

z – Distance, coordinates, normal

Mathematical symbols and operators

$\{\}$ – Columns

$[]$ – Rectangular, or square matrix

$\dot{}$ – Time differentiation; $\dot{u} = du/dt,\ \ddot{u} = d^2u/dt^2$

∇ – Gradient operator; $\partial/\partial x + \partial/\partial y + \partial/\partial z$

Δ – Difference

K_0 – Bessel function of the first kind, zero order

1 INTRODUCTION

The joining of materials to produce an assembly or structure from parts or structural elements, is an important part of the manufacturing process. This process of joining, in which materials are brought together to become one, to form primary (and, occasionally secondary) metallurgical bonds under the combined action of heat and pressure, is commonly defined as welding [Messler, 1999].

Friction Stir Welding (FSW) is a solid-state process of the non-fusion welding processes. An offshoot of conventional friction welding, developed in 1991 by The Weld Institute (TWI) [Thomas *et al.*, 1995], a research and technology center based in the United Kingdom. Non-fusion welding can be defined as the process of joining materials through plastic deformation due to the application of pressure at temperatures below the melting point of the base material(s) and with the added assistance of solid-state diffusion. A key feature of non-fusion welding is that welds can be produced without the need for melting or fusion. This process overcomes the disadvantages that are normally associated with the traditional welding techniques, especially with high strength "difficult to weld" aluminum alloys and the ability to successfully join materials that would otherwise be normally incompatible if fused. The advantages are defect free

welds having good mechanical properties, and due to the lower welding temperatures, resulting in reduced component distortion.

1.1 The FSW Process

As a non-fusion form of welding, the FSW process can be described as the use of a mechanical effect, friction, to transfer the required activation energy transforming the materials to be joined into a viscous state. Once this stage has been reached the effect of stirring then results in the intermixing or diffusion of the materials in the solid-state phase and upon cooling forming a direct bond.

The FSW technique involves the use of a cylindrical shaft tool, consisting of a driven-end and a free-end. The free-end having a profiled shoulder with a projecting pin of smaller diameter. The two abutted or overlapping workpieces are initially securely clamped onto a backing plate and held in place during welding. As the tool is rotated, as shown in Figure 1.1(a), the free-end is slowly lowered in the direction normal to the surface between the two fayed workpieces. As the shouldered pin makes contact with the surface, heat is generated by friction, which forms a shaft of plasticized material around the pin, see Figure 1.1(b) and (c). The tool is then advanced along the joint surface as in Figure 1.1(d), and the combined action of the rotating shoulder and pin produces a mixing of the material ahead of, and behind the pin. Coupled with the downward force of the tool and the mechanical stirring of the pin, the plasticized material recombines on the trailing side of the tool where a weld forms. As the tool is removed, at the end of a

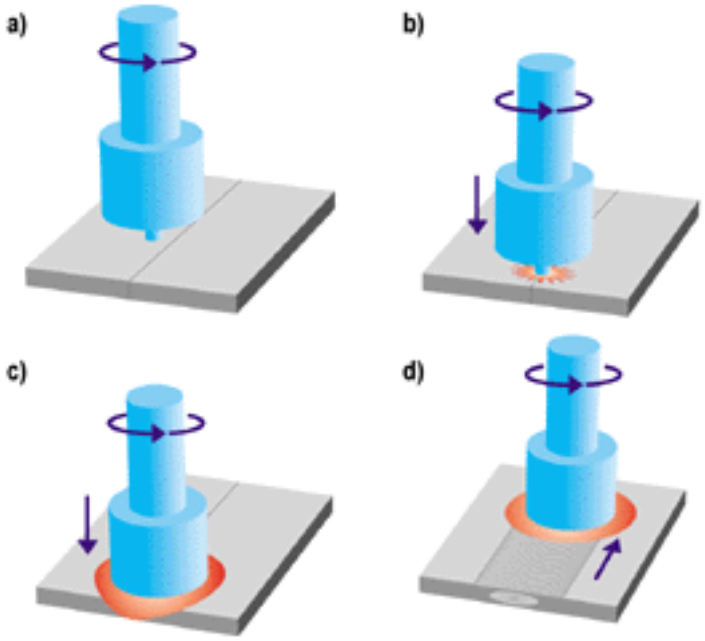

Figure 1.1: The Friction Stir Welding Process, (a) preparing to plunge, (b) plunging pin into material, (c) force applied on shoulder, and (d) transversing along the weld line.

weld cycle, a *keyhole* or crater is formed.

1.2 FSW Applications

Significant effort in the past few years has been applied into putting FSW to use, in full-scale production, however the limitations due to the availability of scientific information and lack of understanding the process completely has been a major disadvantage. In the shipbuilding and off-shore industries, the use of FSW has been seen as an advantage due to simplified manufacturing process and weight reduction.

The aerospace industry, which demands low weight and predictable joint properties have successfully implemented the FSW process, but these are still limited. Lockheed-Martin, Boeing and Airbus have initiated projects to further utilize the process in future applications. Boeing uses FSW to weld the propellant tanks for the Delta II, III and IV launch vehicles, as well as non-structural parts for its civil aircraft. The use of FSW in complex parts requiring curvilinear paths has been successfully demonstrated by Boeing for use in complex landing gear door and FSW sandwich assemblies for a fighter aircraft fairing. Airbus has successfully welded the thinnest FSW weld using 0.3 to 0.4 mm foils in laminate construction. NASA* has successfully welded the External Fuel Tanks for the Space Shuttle program [Technology Transfer Dept., 2001; Heston, 2002], and Eclipse Aviation is in the process of building the first FSW aircraft, using FSW to replace the rivets commonly found in aircraft construction [Hansen, 2003]. This has great potential in reducing costs, and Airbus is presently conducting research to use FSW in the skin-to-skin fuselage connection. This could lead to a reduction in cost, weight, and with an improvement in joint quality.

The automotive and transportation industry have conducted studies into the FSW process, such as high-speed train construction in Japan [Kawasaki *et al.*, 2001]. Developments in the automotive industry have been made by Mazda, where FSW is used in the new RX-7 model. Ford has also began production of FSW to join panels. In Sweden, car seat frames are being welded using dual FSW weld heads. As the use of aluminum is on the increase in the automotive

*National Aeronautical and Space Agency

industry, especially in engines, drive trains, heat exchangers, wheels and bumper reinforcements and with recent developments in the use of aluminum for complete car bodies, this has lead to investigations into FSW techniques to replace the conventional welding processes for joining aluminum. The resistance spot weld (RSW) when applied to aluminum alloys results in greater electric power consumption and an increase in the electrode usage, together with an increase in welding distortion of the components. Therefore other fastening techniques such as riveting and clinching are used instead of RSW [Sakano *et al.*, 2001] and compared to fusion welding techniques FSW requires less energy and has better joint quality properties making it an ideal method for joining aluminum alloys. FSW spot welding has many advantages, in that it would be easy to automate and require no skilled welders, studies are currently under investigation.

Recent developments in the commercialization of studies into the feasibility of the FSW process has put more emphasis into understanding the process parameters and finding ways to make the process more predicable.

1.3 Motivation

The motivation for this research is the need to understand the current limiting factor in the FSW process, the *keyhole*. Understanding the elimination of the *keyhole* with the use of a retractable pin and the influence that pin retraction has on the material behavior, mechanical and material characteristics would be essential to take FSW out of the laboratories into industry. At present there is a retractable tool

developed by NASA [Technology Transfer Dept., 2001] in cooperation with MTS Systems Corporation and MCE Technologies Inc., in the USA, which successfully eliminates the *keyhole*. By closing the *keyhole* without the need to rework the weld or additional filler materials, lends the FSW process to new applications and procedures. Hence, it makes sense to approach this study with the development of a simple modular tool which can be used to simulate pin retraction and reveal the material flow at this point in weld cycle.

1.4 Objectives

The primary objective of the this dissertation will be to investigate the effects that a retractable pin has on the material characterization during the pin retraction cycle. The material flow patterns occurring in the welded aluminum will contribute to a better understanding in the design of retractable pin tools and give further insight into the process parameters required to achieve completeness in the weld cycle. This will be performed by considering several sub-objectives and delimitations in support of the main objectives.

1. The design and manufacture of a simple experimental tool for research purposes, to simulate the retraction characteristics of a retractable pin tool. Since the method of actuation will influence the design, an electro-mechanical, hydraulic or pneumatic system are proposed. The design shall limit the pin movement to <6 mm. The influence of heat on the tool will need examination and both the pin and shoulder shall be modular in design to allow for further investigations. The need for calibration of the

tool, to evaluate pin movement, with both static and dynamic calibration will have to be considered.

2. Investigate and evaluate the process of pin retraction by using Aluminum alloy series 2xxx and 5xxx, with 6 mm plates. In addition to the use of existing sensors, which depends on the status of the host machine (e.g. force in the x-,y-,z-axes of the tool, pin temperature), a pin position sensor and pin force will be required to give an indication to the difference between pin and shoulder. The length of the weld before retraction takes place will be limited to <20 mm, with emphasis on the point of pin extraction. The rate of pin retraction will be limited to be linear and with the possibility of the options in the rate of retraction with respect to time.

3. Analysis and visualization of the flow dynamics in the region of pin retraction will require an examination of the existing material marker techniques. The use of different alloys, embedded alloys and layered plated alloy will require investigating. A method to give a reliable thermal footprint around the point of retraction needs consideration. The heat transfer visualization using methods of embedded thermocouples in the plates or with thermal imaging techniques would need verifying. Existing theoretical material flow and heat transfer models will require some evaluation.

4. The region around the tool extraction during welding will be considered for material flow visualization analysis. The evaluation of the weld, using embedded marker flow patterns, and

the use of digital techniques will have to be investigated. Although this will not be performed, the material characterization of the weld quality would provide valuable information for the improvement of the process parameters.

Finally, the following delimitations have been considered to make the study. The design and development of a retractable tool will solely simulate pin retraction and be used for research purposes. The process control parameters have not been investigated and the FSW system available will be used as presently setup. As the function of a retractable pin-tool would enhance the ability to preform profile welds, these will not considered due limitations of the FSW host machine on site.

This research would contribute in principal to the analysis of the flow patterns in FSW associated to retractable pin techniques. A better understanding of the flow around and during pin retraction would ultimately contribute to eliminating the keyhole effect of a normal tool without detrimental effects on the weld quality.

1.5 Overview

This dissertation is divided into two main parts, that of material flow and tool design. Material flow and thermal modeling form Chapter two, where an overview into existing theories and techniques used to visualize flow of material and thermal processes of FSW is discussed. The design and development of the tool is presented in Chapter three, with Chapter four consisting of a description of the tool calibration, following on to the experimental procedure and method of investigation used. Chapter five contains the experimental results

and method of analysis used. The conclusions are discussed in Chapter six, with recommendations for further study as part of Chapter seven.

2 MATERIAL AND THERMAL FLOW

2.1 Introduction

Material flow is described by the motion of a continuous media, or continuum, due to an action upon it, as with fluids, solids have the property that when acted on by forces they deform. Since "flow" is normally associated with fluids, in this context, the meaning of flow is the deformation of a continuum due the resulting mechanical and thermal effects. [Munson *et al.*, 1998; Truesdell and Rajagopal, 2000; Mase and Mase, 1999]

Friction Stir Welding (FSW) is a non-fusion welding process, where the material is deformed with the combination of heat and force. The flow of material forms an important part in understanding the fundamentals of the welding process. As this is thermo-mechanical in nature, a study of material flow should also consider the thermal effects during a weld. Several studies into modeling of material and thermal flow have been carried out to gain an insight into the process, however most of these have concentrated on a shaft-tool*.

An overview of the thermal and material flow studies are presented in this chapter, and the theoretical understanding of the process was

*A standard tool, a fixed pin relative to the shoulder.

used in the development of the experimental tool design discussed in chapter three. As research in the FSW process is continuous, the latest publications at the time were reviewed.

FSW Conventions

The use of a convention to differentiate between the two sides in a friction stir weld, requires clarification, as FSW welds are asymmetrical. It is therefore important to accurately define the intended locations in the weld, with respect to tool rotation and feed directions. The following convention, as described in Colligan [1999]; Reynolds [2003], and Guerra *et al.* [2003], referring to Figure 2.1, the assumption is made that the tool is moving relative to the workpiece and that the workpiece is fixed. The rotational motion of the tool and the transverse motion are in the same direction, the side

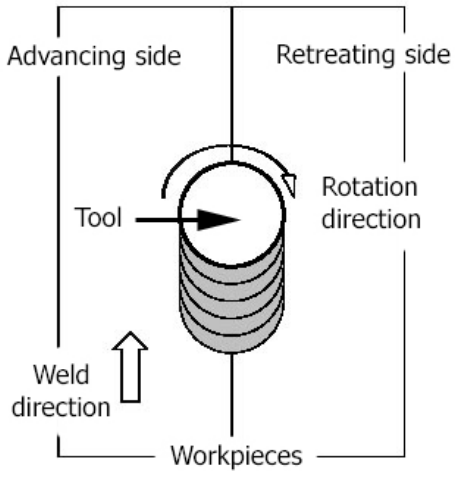

Figure 2.1: Schematic drawing of the FSW conventions.

is referred to as the *advancing side*. The opposite side is referred to as the *retreating side*, where the rotational motion of the tool opposes the feed direction.

2.2 Material Flow

The study of the material flow in a friction stir weld was investigated by Colligan [1999], further work by Reynolds and Siedel [2001] working on different marker and visualization techniques. Studies by Murr *et al.* [1999] and recently by Guerra *et al.* [2003] also illustrate material flow in a FSW weld. The different approaches and resulting analysis of these are presented, as they will form the basis on the material flow, relating to a retractable pin welding tool. Unfortunately no publications concerning material flow with a retractable pin welding tool, have been published to date.

Colligan

Colligan devised two techniques to visualize flow patterns in friction stir welds. One technique, using steel shot, small steel balls (diameter 0.38 mm), as a tracer. These being embedded at different positions along a butt joint, in 6.4 mm thick aluminum alloy, 6061-T6 and 7075-T6 plate, illustrated in Figure 2.2, as used by Colligan [1999]. A weld was run along the "seeded" butt joint and stopped at a point along the tracer pattern. This stopping of the forward motion of the weld tool, preserved the steel shot distribution around the weld, and revealed the path that the tracer took in the material. After a number of techniques had been evaluated, Colligan machined

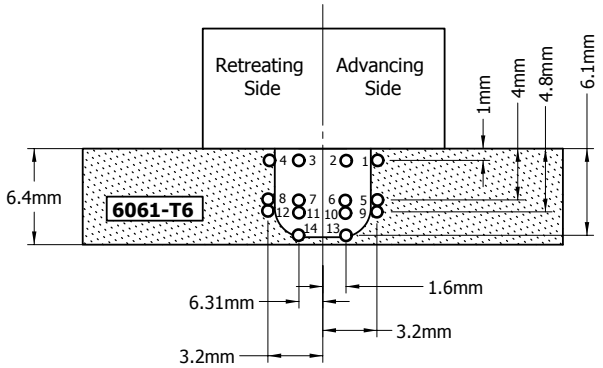

(a) Tracer position in a Al6061-T6 weld sample.

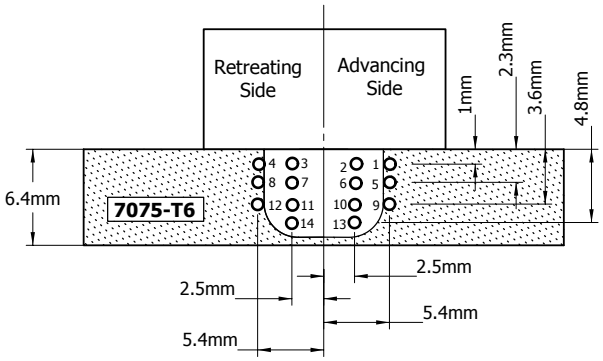

(b) Tracer position in a Al7075-T6 weld sample.

Figure 2.2: Schematic showing placement of the steel shot as used by Colligan (1999).

small grooves, 0.75 mm high by 0.3 mm deep, parallel to the weld direction at various depths and distances from the weld centerline. After inspecting each of the welds, with the use of radiography, to reveal the tracer movement around the pin, and after the passage of the tool.

The second technique, "stop-action", involved stopping the forward

motion suddenly and simultaneously retracting the tool at a rate that caused the pin to unscrew it self. This would leave the threads of the pin intact and attached in the *keyhole* of the weld [Colligan, 1999]. By sectioning the *keyhole* at the end of a weld, Colligan studied the flow of material within the threads of the tool.

The results and analysis of the welds, referring to Colligan, are illustrated in the following Figures 2.3 to 2.4, Colligan states that from the visual studies, not all the material is "stirred" and much is actually extruded, around the pin. Further conclusions made by this author, were that the "stirred" material originated from the upper portion of the tool pin welding path. This material then being forced down in the weld by the threads on the pin and deposited in the weld nugget. The remaining material would then be simply extruded around the retreating side of the welding tool pin, rising in the weld as it goes around the pin. This can be shown in the Figure 2.4(b) in positions one, two and three, where the upper portion of the material is deposited roughly in the middle of the weld path.

Considering the Figures 2.3(a) and 2.4(a), the plan views show two general categories, as described by Colligan, where the steel shot was reoriented and deposited as a roughly continuous line behind the pin. Then there are those with the steel shot deposited behind the pin chaotically, which have features similar to shear-flow turbulence [Lesieur, 1997]. The interpretation of the FSW process by Colligan is one of both stirring and extrusion of the material.

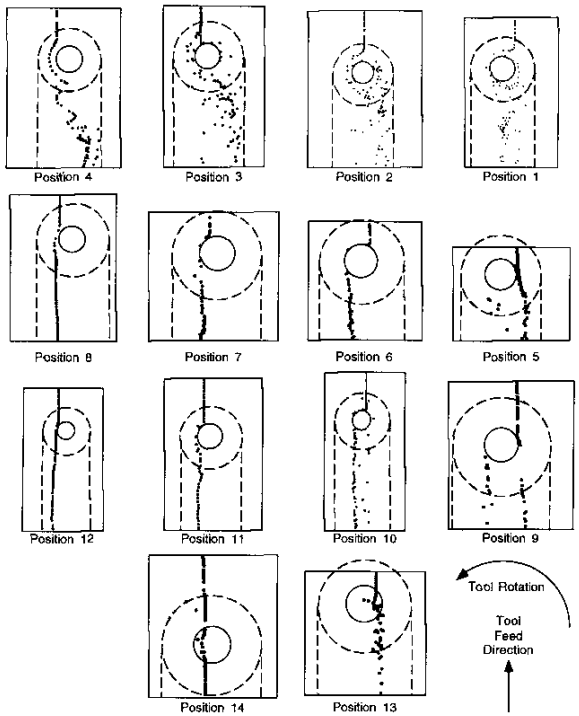

(a) Plan view.

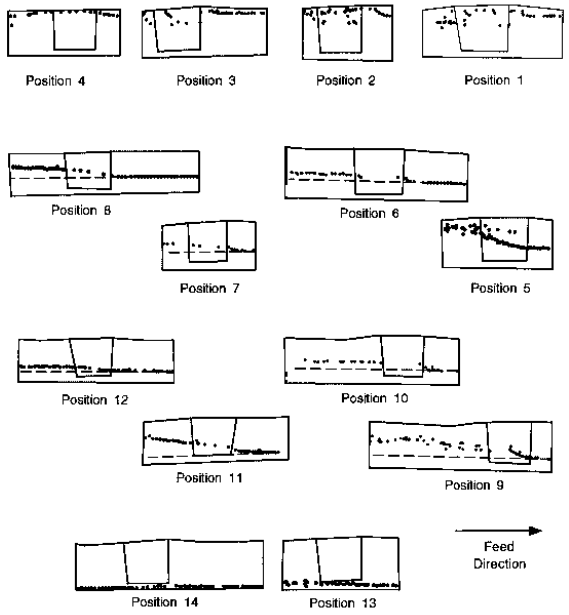

(b) Side view.

Figure 2.3: Drawings of each radiograph for the Al6061 welds, the positions relate to Figure 2.2(a), (Colligan, 1999).

(a) Plan view. (b) Side view.

Figure 2.4: Drawings of each radiograph for the Al7075 welds, the positions relate to Figure 2.2(b), (Colligan, 1999).

Reynolds

Reynolds and Siedel analyzed flow using a technique of inserting markers into the weld to gain information on the material transport and flow variations through the thickness of the plates. The markers consisted of 5454-H32 aluminum thin sheets, placed into the faying surface of the welded 2195-T8 aluminum plates. The markers, a total of six, 2.7 mm high and 1.8 mm thick, were placed at three different heights, to cover the top, middle and the bottom of the welded plate. The inserts were also placed in both the advancing and retreating side of the plates, see Figure 2.5. The staggering of the inserts was done so the possibility of mixing between the markers would be prevented. Following welding, the area to be studied was elucidated

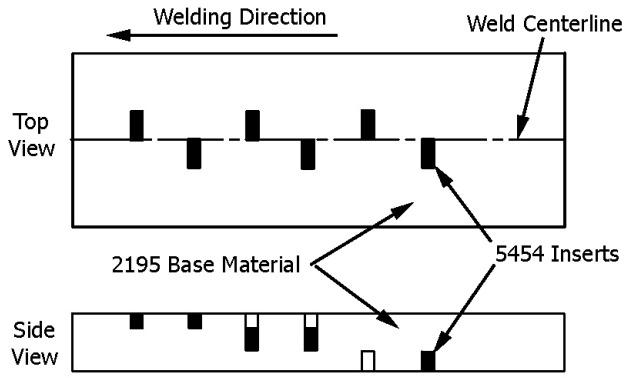

Figure 2.5: Schematic drawing of the marker configuration, (Reynolds and Siedel, 2001).

by milling 0.25 mm thick slices, etched in Keller's reagent[†] and the images digitized to indicate the marker flow, by combining the

[†]Keller's reagent - 150 mL H_2O, 3 mL HNO_3, 6 mL HCL, 6 mL HF

digital images to form a three-dimensional visual flow plot.

The authors concluded that the flow was asymmetric about the weld centerline, and the flow patterns were different on the advancing and retreating sides. It was also noted the maximum material movement was no more than one pin diameter behind its original position. The upper part of the weld showed material of substantial quantities was transfered from the retreating to the advancing side. The movement of this material caused vertical mixing in the weld and a complex circulation of material around the longitudinal axis of the weld. Reynolds and Siedel, attribute this to the influence of temperature in the weld. Reynolds and Siedel explained since the FSW process is a constant-volume process, with the shoulder, pin and the undeformed base material forming a flow restriction. This "stirring" of the material occurred around the rotating tool shoulder which has a direct influence on the material transport. As the material was transported from the retreating side to the advancing side, this caused material from the top of the advancing side to move downward within the pin diameter. Upon approaching the root of the weld, material transport was restricted by the backing plate, resulting in a detected upward motion on the retreating side within and near the pin radius. The extrusion around the pin combined with the "stirring" action at the shoulder, produces within the pin diameter a secondary, vertical circular motion, opposing the rotational direction of the tool, around the longitudinal axis of the weld.

The influence of deformation heat due to the tool rotation in workpiece, leads to a reduction in flow stress of the welded material,

thus allowing the material in the weld zone to flow. Therefore as Reynolds and Siedel showed, by increasing the heat input via the tool, this results in reduced flow stresses and increases the "mobility" of the material in the weld. The work done by Reynolds and Siedel illustrated that the movement of material in a FSW weld is due to two tool motions, translation and rotation. However, also acknowledging the limitations of the method used, as only the final positions are shown and not the actual flow paths.

Guerra

Following on work done by Colligan [1999]; Reynolds and Siedel [2001], Guerra *et al.* [2003] used a technique, with some similarity to those previously discussed. The material flow visualizations were made using two different marker tracer methods. The first used a thin 0.1 mm pure copper foil placed along the weld faying surface of 6.3 mm Al6061 plates. The tool and workpiece translation were stopped suddenly to produce a "frozen"pin in the weld, similar to that used by Colligan [1999]. Guerra *et al.* acknowledged the assumption that the stopping operation was to be considered instantaneous, due to the loads on the machine during welding. The other method described by Guerra *et al.* were welds made with 6.3 mm plates, in which the top half was Al2195 and the bottom half with Al6061 aluminum. After welding the samples were prepared into plan and transverse metallographic sections through the frozen pin. These were then etched using Keller's reagent.

The large circular feature in the center of Figure 2.6 is the "frozen" pin cross section. The area surrounding the pin indicated with **A**,

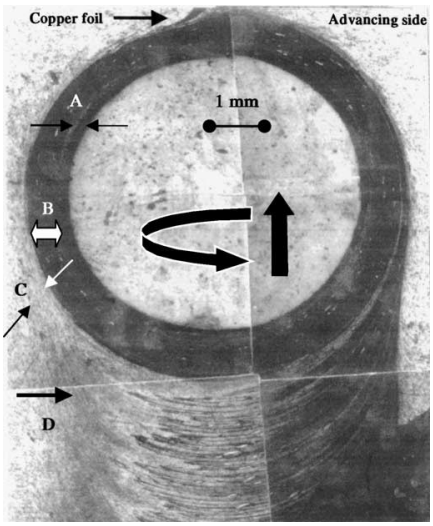

Figure 2.6: Plan view at mid thickness of weld. A copper foil marker on a faying surface of the 6061 aluminum, as seen at the top. **A** Gap without material. **B** Rotational zone, or rotating with the pin. **C** Transition zone of material that is entrained by the rotating pin. Small bright particles in **B** are from the copper foil (Guerra *et al.*, 2003).

between the arrows, is an open space, with no material. Similar to what Colligan [1999] found in the "stop action" studies, when the pin was unwound from the material. The region **B**, shows an approximate circular region and referred by Guerra *et al.* as the "rotational zone". The thickness was determined by the authors, to be about three times thicker than the distance the pin has moved in one revolution, also detected by Reynolds and Siedel [2001]. This region was shown by the authors to rotate at approximately the same velocity as the pin.

Moving away from the "rotational zone" is the region denoted **C**, this zone, the "transition zone", is asymmetrical with the retreating side twice as thick as the advancing side. Guerra *et al.* believe that

in this region the velocity gradient, lies from the inner section where the velocity corresponds to the pin, decreasing to zero toward the outer edges.

Another observation made by Guerra *et al.* was that the threads of the pin created a secondary vortex or vertical flow of material within the rotational zone. This material flowed from the outer edge of the rotational zone, inwards around the shoulder and was pulled downward by the action of the threads to the base of the weld. The trajectory was complex and followed a helical path around the pin, possibly due to the threaded pattern of the pin. As noted previously, this confirmed what Reynolds and Siedel [2001] also observed.

Guerra *et al.* proposed that the velocity of this vertical flow could be estimated by taking into consideration the vertical velocity generated by the threads. Assuming that a portion of material is influenced in a downward motion by the action of the threads, let n be the number of threads, then it would take $2n$ revolutions to move down and up, within the rotational zone. During which time the pin has transversed a distance, x mm or approximately n times the radius of the rotational zone. Therefore a piece of material, once entering the rotational zone would take "roughly about one-half of a round trip up and down in the vortex flow before it leaves the rotational zone" [Guerra *et al.*, 2003].

The vertical motion during FSW welding is clearly illustrated in the cross sectional view, taken perpendicular to the weld direction, of Figure 2.7. The upper portion of darker material consisting of 2195 aluminum and the bottom section of 6061 aluminum (the darkness

is due to the etching of the sample with Keller's reagent, with the Al2195 etching dark while the Al6061 remains light). The downward

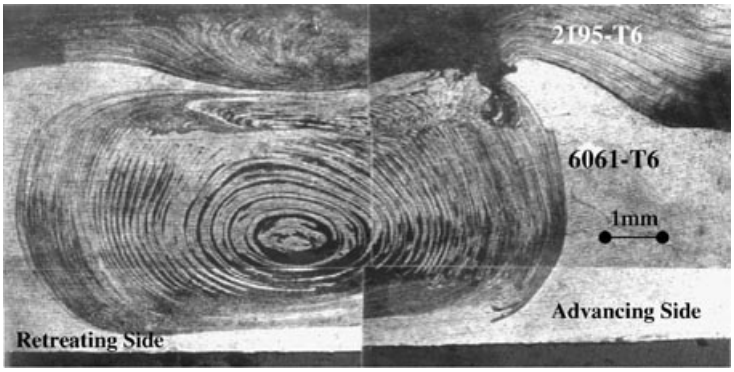

Figure 2.7: Weld showing the large vertical movement ,with the Al2195 on top and the 6061 aluminum below, during welding (Guerra *et al.*, 2003).

movement as described by Guerra *et al.*, shows the Al2195 material being carried down by the vortex flow of the pin, in the central region of the weld, is balanced by the upward flow of the Al6061 material in the outer rotational zone.

Figure 2.8, a cross-section of the "frozen" pin, shows that the flow in the upper section, approximately one third of the weld, is influenced by the shoulder and not by the threads on the pin. This having a different flow pattern to that of the lower section around the base of the pin. Guerra *et al.* also ran welds where the tool rotation was clockwise and counter-clockwise using the same tool, this showed differences in the vortex circulation directions between the two. However the interactions between the shoulder flow and central vortex has yet to be understood, but the authors believe that this interaction may cause the differences between clockwise and

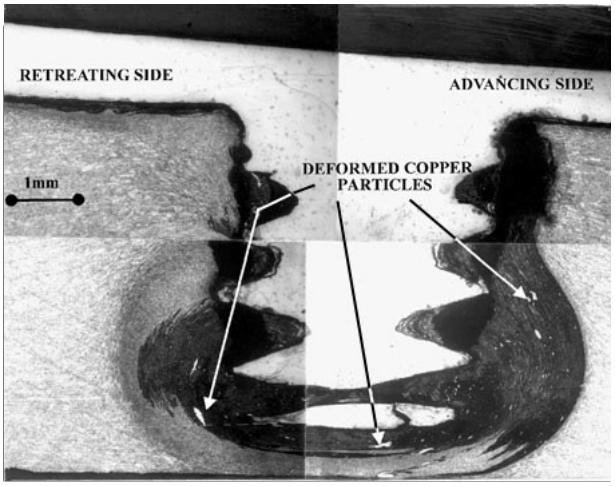

Figure 2.8: Weld showing the large vertical movement ,with the Al2195 on top and the 6061 aluminum below, during welding (Guerra *et al.*, 2003).

counter-clockwise welds.

The conclusions from the work done by Guerra *et al.*, showed that the movement of material around the pin, in a FSW weld, could be attributed to two processes that from the advancing and the other from the retreating side. Firstly the material on the advancing front side, enters and advances with pin within the rotational zone. This material was found to be highly deformed and was shed into arc-shaped features (onion-rings) behind the pin. The material from the retreating side in front of the pin was drawn-off and without rotating around the pin, filled the void on the retreating side left by the pin wake. The thermo-mechanical properties and histories of the material moved by these process was found to be very different. As with [Reynolds and Siedel, 2001], Guerra *et al.* also noticed large vertical or vortex movement of material within the transitional zone. This was caused by the influence of the threads on the pin,

where the material entering this region followed a helical trajectory formed by the rotational motion, vortex flow, and the translational motion of the pin. The action of the shoulder at the top of the weld, caused material to flow differently than those influenced by the threads on the pin. Differences were seen between the upper region to that of the lower region, which is largely dominated by the pin, especially when the rotation of the same pin was either clockwise or counter-clockwise.

2.3 Thermal Flow and Analysis

Thermal modeling attempts of the FSW process have initially been mostly analytical in their approach. Recently various models using finite element methods (FEM), computational fluid dynamics (CFD) based on viscoplastic flow models have replaced the analytical methods. In this section an outline of the thermal model development is given, to provide an understanding of the the thermal effects in the FSW process.

Background

The initial attempt at modeling the FSW process, began with the Rosenthal equation for a uniformly moving point or heat source to define the input [Russell and Shercliff, 1999; Khandhar *et al.*, 2003]. Rosenthal's approach was the assumption that the energy input from the heat source used (in this case to make a weld) was uniform and moved with a constant velocity v along the x-axis of a fixed

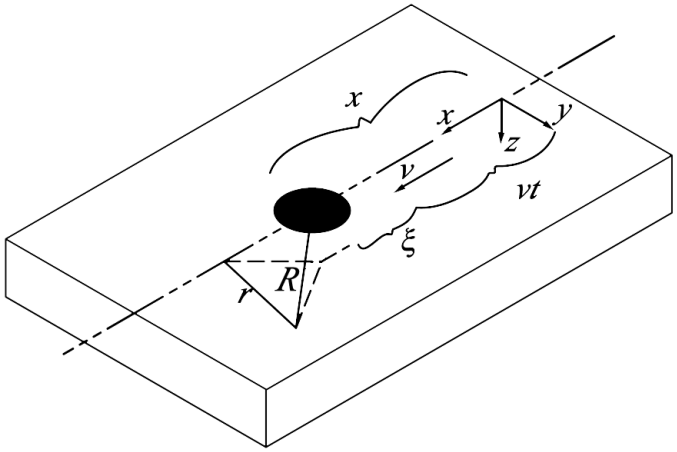

Figure 2.9: Schematic for Rosenthal's equation (Messler, 1999).

rectangular coordinate system, as shown in Figure 2.9. The transfer of heat is determined for the time-dependent conduction of heat, which can be generally expressed by the general equation of heat flow with respect to time:

$$\rho c\dot{T} = \nabla(k\dot{T}_i) - \rho c v_i \dot{T}_i + \dot{q} \tag{2.1}$$

where

i = represents the coordinates (x, y, z) (mm)

T = temperature (K)

$\dot{T}$ = rate of change of temperature

k = thermal conductivity ($\mathrm{Jmm^{-1}s^{-1}K^{-1}}$)

ρ = density ($\mathrm{gmm^{-3}}$)

c = specific heat ($\mathrm{Jg^{-1}K^{-1}}$)

v = velocity ($\mathrm{mm\ s^{-1}}$)

$\dot{q}$ = rate of heat generation (Wmm^{-3})

The coordinates represent the following:

x = coordinate in the direction of the weld (mm)

y = coordinate transverse to the welding direction (mm)

z = coordinate normal to weld surface (mm)

Rosenthal simplified the heat flow equation, Eq. (2.1), in two ways, firstly by assuming the thermal properties (thermal conductivity, k, and the product of specific heat and density, $c\rho$) of the welded material remained constant. Secondly by changing the coordinate system from a fixed system to a moving system. However the assumption that the thermal properties be treated as constants, has its flaws, as these properties typically are different with changes in temperature [Messler, 1999; Dorodnitsyn and Kozlov, 2003]. The moving coordinate system poses no problems, by simply taking the ξ as a replacement for x, where ξ is the distance of the point heat source from some fixed position along the x-axis. By taking the velocity v into consideration (where there is only one velocity component, in the x direction), where t is time then

$$\xi = x - vt$$

This is illustrated in Figure 2.9. By then taking the Eq. (2.1) with the constant thermal properties and differentiating with respect to ξ, the result is

$$\ddot{T}_\xi + \ddot{T}_y + \ddot{T}_z = -\frac{c\rho}{k}\left(v\dot{T}_\xi + \dot{T}_t\right) \tag{2.2}$$

where the notation $\ddot{T}_\xi$ represents the second derivative of temperature with respect to ξ, that is $\frac{d^2T}{d_\xi{}^2}$. Further simplifying by assuming the temperature distribution around the heat source moving at a constant velocity will stabilize and therefore putting $\dot{T}_t = dT/dt = 0$, this results in

$$\ddot{T}_\xi + \ddot{T}_y + \ddot{T}_z = -\frac{c\rho}{k} v \dot{T}_\xi \tag{2.3}$$

Considering that Eq. (2.3) is in a simplified form and with the exception of the thermal properties assumptions, reasonable results can be obtained, if numerical methods are used. These are by using a weighted average on the thermal properties based on the weld cycle or solving the simplified heat flow equation several times using a value of the thermal property in a different temperature range each time and seeing the effect.

Rosenthal solved the heat flow equation, Eq. (2.3), for thin plates in which the heat flow is basically two dimensional. Giving the solution

$$T - T_0 = \frac{q}{2\pi k} e^{-v\xi/2\alpha} K_0 \frac{vR}{2\alpha} \tag{2.4}$$

where

$$\begin{aligned}
q &= \text{heat input from welding source (Jmm}^{-1}\text{)} \\
k &= \text{thermal conductivity (Jm}^{-1}\text{s}^{-1}\text{K}^{-1}\text{)} \\
\alpha &= \text{thermal diffusivity } = k/\rho c, \text{ (m}^2\text{/s)} \\
K_0 &= \text{a Bessel function of the first kind, zero order} \\
R &= (\xi^2 + y^2 + z^2)^{1/2} \text{ , the distance from the heat source} \\
&\quad \text{to a particular fixed point (m).}
\end{aligned}$$

Thermal Models

Initial studies in FSW related the process to existing models from laser welding and other fusion processes, such as electric-arc welding. Most of the work done in FSW was empirical testing through trial and error, modeling of the process can only lead to the better understanding of the parameters involved.

Russell and Shercliff [1999], developed a model based on the Rosenthal equation for a moving point source, as described in the previous section, and adapted it for the FSW process. By defining two critical stages in FSW, the representation of heat generated by the welding tool and prediction of the temperature field developed in the workpiece by conduction. The model replaced the heat generation with simplified heat inputs such as the point source, line source and distributed surface heat input.

Frigaard *et al.* [1999] used the finite difference approach to model and calculate two and three dimensional heat flow models. The model predictions by Frigaard *et al.* showed four stages to a FSW weld,

- **Stationary heating period**: The material beneath the shoulder is preheated to a certain temperature (about 400°C for aluminum alloys) to accommodate the plastic deformation during welding,
- **Transient heating period**: The heat starts to build up around the shoulder as the tool moves until saturation occurs,
- **Pseudo steady state period**: The thermal field around the tool remains constant during the welding operation,

- **Post steady state period**: The reflection of heat from the end plate surface leads to additional build-up of heat around the tool shoulder.

They further identified a process parameter q_0/vd (kJmm^{-2}) where q_0 is the net power, v is the welding speed, and d the plate thickness, that determines the pseudo state temperature distribution in thin plate welding. The material in front of the weld had to be preheated to accommodate plastic deformation during welding, they found that the thermal contour to be axis-symmetric around this point at a temperature of approximately 450°C. They showed that the heat input per unit length can be increased by raising the net power, q_0, either by increasing the shoulder radius or the rotational speed. Frigaard *et al.* noted the frictional coefficient, μ, would be constantly changing from one at the dry start toward zero for local melting, the authors proposed a value $\mu = 0.4$.

North *et al.* [2000] presented work done on determining the material viscosity of 6061-T6 aluminum alloy, using techniques similar to that used in high molecular weight polymers. The authors questioned the approach of a solely frictional heat generating model, and proposed a model to the determine the size of the plasticized region ahead of the tool. They concluded that the viscosity of the Al6061 material decreased as the rotational speed of the tool increased, and this decrease corresponded with fluid flow relations, indicating that viscosity is inversely proportional to angular velocity. The temperature values around the pin were found to be around 582°C, close to solidus temperature. North *et al.* determined that width of the plasticized region ahead of rotating pin depended on the ratio of

the square of the angular velocity and travel speed.

Earlier work by Smith *et al.* [1999] using the similar techniques as North *et al.* [2000], noted the following, heating is derived from friction and the numerous adhesions and seizure events at the beginning of the plunging process. Also after initial heating, they believed that heat generation was due to viscous heat dissipation of mechanical energy. This implies that there is no slipping, so therefore the material flow rate at the contact point of the tool and the material, is the tool velocity. The authors found that, the measurement of the temperature of aluminum near the material flow zone proved difficult. They also showed that the principles of fluid mechanics applied to FSW, and that the effect of viscous heat dissipation within the weld as opposed to surface frictional welding provided the heat generation. The use of an infinite sea viscometer, as used by North *et al.*, predicted flow profiles and temperature distributions during plunge testing. The plunge testing showed an isothermal within 250 microns of the tool and the effect of the shear rate on viscosity as being large.

Askari *et al.* [2001], presented work on a three dimensional model using CTH code, which is a three dimensional code that solves the time-dependent equations of continuum mechanics and thermodynamics. This code uses the Eulerian approach, where the mesh is fixed and the material flows between these fixed cells. The Eulerian approach favors FSW due to the large material deformations that occur, whereas the Lagrangian approach, links the mesh to the material and deforms with the body, resulting in excessive mesh distortions. The authors approach was different and the primary

advantage was that the workpiece was teated as a solid rather than a fluid. This material model used was an elastoplastic model, where previous models used the Johnson-Cook plasticity model, which contains a approximation to the thermo-viscoplastic response of aluminum and other ductile metals. The author noted that the shoulder region close to the pin produced the highest temperatures, and the flow stress distribution corresponded to this temperature pattern. Also that the advancing side showed to be slightly hotter than retreating side.

A recent development in numerical modeling techniques in which the combination of both Eulerian and Lagrangian methods, was used by Aramayo *et al.* [2002]. The technique, Arbitrary Lagrangian-Eulerian (ALE) has the advantage of combining the solid Lagrangian formulation with the Eulerian flow. Therefore not only the flow and temperature of the workpiece can modeled, but also to include the stress and strains during welding. However after developing a CFD and an ALE model the authors concluded there were limitations in coupling the flow fields with the temperature fields generated by friction and by using the material models that incorporate temperature dependent stress-train rate and viscosity effects.

Dong *et al.* [2001], presented a coupled thermomechanical analysis of a FSW weld, using simplified models. The authors found that, the frictional heating dominated the upper portion of the weld and plastic work induced heating in the lower section of the weld. The plastic slip zone was due to interactions between the tool and the base material, they proposed that the stir pin geometry (shoulder diameter and pin height), and the workpiece thickness played a role

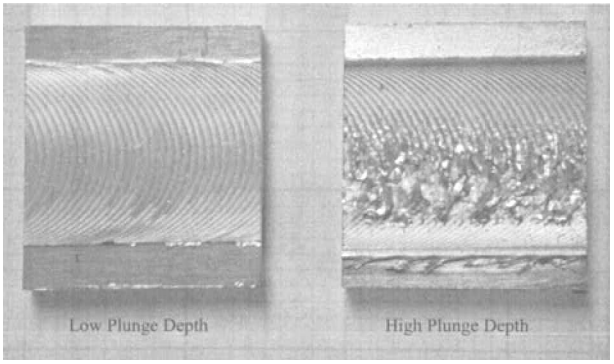

Figure 2.10: Surface welds with (a) low and (b) high plunge depths: rotation speed 475 rev min^{-1} (Colegrove and Shercliff, 2003).

in the appropriate formation of the slip zone. They confirmed the relationship between the translation speed to the rotation speed as an important welding parameter.

Colegrove and Shercliff [2003], using experimental and theoretical techniques, concluded that the different tool materials exerted different surface shear stresses on the welded material. The peak temperature of the Al7075-T7351 when welded was found to be near the solidus, therefore the temperature limited heat generation, and the changing of rotational speed had little effect. Surface scale was found to be a problem on several welds, the authors found that on thick section welds, it was worsened by high rotation speeds and on thin section plates by large plunge depths. Colegrove and Shercliff showed that the relationship between the weld power, weld speed and the tool area exists, by adapting the Rosenthal equation into the equation, $Q = 3Av^{0.5}$ where Q is the power (W) and v is the welding speed (mms^{-1}), A is the tool surface area (mm^2). They proposed a relationship of $A \approx 80d$ where d is the material thickness (mm).

Khandhar *et al.* [2003], developed a three-dimensional model to enable the prediction of temperature distribution during FSW welds in aluminum 6061-T651 plates. The moving heat source, Rosenthal's equation, was coupled with the actual machine power input. The use of axis-symmetric finite element models based on torque were developed by distributing the power to the different interfaces between the tool and the workpieces, based on the torques generated at the different tool surfaces. Certain limitations were noted by the authors, such as the uncertain variables, normally approximated, for example, thermal contact conductance and the convection coefficient at the bottom surfaces. The authors also proposed that the backing plates may have a greater influence on weld quality.

Chen and Kovacevic [2003], used a three-dimensional thermomechanical model to show the stress evolution in an FSW weld of 6061-T6 aluminum alloy. The results showed maximum temperature gradients in longitudinal and lateral direction being located just beyond the shoulder edge. The authors found that the longitudinal residual stress is greater than the lateral stress at the surface of the weld. They noted that the high stress is located in the region extending down from the crown to the mid-thickness of the weld.

Song and Kovacevic [2003*b*], presented a comprehensive three-dimensional heat transfer model, using a moving coordinate system, to reduce the difficulty of modeling the moving tool. The authors concluded that the difficulty in predicting the temperature distribution near the rotating pin was reduced. This work was continuation of the work [Song and Kovacevic, 2003*a*], where the following were

noted, the local temperature immediately beneath the tool shoulder could be very close to the material melting temperature, also noted by Askari *et al.* [2001]; Colegrove and Shercliff [2003]; Chen and Kovacevic [2003], if the input heat influx is high enough. They also showed that the heat transfer in the section perpendicular to the welding direction was assumed to be quasi-steady during the main welding period.

2.4 Summary

The material presented in this chapter relates to work on the theoretical understanding of the FSW process, together with the ability to predict the effects of the welding parameters being essential for the optimizing and controlling the FSW process. The attempts to analyze and understand the flow in a FSW weld have been limited to by assumptions in either the material flow visualization or in the thermal analysis. Problems exist in the prediction of the material flow due to the nature of the process, where trajectories maybe either regular or irregular and unpredictable. Further more, when irregularity is observed in an experiment one may ask whether this is due to chaos or to randomness [Kreuzer, 1991].

Another problem is the use of fluid mechanics to describe flow in a solid. Since the material models take on non-Newtonian fluid characteristics, such as the Bingham Plastic Model, first proposed in 1922 by E.C. Bingham, where the

$$\sigma_{shear} = K + \eta \frac{dv}{dy}$$

as opposed to Newtonian where $K = 0$. This acts as a solid for small values of shear and as fluid as the shear stresses increase.The viscosity of the material in FSW weld has been investigated but the changes due to temperature have yet to be defined. As an increase in viscosity results in a greater resistance to shearing, it is therefore the statement "Stress is Proportional to the rate of deformation" which becomes appropriate in the study of FSW models.

By having the material in a FSW weld behaving as a fluid could possibly be misleading, the work on a reliable, predictable model of the process. Since the FSW process is a non-fusion process, whereby the material is not in a molten state and therefore remains a solid. This difference in the material definition, influences both the material flow and thermodynamic characteristics of the weld parameters in FSW. The combination of a nonlinear solid material flow model with the true thermodynamic characteristics has yet to be attempted, partly due to the complexity of the models, and the unpredictable, chaotic nature in which the material is welded. The process itself remains simple, however the physics behind the process falls within the nonlinear, chaotic dynamics of physics.

3 TOOL DEVELOPMENT

Design, is the essential purpose and basic function of engineering. The methodology to create engineering design, begins with the recognition of a need and the conception of an idea to fill that need. The engineering design process, can be simplified into the following stages:

- **The Problem definition**. A stage of identifying and analyzing a need prior to initializing conceptual design. The analysis is concerned with the functions and the constraints of the design space.
- **The Conceptual design**. A conceptual design stage involves the process of generating and creating novel ideas and implementing fundamental ideas that satisfy the identified need.
- **The Realization**. A stage of finalizing the design details through which a concept is turned from a conceptual idea into an overall product or system layout.

Figure 3.1 shows the process in more detail and defines the process flow. A brief description of design methodology with emphasis on two theories of design, axiomatic design and parametric conceptual design will form the basis of this chapter. By using a mixture of both processes to design the experimental retractable pin welding tool.

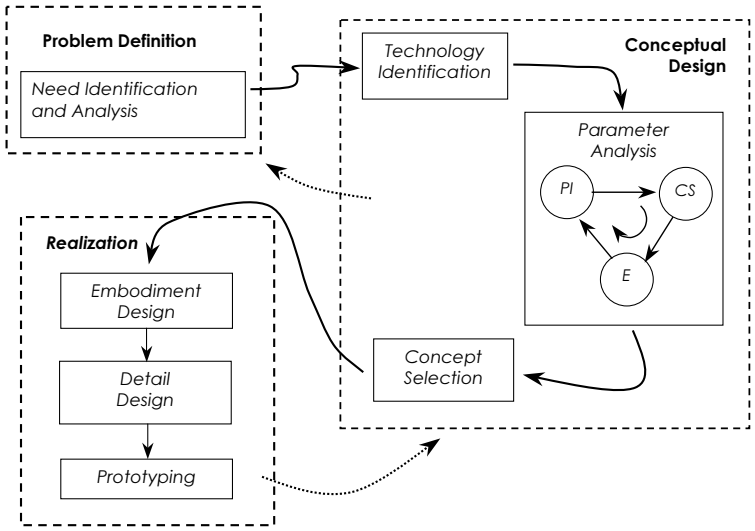

Figure 3.1: Overview of the engineering design process (PI-Parameter Identification, CS-Creative Synthesis, E-Evaluation).

3.1 Design Methodology

Design, can be best described by the derivation, from the Latin word *designare*, which when translating the roots *de* meaning "from" and *signare* "to draw". Therefore the main purpose of engineering design, is to produce creative solutions, drawn from the knowledge the engineer has at hand, in the form of new materials, processes, powerful computers and software, to facilitate design conception and analysis.

Since engineering, as a part of the applied physical sciences, is concerned with understanding and transforming the natural physical world by creating new devices, systems and processes. This process of creation is generally termed *engineering design*, as with all the sciences, several models, or theories have been developed to address

the design process.

Essentially there are two main thoughts of design methodology, one where the engineer, follows a flowchart, very much like that of a computer program, evaluating whether the conditional clauses (functional requirements) have been met, refining and repeating steps as required [Shigley, 1986], similar as shown in Figure 3.1. Another more recent method is that of Suh, as shown in Figure 3.2,

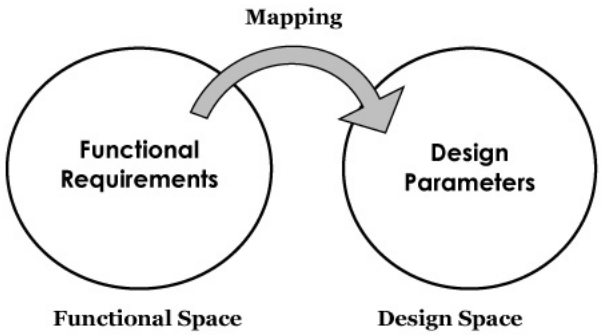

Figure 3.2: Engineering design as a functional mapping.

where the process is characterized by mapping. Thompson [1999] states design can be represented as a "mapping process from the functional space to the physical space to satisfy the designer-specified functional requirements". There is however a commonality in the different processes, with problem identification through to a final solution, engineers make decisions based on modeled behavior, needs and constraints. The process as shown in Figure 3.1, would be a true representation for all design processes.

The following two sections deals with, a discussion of the axiomatic system of design, and the conceptual stage of design. Concentrat-

ing on the latter as this being an important part of any design method.

3.1.1 Axiomatic Design

"Axiomatic design" as proposed by Suh, where the model of a design process is based on the transfer from the functional space to the physical space [Thompson, 1999; Suh, 1998, 1999]. The functional space consists of functional requirements (FRs), and the physical space contains design parameters (DPs). The FRs are defined as the minimum requirements to characterize the design goals. A design needs to meet the defined FRs, and to achieve this a system of DPs, which affect the behavior of the FRs are satisfied [Suh, 1998].

Suh presents design as a sequential process, where the most important functional requirements need to be identified first, then a physical solution created leading to new, lower-level FRs and continuing till all the FRs are met [Melvin, 2003; Suh, 1999]. Two axioms are required to satisfy the principals of the technique:

1. **Axiom 1 (Independence Axiom)** *Maintain the independence of the functional requirements.*

2. **Axiom 2 (Information Axiom)** *Minimize the information content of the design.*

Therefore many corollaries can be derived from these two axioms to offer the designer assistance in synthesizing physical solutions to satisfy FRs.
Some examples are:

Corollary 1 *(Decoupling of Coupled Design)*

Decompose, or separate parts, or aspects of a solution if FRs are

coupled or become interdependent in the designs proposed.

Corollary 2 *(Minimization of FRs)*

Minimize the number of FRs and constraints.

Corollary 3 *(Integration of Physical Parts)*

Integrate the design features in a single physical part if FRs can be independently satisfied in the proposed solution.

Corollary 4 *(Use of Standardization)*

Use standardized or interchangeable parts if the use of these parts is consistent with the FRs and constraints.

Corollary 5 *(Use of Symmetry)*

Use symmetrical shapes and, or arrangements if they are consistent with the FRs and constraints.

Corollary 6 *(Largest Tolerance)*

Specify the largest allowable tolerance in stating the FRs.

Corollary 7 *(Uncoupled Design with Less Information)*

Seek an uncoupled design that requires less information than coupled designs in satisfying a set of FRs.

Mathematically;

$$FR_i = A_{ij} DP_i \quad \text{where} \quad i, j = 1, 2, \ldots, N \tag{3.1}$$

In Eq. (3.1), FR_i and DP_i are vectors representing Function Requirements and Design Parameters respectively and A_{ij} relates to the design matrix [Suh, 1998, 1999]. For example, if a design matrix

contained the following design equation:

$$\begin{Bmatrix} FR_1 \\ FR_2 \end{Bmatrix} = \begin{bmatrix} A_{11} & 0 \\ A_{21} & A_{22} \end{bmatrix} \begin{Bmatrix} DP_1 \\ DP_2 \end{Bmatrix} \tag{3.2}$$

where A_{11} signifies the effect of DP_1 on FR_1, and A_{21} signifies the effect of DP_2 on FR_1, etc. When the design equations represent conceptual levels of design, it is common for the elements of the matrix, A_{ij} to be represented by 'X' when there is an effect (non-zeros), and a zero, '0' when there is none. For example if in the following equation A_{11} and A_{22} are coupled to either DP_1 or DP_2 whereas A_{21} is uncoupled, zero:

$$\begin{Bmatrix} FR_1 \\ FR_2 \end{Bmatrix} = \begin{bmatrix} X & 0 \\ 0 & X \end{bmatrix} \begin{Bmatrix} DP_1 \\ DP_2 \end{Bmatrix} \tag{3.3}$$

Therefore to satisfy the Independence Axiom, the design matrix must be diagonal or triangular. In the Eq. (3.2) the triangular matrix shown represents a decoupled design. This would require that the value of DP_1 be set before that of DP_2. When a design matrix is a diagonal matrix, this represents a uncoupled design, and the DPs maybe set in any order. The uncoupled design matrix allows for the design tasks to be mutually separable and therefore allowing tasks to be conducted concurrently, the designers aim is to achieve this form of design matrix. Most of the real world problems are either decoupled or coupled forms. However coupled design is not necessary bad design just time consuming. To achieve decoupled or uncoupled design, there are certain principals to follow:

- Use standard parts
- Use of symmetrical shapes and arrangements

- Reducing the information content in design
- Adding additional design parameters to make the number of FRs equal to that of the DPs

Axiomatic design firstly addresses the general requirements of a system, and breaks these down into sub-requirements. As the system is broken down, it is necessary to specify a set of FRs, move into the physical space with the conception of a design solution and specification of DPs, and then proceed back to the functional space as required. This form of iteration also termed zigzagging, between functional and physical space, which progresses from a general to a detailed description.

3.1.2 Parametric Conceptual Design

The process of parametric conceptual design can be broken down into three main stages, with reference to the proposed design methodology of [Kroll *et al.*, 2001], Figure 3.1, the problem definition followed by the conceptual design and finally that of realization.

The problem definition stage, is also the termed "Need Identification and Analysis", here identifying what the real need is and analyzing the need such that the best possible solutions meet this need. Once a need has been identified this statement forms the basis for the design process. The "Need Analysis", is where the functions and constraints are defined and clearly formulated to define the solution space. An imaginary solution space can be defined as the space where the functions can be realized, with the "Need Identification" forming the purpose, or primary function, this can be broken down

into secondary or subfunctions. These subfunctions are further refined as they are directly related to the need and are solution specific. The constraints are defined, this then identifies the outer limits of the solution space. Ideally a solution space would be infinite.

The functions can be further defined into the following categories, performance, size, value, safety and special considerations [Kroll *et al.*, 2001].

- **Performance:** deals with functions, which are the actions or activities that a product should perform.
- **Value:** not only the monetary but also related to the original need, the function of the product and the level of performance attempted.
- **Size:** relates to the constraints on the dimensions, shape, weight and other physical properties.
- **Safety:** deals with issues concerning, operation safety, health and the environment.
- **Special:** concerned with market conditions, trends, government regulations and other special or unusual task-related circumstances.

The conceptual design stage is best described as the thought process of generating and implementing the fundamental ideas, characterizing a product or system. The idea of conceptual design differentiates between products of similar type through innovation, novelty, performance, robustness and development time. The methodology for conceptual design is called parameter design as

presented in Figure 3.1, where PI represents *Parameter Identification*, CS as *Creative Synthesis* and E as *Evaluation*.

The element of parameter identification, comprises of the recognition of the main parameters in the problem and developing a key understanding of the problem and pointing to potential solutions. The second part of parameter analysis is creative synthesis, this represents the generation of physical configurations, as the process is iterative, many physical configurations tend to be generated. These then influence the design solution by having new sets of parameters which stimulate the direction of the design.

The process of moving from the physical back to the parameter stage is handled in the third phase of the parameter analysis methodology, the evaluation stage. This stage is important since the degree of physical realization of the solution needs to be addressed. Finally the step of Technology Identification is where new or existing technologies are investigated as starting points or initial conditions, for parameter analysis.

The final stage of Realization is where the design is turned into a product or system layout, here there are three or more steps that need attention.

The embodiment design stage, defines a point where the most promising concept is selected for further development, this is also known as the preliminary design, layout design or configuration design. The layout drawings are drawn up and noncritical issues are addressed, such as, materials, preliminary calculations of component sizes, the concerns of “transmission of forces”, manufacturing

process, easy of assembly by reducing the components.

The detail design stage, is where the design is checked through comprehensive calculations of strength and properties, of precise dimensions and tolerances, material specific specifications and other considerations of the final design stage are taken into account.

A prototype is then produced and testing continues the process, at this stage in the process, often the product is improved or at times redesigned, until the product is fit for the market.

3.2 Retractable Pin Tool Design

3.2.1 Background

The Friction stir welding process has been around for several years and has been continuously developed. Friction Stir Welding (FSW) uses the principle of the force of friction to generate heat, this results in the material, to be joined, to be transformed into a plasticized state and with the action of the pin, extending from a profiled shoulder, to stir the two materials into each other to form a solid-state bond without needing to add fillers or external heat.

The welding tool consists of a shaft, in which one end is a free-end and the other driven. The driven-end is that which rotates the tool, the free-end consists of a shouldered pin, which is lowered onto the surfaces between the two fayed workpieces which are to be joined. The shouldered pin on the free-end of the shaft-tool being of fixed length, generates the frictional heat to plasticize the material around the pin. The shaft-tool is then moved transversely along the fayed

join line, whereby the stirring action of the pin, moves material from the front to the rear of the pin, thereby mixing the materials and forming a solid-state bond.

Present friction stir welding tools, in which the pin is of fixed length, have the disadvantage of being able only to weld materials of same thickness and leaving a crater or *keyhole* (as shown in Figure 3.3) in the welded workpieces, plates **A** and **B**, upon tool retraction. The *keyhole* effect has limited the friction stir welding process from more complex joining applications, such as those used in the aerospace and automotive industries. Figure 3.3, shows the elimination of the *keyhole* would complete the weld and make the process more acceptable to industry.

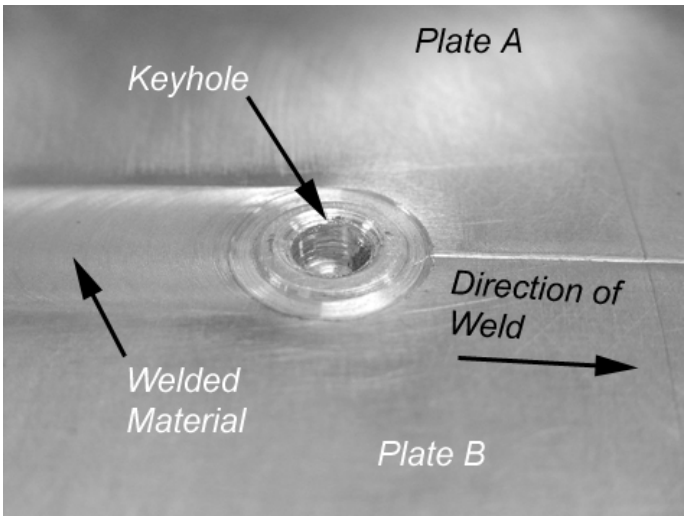

Figure 3.3: The *keyhole* in a friction stir weld.

3.2.2 Problem Definition

Need Identification

Since the welding tools used in the present form of FSW have the pin fixed relative to the shoulder face of the shaft tool. It would require that the action of the pin during a FSW weld needs to be identified.

- *Stirring:* As the pin rotates, this causes the material to deform around the pin and forcing the plasticized material to flow from one workpiece into the other and with a profiled pin the material would also flow vertically downwards relative to the weld [Colligan, 1999], thereby forming a solid-state bond.
- *Length:* The pin length controls the amount of material affected by the stirring action, in relation to the thickness of the workpieces.

Therefore the pin facilitates the action of material intermixing, whereas the length of the pin, governs the thickness of the material to be welded. So to reduce the above to form a problem statement, or identify the need, the action of stirring should remain a constant. This means, for a FSW weld, the pin rotates and the action of changing the length of the pin needs to be addressed.

Stating the "Need Analysis" statement simply, as follows: "a pin that can have a variable length, along its axial axis, whilst rotating and to able to control this length." This is only a generalization and a more detailed break down is required. This is achieved by defining the functions and constraints into smaller statements. The following categories of the functions and constraints, performance, value, size,

safety and special considerations as defined by [Kroll *et al.*, 2001]. Briefly the categories of the functions and constraints relating to the design of the retractable tool are considered:

- *Performance*, the welding tool requires a pin to be variable along its axial axis, and be able to withstand the forces resulting from the welding process. Here data from previous tests carried out on the FSW process are considered, e.g. from the published results of Johnson [2001] and Ding [2000]. The limits due to the existing machine on which the tool will be tested were also considered.

- *Size*, here the limits in the overall size of the tool were considered as the space around the machine, as stated above, is limited. The possibility of adapting the tool for future use with robots was considered as a constraint but not implemented.

- *Value*, this consideration has a two fold function, the cost had to be within a respectable limit for an experimental tool and yet be able to deliver the desired performance.

- *Safety*, since this was an experimental tool a fair amount of operational safety was built in, as the process is not environmentally hazardous, this was not considered.

- *Special*, as the process of FSW is still in its infancy and continuously developing, an investigation into the patents issued was conducted.

3.2.3 Literature Survey of Existing Concepts

The most published movable pin tool for the use with friction stir welding has been the one developed by NASA [Technology Transfer Dept., 2001]. Several others have been published as patents, and most using a variety of differing technologies, these will be discussed in this section.

Wykes

This tool presented by Wykes [1997] can move the pin relative to the shoulder and further, the shoulder circumference can also be adjusted during the welding process. This can be seen in the Figure 3.4,

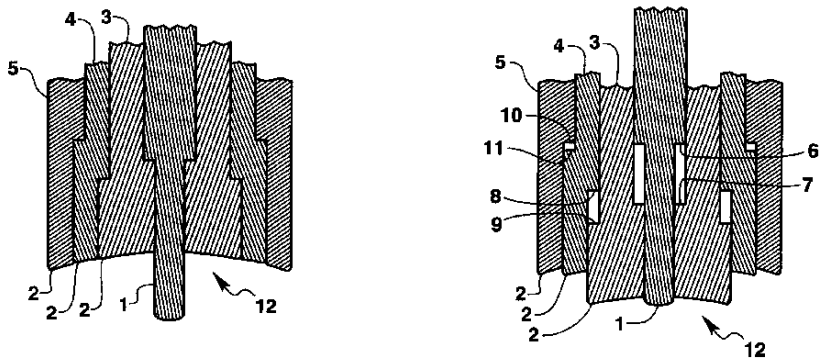

(a) In the extended position. (b) In the retracted position.

Figure 3.4: Wykes (1997).

where the pin moves independently to the different shoulders denoted by *'3'*, *'4'* and *'5'* in the Figures 3.4(a) and 3.4(b). Actuation of the pin and shoulders is not defined. Both the problem of the different thicknesses and the closure of the *keyhole* are addressed in this design configuration.

Colligan

The tool as presented by Colligan [1998] comprises of an shaft tool which characterizes those used in the FSW process, with the pin movement achieved by the spring denoted by *'50'* in Figure 3.5, which allows for the pin *'40'* to move by compressing the spring *'50'* relative to the shoulder *'38'*. Colligan [1998] describes one embodiment of the tool, as being used in conjunction with an apparatus that allows the shoulder of the tool to ride on and track the workpiece surface. However this design solves one problem, by

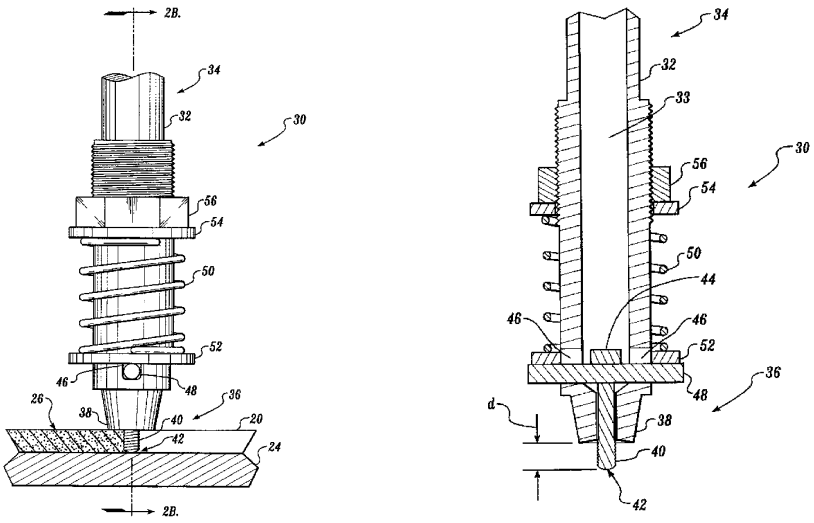

(a) Side view. (b) Sectional view.

Figure 3.5: Colligan (1998).

allowing for the welding of workpieces of different thickness, but it does not address the problem of closing the *keyhole*.

Holt and Lang

This design by Holt and Lang [1998] is a hydraulically actuated welding tool, which has an actuating plunger with a pin like end. This can be seen in the Figure 3.6 where the pin / plunger component *'19'* and the pin *'4'* moving in the shoulder body *'9'*. The actuation

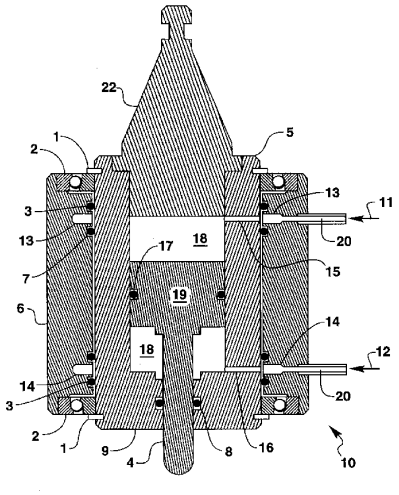

Figure 3.6: Holt and Lang (1998).

in the downward direction relative to the shoulder as in Figure 3.6 takes place, when the volume of fluid in chamber *'18'* above *'19'* is increased, and correspondingly the fluid in chamber *'18'* below *'19'* is decreased and the reverse to move the pin upward. The design is very simple and embodies similar design concepts as with the designs of those in this section. The design, covers the problem of the *keyhole* elimination and also allows for welding of materials with differing thicknesses.

Ding and Oelgoetz

This tool effectively has been used by NASA [Technology Transfer Dept., 2001], according to Ding and Oelgoetz [1999] comprises of an auto-adjusting pin, where the pin is adjusted electro-mechanically or hydraulically. The pin moves independently to the shoulder, as with the tool designs of Wykes [1997], and Holt and Lang [1998].

Reference to the Figure 3.7, the pin '*33*' moves in the axial channel

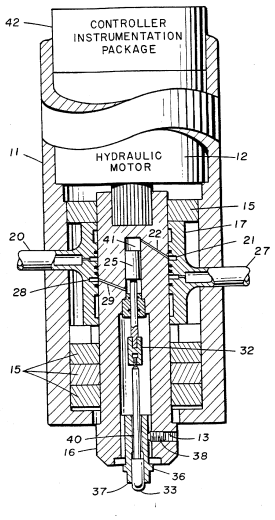

Figure 3.7: Ding and Oelgoetz (1999).

located in the shoulder '*37*', and is moved with a hydraulic or electro-mechanical actuator. The method of hydraulic actuation is shown in the Figure 3.7. A differing aspect to this design is the use of modular components, such as the pin and shoulder, and the compactness of the design which allows it to be used on a variety of platforms. A major advancement in this tool design has been the development of the control system to form a closed-loop feedback

Figure 3.8: NASA's retractable pin tool.

system to control the pin. This tool addresses both the different thickness of the welding material and the elimination of the *keyhole* effect.

Strombeck and Dos Santos

The solution provided by von Strombeck and Dos Santos [2002] is where a movable pin is extended through the workpiece to form another shoulder on the back surface of the workpiece. This second shoulder which moves independently to the first, forms the backing plate, as in the conventional Friction Stir Welding process, however eliminating the need for a fixed structure, therefore ideal for robotic use. The use of two shoulders also allows for the weld to be seen as a "two pass" weld. This means that a weld is carried out on both sides of a workpiece. According to von Strombeck and Dos Santos [2002] this tool does not induce warping of the workpieces and plasticized material cannot escape.

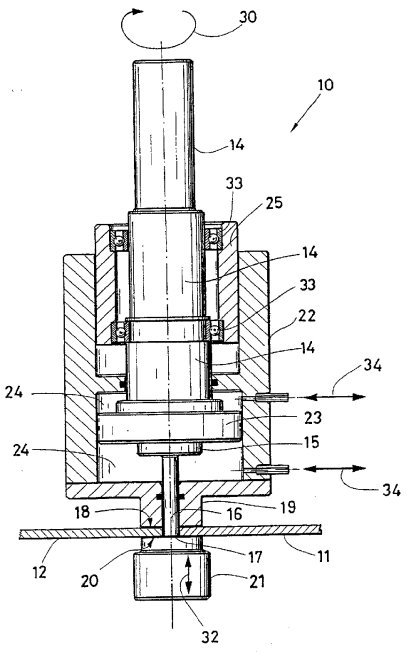

Figure 3.9: von Strombeck and Dos Santos (2002).

The forces produced by Friction Stir Welding on the workpieces are eliminated due to the nature of the tool, the force applied by the first shoulder *'18'* on the Figure 3.9 and that of the second shoulder *'20'* are opposing therefore the total force on the workpiece is eliminated.

This form of tool has been successfully used by the MTS Systems Corporation, shown in Figure 3.10. This design of weld head, solves the problem of the *keyhole* using a different approach, with the resulting *keyhole* effect is eliminated from the process. This tool addresses the problem of different material thicknesses during welding.

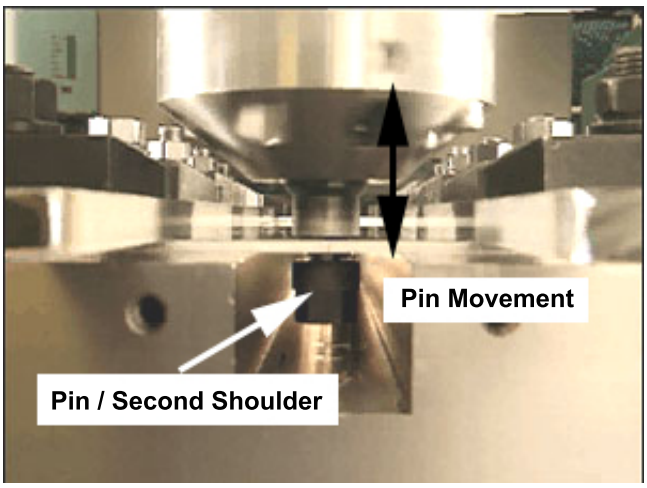

Figure 3.10: An AdAPT (Adaptable, Adujustable, Pin Tool) bobbin type tool (from MTS Systems Corporation (2002)).

3.2.4 Parameter Concept Analysis

The design concept was to have a actuating device to lift and lower the pin onto the surface, there are several ways in which one can transmit this motion, these being, electrical, mechanical, hydraulic and pneumatic. Each is used to transmit power (force over a distance in time) and modify motion (accelerate, decelerate), and each method has its special capabilities and limitations [Rohner and Smith, 1989]. After a literature survey into existing ideas and patents was completed the next stage of the design process was carried out, that of identifying the requirements and constraints. Once defined, a look at existing technologies to fulfill the defined requirements was investigated.

Design Requirements

Before the process of design can continue the requirements and constraints have to be clearly defined. The design requirements and constraints (*shown in italics*), are listed below:

1. Pin movement to along the axial axis, *limited to around 6mm with respect to the shoulder*.
2. The actuator must be capable of reacting to forces on the pin in both directions.
3. Control the effect of heat on the tool, especially around the actuator.
4. Maximum rotation of the tool: 500 rpm.
5. Monitor temperature of the pin.
6. The tool assembly must be modular.
7. *Must fit into existing machine set-up.*
8. Have components that are symmetrical or are similar to lower the production costs.

Technology Identification

From the investigation into the existing tools and those in the patents, it was apparent that the method of actuation will play a crucial role in the design of the tool. Since the tool is rotating and needs to be moved along the axial axis relative to the rotation, the method of actuating was investigated.

Table 3.1: Performance data for different actuators

No.	Actuator Type	Expansion	Shear	Efficiency
		%	Nmm^{-2}	%
1	Hydraulic cylinder	30	21	92
2	Pneumatic cylinder	76	1	88
3	DC motor [a]	70	0.07	50

a - Direct Current

Table 3.1 illustrates the different types of actuation and the corresponding performance data. The comparison between the rotation motors and the linear actuators was based on the conversion consisting of a mechanical spindle with a nut, with a 1 mm pitch. Therefore the length of the spindle relates to that of the motor [Heinz, 1996]. *Expansion* is the stroke relative to the length of the inner actuator where the energy is generated, for example, the internal length of a hydraulic cylinder. The effective stroke of an electric motor is 70% of the specified spindle length.

Shear, denotes the linear force relative to the force-generation surface, for example, the cross-sectional inner surface on a hydraulic cylinder. The force on the the rotor and the rotor lateral surface is used to calculate the *transverse shear* in electric motors.

Efficiency is derived from the supplied energy divided by the energy transmitted to the actuator, not including the associated losses.

Considering the data from Table 3.1, by looking at the efficiencies it was decided to continue with either a hydraulic or pneumatic form of actuation. The DC motor solution, would have required complex

Table 3.2: The differences between hydraulic and pneumatic actuators

	Hydraulic actuator	Pneumatic actuator
Medium	Fluid, usually hydraulic oil Supply from tank, oil sump Virtually incompressible Self-lubricating Viscosity extremely temperature-sensitive	Gas, usually air Supply from surrounding air Compressible Auxiliary lubrication needed Viscosity fluctuations virtually irrelevant
Pressure	to approx. 30MPa	to approx. 1MPa
Lines	Supply and feed lines	Pressure connection Return direct to environment

mechanisms to convert the rotational motion into linear, and further complicating the tool. Since one of the constraints, using the existing machine, would have been compromised and a functional requirement was to have a simple tool. A detailed investigation into the two types, hydraulic and pneumatic, was conducted. The difference with the two types of actuators can be clearly seen in Table. 3.2, however there are also differences in their applications, due to the difference, in the compressibility of the two mediums. As described below:

Hydraulic actuator: Positioning applications with high load rigidity, demanding requirements for synchronization and positioning precision within closed-loop control system.

Pneumatic actuator: Actuators with limited force requirements, positioning via mechanical contact, operation in an open-loop control system.

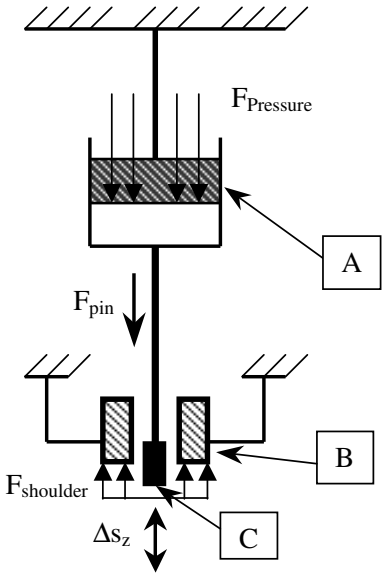

Figure 3.11: A simple schematic of the model using a hydraulic or pneumatic actuator, where **A** is the actuator, **B** the shoulder and **C** the pin.

3.2.5 Analysis of Design Parameters

A simple conceptual model was developed to obtain a better understanding of the needs as this was new technology and there being limited references. The model formed part of the design analysis, data was obtained from published articles by Johnson [2001] and Ding [2000] where the forces were measured, these are tabled in Table 3.4. In Figure 3.11 the forces that will influence the design are shown, note the rotation of the tool has not been included.

Once the data and model were analyzed the conceptual design was redefined implementing the appropriate technology and allowances of the constraints. Figure 3.11, the forces and the required movement

of the pin ΔS_z have been included, to make the design analysis simple and to define the problem areas. The main load bearing structure would need to direct the applied stresses on the shoulder **B** through to the point W_1. An estimation of the forces acting on the system was taken from existing tests conducted on the FSW tools and from tests conducted on the machine to be used for this experimental tool.

The data from Johnson [2001] relates to a shaft tool, where the pin is fixed relative to the shoulder, therefore the force $\mathbf{F_z}$ is a combination of pin and shoulder forces. Various tool geometries were used by Johnson [2001], these are listed in Table 3.3, and an adjustment of the forces to a calculated equivalent force for the analysis was carried out.

The data published by Johnson [2001], Table 3.4, can be split into the components of force on the shoulder and the pin. The required pressure on the material, using the 20 mm and 25 mm shouldered tools is exactly in proportion to their respective areas. Since the shoulder is fixed relative to the pin, see Figure 3.11, the magnitude of the forces

Table 3.3: Tool geometry as used by Johnson (2001) for the force characterization of FSW welds

Tool	Shoulder Diameter *mm*	Center Pin Diameter *mm*	Pin Length *mm*
K1	25	10	6.1
K2	25	8	5.8
K3	20	8	5.6
K4	20	9	6.15

Table 3.4: Selected force and torque measured data for a FSW shaft tool (Johnson, 2001)

Alloy	Tool	Rotation rpm	Speed mm/min	Force F_x kN	Force F_z kN	Torque Nm
2014-T6	K1	500	80	1.4	13.5	55
	K2	500	80	3.7	22.5	41
		500	80	3.8	23.5	42
	K3	500	80	4.2	17.5	32
	K4	500	40	1.9	14.5	31

applied on the shoulder will be needed for the tool design. The force in the z-axis on the pin during welding is assumed to be relatively small compared to that of the shoulder, due to the hydrostatic pressure on the tool. So the total force $\mathbf{F_z}$ was used as an indication of the force, which applied on the tool as a compressive force.

According to data from Johnson [2001] (Table 3.4), it can be shown that a force $\mathbf{F_z}$ of between 14 kN to 24 kN can be expected on the shoulder with the other parameters kept constant, this would mean a tool would need to resist a compressive force of this magnitude.

In the FSW process there are significant forces exerted on the tool, however these have been considered only on a shoulder-pin tool*.

Upon analysis of these forces, most are focused on the shoulder as it is directly responsible for the plunge depth and partial generation of the frictional heat. When the total forces are assessed, the force of the pin needs to be evaluated independently to that of the shoulder. As the shoulder is pushing against the weld material surface, an oppos-

*This refers to the standard fixed pin shaft tool used in the FSW welding

ing force is pushing against the tip of the welding pin [Ding, 2000]. Thus the pin force had to be considered to give an indication into the size and force required for the actuator.

Considering the work from Ding [2000], where the force characterization on the pin was measured, during static and dynamic welds, formed a basis on which the design constraints could be evaluated. As this was the only published data on a retractable pin tool, available for this research, it was used to separate the ratio of force on the shoulder with that of the pin from the data measured by Johnson [2001]. The pin-shoulder configuration as used by Ding [2000] consisted of a shoulder diameter of 24 mm and a pin diameter of 9.6 mm. The results were converted assuming all other parameters remained constant. The data was given in units of Pressure **P** (MPa), these had to be converted to units of force **F** (N), using the relationship;

$$\mathbf{F} = \mathbf{P} \cdot Area$$

The area (mm^2) in this case was that of the pin, using the pin diameter given as 9.6 mm. After conversion and relating it to two different pin diameters, the data shows that a small pin diameter would require less actuation force. The role played by the pin with respect to heat generation had to be considered.

The shoulder with a diameter of 20 mm and 6 mm for a pin diameter, was considered for the tool design, taking the data from Table 3.4 and Table 3.5 into consideration.

Table 3.5: Pin pressure converted to force, where S1-S6 are the static plunge data and D1-D4 the dynamic plunge data, taken from Ding (2000)

No.	Pressure, MPa	Force F_z, kN Pin diameter 9.6 mm	Force F_z, kN Pin diameter 6.0 mm
S1	26.73	1.935	0.756
S2	28.96	2.096	0.819
S3	26.20	1.896	0.740
S4	28.32	2.050	0.800
S5	28.86	1.727	0.675
S6	28.99	2.098	0.819
D1	29.303	2.120	0.829
D2	32.219	2.332	0.911
D3	31.17	2.256	0.881
D4	36.34	2.630	1.027

3.2.6 Concept Selection

Method of Actuation

The actuator would need to move the pin into the plate at the start of the welding process. Once the forces have been defined, a system had to be considered, either a hydraulic or pneumatic actuator. As discussed in the previous section, a 25 kN force on the shoulder and a force on the pin of around 1 kN would be applied to the tool and form the basic requirements for the design.

A problem with an actuator that can withstand forces of 25 kN, would be the need to fulfill the constraint concerning the available space on the existing machine, to which the tool would have to be

fitted. An actuator capable of this and also be small enough to fit on the machine would require designing. A simpler solution where the pin would only require actuation, meant that a smaller diameter actuator was needed.

The search for a hydraulic actuator, initially considered the better solution, was conducted using the data gathered from the technology identification phase. However the complications of a hydraulic system, accumulators, pumps to deliver the pressure, and the possibility of contamination, weighed against using this form of actuation.

Pneumatic actuators however do not have the capacity to deliver the required force of 1 kN without having a large diameter piston. The advantages of pneumatic transmission being clean, the risks of contamination are limited as air is freely available and easily exhausted back into the atmosphere. Actuators running on air, are simple and inexpensive, fulfilling another design requirement.

Now that the system of actuation had been decided, a solution to provide the movement had to be found. After a comprehensive search, a pneumatic muscle type actuator seemed a possible solution. The primary advantage being a force to diameter ratio ten times greater than that of a normal pneumatic piston actuator.

Fluidic Muscle

The most common type of pneumatic artificial muscle type actuator is the McKibben Muscle. The actuator as described by Chou and Hannaford [1996], converts pneumatic or hydraulic energy into me-

chanical, by transferring the pressure applied on the inner surface of its bladder to cause a shortening tension. Recent developments from Festo AG & Co., who have introduced the Fluidic Muscle, consisting of a combination of an impervious flexible tube and a covering of tightly woven threads in a diamond-shaped pattern flanked on each end with a end-fitting [Festo AG., 2003; Nakamura *et al.*, 2002]. The

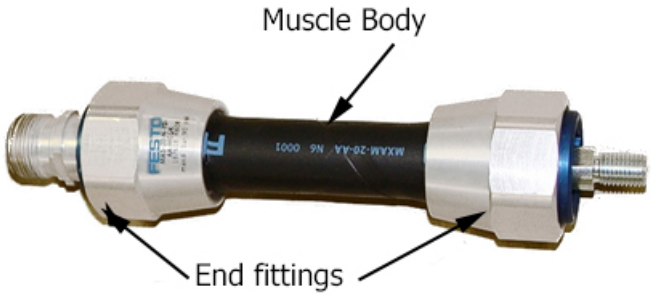

Figure 3.12: A Festo Fluidic Muscle showing the end fittings and the muscle body.

resulting grid structure is deformed in the peripheral direction, with increasing the internal pressure, an axial direction tension force results.

Since the pin movement was limited to 6 mm of travel and the force on the pin alone as shown in Table 3.5, was less than that of the shoulder, approximately 1 kN. Figure 3.13 illustrates the relationship of muscle contraction, or travel to force, as calculated from software given by Festo AG. [2003], where a maximum force of 1200 N can be attained for the range of 6 mm pin movement. A conceptual design which included the actuator was drawn up. The following concerns where noted, a need for a rotary joint to deliver the pressure whilst

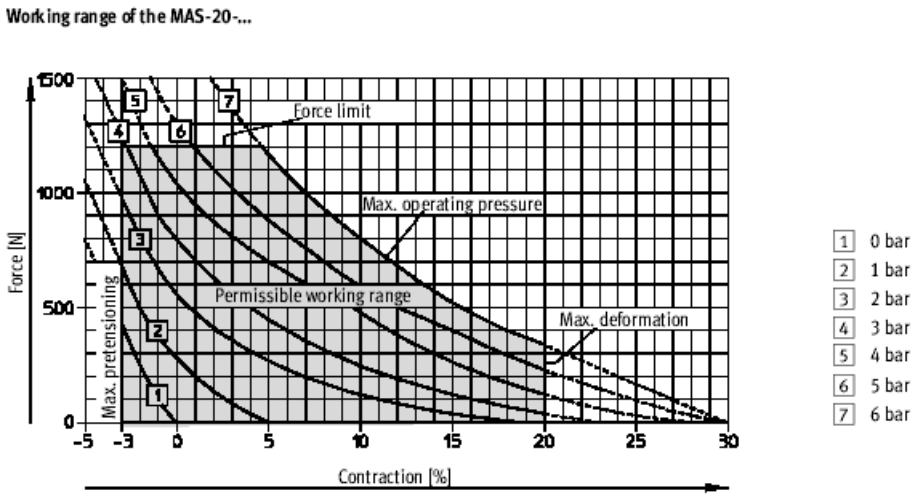

Figure 3.13: Operating range for stroke and pressure from Festo AG. (2003).

the tool rotated, and a support structure to withstand the forces applied to the shoulder.

Considerations in the function application of the muscle where dealt with early in the conceptual phase. As the muscle could be used in its simplest form, as a single-acting actuator against a constant load. Here a load is attached to the actuator and when pressurized, the actuator develops enough force to lift the load. Pretensioning the actuator, with a pressure, would the effectively give the actuator a holding force and thus leaving a small force component for the lifting motion itself.

By letting the actuator behave as a spring, a changing external force would then cause the actuator to follow the action of that force. Having the spring stiffness and the pretensioning force variable, the

actuator could be used as a spring with constant volume or constant pressure, thus being able to produce different spring characteristics.

Both these applications could be used for an actuator in the tool design, as the movement and the retraction force were considered small. Once the actuator system was designed, the components of the support structure were then addressed.

Concept Selection

The concept and its integral components are defined after extensive iteration of the parameter identification, through to the creative synthesis and final evaluation process. The concept design, can be broken into sub-functional concepts, these being, the method of delivering air to the system, a method of supporting the actuator, a system to allow for cooling the rotary joint and the actuator, the modular pin and shoulder assembly.

When the design functional requirements are reviewed, page 56, with the pin movement through an actuation system using a Fluidic Muscle arrangement. The ability to react to forces of a magnitude, as defined in Section 3.2.5, could be done using a Fluidic Muscle. The need to have the tool rotating, a prerequisite design parameter, and deliver pressurized air to the system, in the form of a rotary joint would need designing.

The cooling of the actuator, as a defined design requirement, would have to be integrated in the design with the rotary joint. A concept was devised to allow an air cooling system, that could be used in various configurations.

The design requirement of the tool being modular in design, would have to include the support structure and the shoulder and pin assembly. Through systematically evaluating the concept design, and concentrating on points of possible problems, different concepts were applied. Resulting in components that were easier to manufacture and without the need to re-manufacture large components. This also fulfilled the design requirement concerning symmetrical and lowered manufacturing costs.

3.2.7 Design Realization

At this stage of the design process, the conceptual design is defined in more detail. Layout drawings and preliminary calculations where carried out to evaluate and verify the design. In this section, a discussion as to the reasoning behind the resulting designed components is addressed. The design is separated into three embodiments, the rotary joint, the support structure and the shoulder-pin assembly. The actuator locates between the rotary joint and the shoulder-pin assembly and has been dealt with in previous sections, however the link to the other components will be discussed here. The detailed drawings can viewed in the Appendix section of this work.

Rotary Joint

The rotary joint, was needed to provide air pressure to the actuator whilst the tool was rotating. The preferred option was to source one, as this would facilitate the design and production stage. However on the host machine, a limitation due to the data acquisition platform

was encountered, and a rotary joint was designed.

The body of the rotary joint was designed to accommodate an air passageway to supply the actuator. The body also included eight separate passageways through which cooling air could be directed. The slip-ring contained two separate annular passageways with inlets at *(2a)* and *(2b)* in Figure 3.14, one for the actuator and another for the cooling. Separating these passageways, three 'O'-rings were used, the data specifications and design evaluation steps are shown in Appendix B.

The outer ring, was to be held stationary during operation and a support bracket was designed to be attached to the host machine. A Teflon washer was placed between the lower-side of the outer ring and the upper support bracket, to prevent the unnecessary rubbing on the upper support bracket.

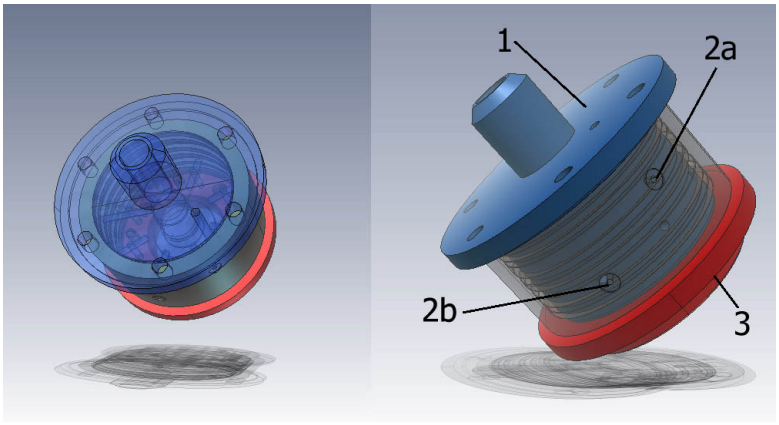

Figure 3.14: Views showing the body *(1)*, air inlets *(2a)*, and *(2b)* on the slip-ring and *(3)* the upper adapter plate.

Support Structure

The support structure, is a load bearing component of the experimental welding tool. This comprises of several components which link the shoulder-pin assembly to an adapter plate on the rotary joint assembly. Since the actuator was unable to take the loads required during the welding process, a support structure was designed to allow for the stresses to flow through the rotary joint and into the host machine structure.

A look at Figure 3.11 shows the forces that will need to be contained and redirected through the structure. The magnitude of these forces being equal those at the shoulder **B**, and therefore at W_1. The structure was considered as a simply supported (fixed-free) column, the fixed-end at the point W_1 and the free-end at **B**. However due to the design concept the structure was broken down into simpler configurations to ease the calculations needed to evaluate the concept.

The design entailed the use of four columns, which had the dual function, that of carrying the load from the shoulder and restricting pin mounting plate movement to one Degree of Freedom (DoF), see Figure 3.15. The columns are attached to the lower adapter plate on which the shoulder is mounted, and a cylindrical tube connecting the upper adapter plate to the lower adapter plate, provides extra support in compression.

Design calculations on the columns and the outer shell, (not shown in Figure 3.15) were done to evaluated the concept. Since a column can be described as a long slender bar subject to axial compression, and with failure in the form of buckling, where by lateral deflection

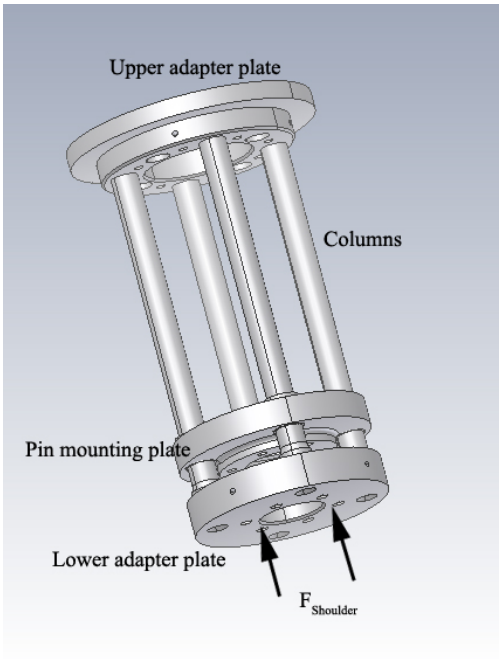

Figure 3.15: A schematic view of the support structure.

the column reaches its buckling stress or critical stress. This being frequently below the limit of proportionality and seldom above the yield stress of the material. Due to the proposed design concept the predictions of bucking loads on the support structure are important for the design evaluation.

Consider a simple column subjected to a compressive load, as in Figure 3.16, the load P shortens the column, irrespective of the value of P. Assuming that the load P has reached the critical value P_{CR}, at this load the displacement is permanent. As $P > P_{CR}$, lateral displacement increases and the column is unstable. The solution of P_{CR} can be found by considering the differential equation for the deflection

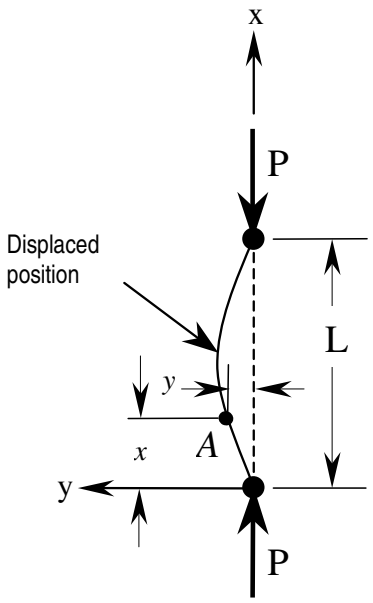

Figure 3.16: Defining a buckling load for a perfect column.

curve

$$EI\frac{d^2y}{dx^2} = M \tag{3.4}$$

therefore the resultant moment is

$$M = -Py \tag{3.5}$$

and substituting into Eq. (3.4) and rearranging

$$\frac{d^2y}{dx^2} + \frac{P}{EI}\,y = 0 \tag{3.6}$$

this resembles a differential equation for simple harmonic motion. For which the solution is

$$y = A \sin \sqrt{\frac{P}{EI}}\, x + B \cos \sqrt{\frac{P}{EI}}\, x \tag{3.7}$$

where A and B are constants of integration, and will have to be determined for the boundary conditions of the problem. The boundary conditions used are $y = 0$ at $x = 0$ and $x = L$, with reference to Figure 3.16. After evaluating using the boundary conditions, this gives $B = 0$, and

$$0 = A \sin \sqrt{\frac{P}{EI}}\, L \tag{3.8}$$

Since if $A = 0$, no buckling occurs. Considering $A \neq 0$ then

$$\sin \sqrt{\frac{P}{EI}}\, L = 0 \tag{3.9}$$

this is then satisfied by $\sqrt{P/EI}\, L = N\pi$, where N is an integer. Solving for $N = 1$ gives the critical load

$$P_{CR} = \frac{\pi^2 EI}{L^2} \tag{3.10}$$

this called the *Euler column formula*.†

The Euler formula forms the basis with which buckling in columns can be calculated, however different conditions require other methods to solve the problem. When the results from the boundary conditions are added, Eq. (3.7) becomes

$$y = A \sin \frac{\pi x}{L} \tag{3.11}$$

†This applies only to rounded-end columns.

which indicates a half sin-wave defection curve. Since the minimum critical load is of importance, which occurs at $N = 1$.

As a column is described as being long and slender, the proportion of length to diameter determines the route to take when solving this type of problem. The *slenderness ratio* is defined as L/k and by using the relationship $I = Ak^2$, A is Area and k the radius of gyration of the column. By rearranging the Eq. (3.10) into

$$\frac{P_{CR}}{A} = \frac{\pi^2 E}{(L/k)^2} \tag{3.12}$$

As Eq. (3.12) shows the critical unit load, not to mistaken with the critical load in Eq. (3.10), has units resembling that of stress (Nm^{-2}). Therefore, from Eq. (3.12) the critical unit load, depends only on the modulus of elasticity E and the slenderness ratio.

When the deflection curves for the different types end conditions are derived, either by solving the differential equation or by comparison. The end conditions and the resulting equations can be summarized with a factor C called the *end-condition constant*, these being theoretical values. The Euler equations can then be written in the following two forms:

$$P_{CR} = \frac{C\pi^2 EI}{L^2}\,, \qquad \frac{P_{CR}}{A} = \frac{C\pi^2 E}{(L/k)^2} \tag{3.13}$$

As there are two types of columns, long and short. *Long columns* which being long enough and sufficiently slender to fail by elastic instability, these can be solved using the Euler formula. However the columns that are short and do not fail by elastic instability are termed *short columns*, where failure occurs when the maximum stress is due to direct compression and to the bending that results from accidental

crookedness and eccentricity reaching a certain value [Young, 1989]. Therefore by calculating the slenderness ratio, and comparing it to a rearranged Euler formula, which is derived from the Eq. (3.13) in the form

$$\left(\frac{l}{k}\right)_1 = \sqrt{\frac{2\pi^2 CE}{\sigma_y}} \tag{3.14}$$

where in Eq. (3.13) P_{CR}/A equals the point at which the critical slenderness ratio is reached. This being where the unit load P/A is equal to the *yield stress*/2 or $\sigma_y/2$. By rule, if the slenderness ratio $(l/k)_1$ is less the l/k then the column can considered as a short column and there several empirically derived formulas which can be applied, otherwise use the Euler formula is required.

As the formulas for short columns are versions of Euler's formula, with empirically adjusted constant to conform to the test results, only the best know are shown. In the following equations as given by Young [1989], the load where failure occurs is P, A represents the cross-sectional area, L the length, and k the least radius of gyration of the section.

Secant formula

$$\frac{P}{A} = \frac{\sigma}{1 + \frac{ec}{k^2} \sec\left(\frac{KL}{2k}\sqrt{\frac{P}{AE}}\right)} \tag{3.15}$$

This formula is adapted for stress due to eccentric loading. Here σ denotes the maximum stress at yield, e denotes the *equivalent eccentricity*(that where a perfectly straight column would cause the same amount of bending), c denotes the distance form the neutral

plane of bending to the outer surface. K is a constant dependent on the end conditions, such that KL is the effective length of the column.

Rankine formula

$$\frac{P}{A} = \frac{\sigma}{1 + \phi(L/k)^2} \tag{3.16}$$

The value of σ is often taken as the ultimate strength and the value of ϕ is $\sigma/C\pi^2E$.

Parabolic or Johnson formula

$$\frac{P}{A} = \sigma - b\left(\frac{L}{k}\right)^2 \tag{3.17}$$

The constant b is generally chosen to make the parabola intersect tangent to the Euler curve for a long column.

Exponential formula

$$\frac{P}{A} = C_1^{\lambda^2}\sigma \qquad \text{where} \quad \lambda = \frac{KL}{k\pi}\left(\frac{\sigma}{E}\right)^2 \tag{3.18}$$

where K,L,k, and σ are as defined in the secant formula. The constant λ combines the column dimensions L and k. the end conditions by K, and the material properties σ and E.

Column Design Calculations

The design calculations for the columns in the support structure were considered to be fixed at both ends, as shown in Figure 3.15, taking the fixed ends as the upper and lower adapter plates respectively.

Table 3.6: End condition constants for Euler columns, with reference to Eq. (3.13), (Shigley, 1986)

	End condition constant C	
Column end conditions	Theoretical value	Recommended value
Fixed-free	0.25	0.25
Rounded-rounded	1	1
Fixed-rounded	2	1.2
Fixed-fixed	4	1.2

However the whole assembly would have to be considered as complex column with one a fixed-end that of the upper adapter plate and a free-end at the shoulder. The calculations for this will be discussed later in this section.

Initial ideal conditions due to space considerations, are for the diameter of the columns to be between 10 to 12 mm and the length was fixed at 160 mm. The load in the z-axis was determined from the Table 3.4, therefore a compressive force of 25 kN was considered as the minimum allowable. The value of C, the end condition for fixed-fixed is defined as 1.2 from Table. 3.6.

Defining the initial conditions as variables:

$$\begin{aligned} \mathbf{F_z} &= 25 \text{ kN} \\ L &= 160 \text{ mm} \\ n &= 4 \quad \text{(safety factor)} \\ E &= 209 \text{ GPa} \end{aligned}$$

$$\begin{aligned} \sigma_y &= 400 \text{ MPa} \\ C &= 1.2 \end{aligned}$$

Consider the column to be a solid round section, therefore determine the second moment of inertia

$$I = \frac{\pi d^4}{64}$$

and taking the radius of gyration k to be $d/4$. By rearranging Euler's equation, Eq. (3.13)

$$I = \frac{P_{CR} L^2}{C\pi^2 E}$$

Substituting the values given and considering the safety factor so that $P_{CR} = n\mathbf{F_Z} = 4(25) = 100$ kN, and solving for I gives

$$I = \frac{100(160)^2}{1.2(\pi^2)209} \frac{10^3(10^{-3})^2}{10^9}$$

$$I = 1.034(10^{-9}) \text{ m}^4$$

using I to find the diameter d

$$d = \left(\frac{I(64)}{\pi}\right)^{\frac{1}{4}} = 12.05 \text{ mm}$$

which gives a radius of gyration $k = d/4$ of 3.00 mm, then using the relationship $L/k - (L/k)_1 \geq 0$ for a long column and < 0 for a short column. This relationship of the slenderness ratios gives the indication to which failure is likely to occur in the column.

Having calculated the diameter and the radius of gyration, and by evaluating the difference between the slenderness ratios L/k and

$(L/k)_1$. Thus the slenderness ratio $L/k = 160/3 = 53.33$ Next the check for a Euler column, using Eq. (3.14) gives

$$\left(\frac{L}{k}\right)_1 = \left(\frac{2C\pi^2 E}{\sigma_y}\right)^{1/2} = \left[\frac{2(1.2)(\pi^2)(209)(10)^3}{400}\right]^{1/2} = 111.2$$

Subtracting $L/k - (L/k)_1 = 53.33 - 111.2 = -57.92$, therefore it is indeed a short column. We now define the diameter for a short column from the Parabolic equation, Eq. (3.17)

$$d = 2\left(\sqrt{\frac{P_{CR}}{\pi\sigma_y} + \frac{\sigma_y L^2}{C\pi^2 E}}\right)$$

$$d = 2\left[\sqrt{\frac{100(10)^3}{400(10)^6\pi} + \frac{400(10)^6(0.16)^2}{1.2(\pi^2)(209)(10)^9}}\right] = 1.6 \text{ mm}$$

This however would be the minimum required diameter to sustain the defined loads and criteria for a column.

The evaluation of the loads in this region on the design was done with the use of Finite Element Analysis (FEA), using COSMOS DesignStar software. The FEA analysis was done on the assembly of columns, including the upper and lower adapter plates. This confirmed the buckling that could occur if the load was increased to 35 kN, and it showed that the support structure was to be treated as a single column, with a fixed-end and the free-end, with three DoF. Thus an outer shell tube had to be designed to fit between the upper and lower adapter plates to prevent the deflection as shown in Figure 3.17. This shell structure had also to allow air to flow through whilst rotating, to keep the actuator cool. The design calculations were for a tube in simple compression, and ignoring the holes at first, the maximum force in the z-axis was calculated to be 77 kN.

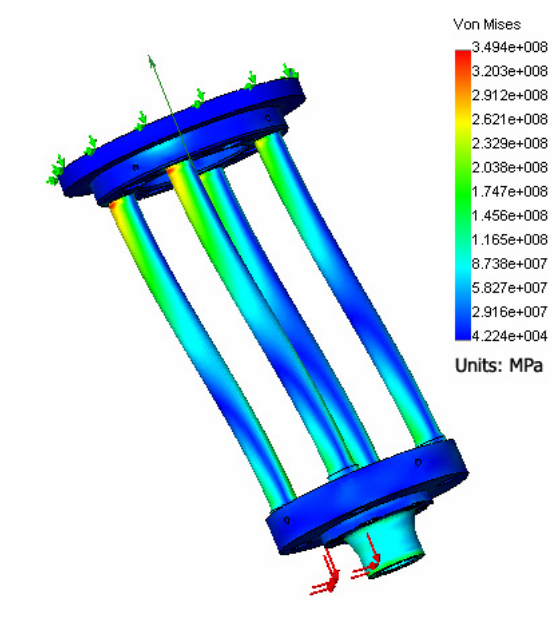

Figure 3.17: FEA study of columns in support structure.

The FEA analysis, in Figure 3.18, of the tube in compression and in bending along the y-axis was done to finalize the design. The arrangement of the holes in the tube, showed as expected to be stress raisers. The localized stress at 50 MPa did not affect the upper or lower adapter plates, this was considered acceptable for the functional requirements of the experimental tool.

Shoulder and Pin

The two final components of the welding tool, are also the most important, it is here where the welding process takes place. The shoulder and pin were designed to be modular, for two reasons; firstly to facilitate the development progress, and secondly since these components take the loads and heat cycles directly, therefore

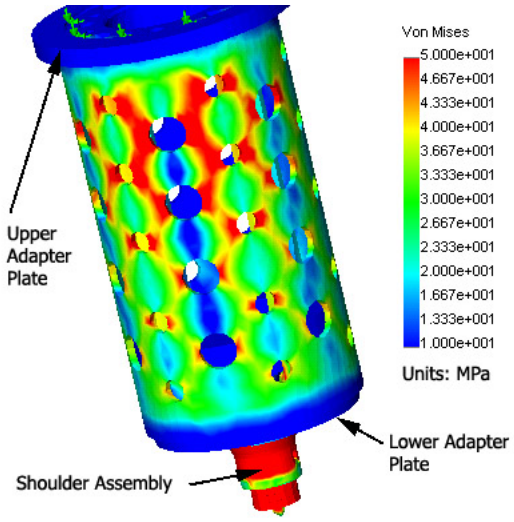

Figure 3.18: FEA study of the compressive and bending stresses in the outer tubular structure of the tool.

will be requiring replacement more often.

The profile shape of the pin was left simple as it was not known how the material would react during the welding process. However when the shaft-tools as described in Section 3.2.1 on page 45 were looked at after welding, pickup was noticed on the shoulder face and in the threaded part of the pin. As the pin would be moving during a welding cycle and having no information on the profiles from existing retractable pin tools, it was decided to pursue a safe route, where the cross-sectional profile would remain constant and circular. If the profiles, as of the existing tools were used, it would have required complex shape analysis and tolerances to prevent material from entering into the shoulder channel, in which the pin moves.

The shoulder surface, also important due its influence on the weld

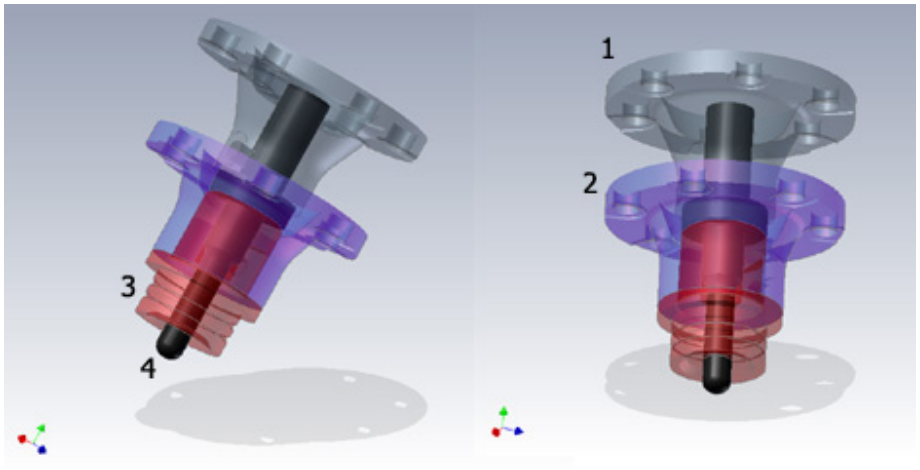

Figure 3.19: A view of the shoulder and pin assembly.

process, as the initial contact in this form of tool and it required a surface capable of generating enough heat, locally, to allow for pin penetration. The shape of the surface of the tool, had a small concave section around the pin area, to allow for hydrodynamic pressure of the material to be accommodated.

The shoulder *(3)* and pin *(4)* are mounted into flanged brackets *(1)* and *(2)* as shown in Figure 3.19, the design of these components was to allow for the loads to be directed away from the shoulder and pin into the surrounding components. The conical shape of the flanged brackets was an effective way of dissipating the load and taking care of the resultant heat build-up on the components and diverting it away to the outer tube of the support structure.

The evaluation of the loads in this region on the design was done with the use of FEA, the conditions applied were for a worst case scenario, where a load of 45 kN would be applied directly to the shoulder face, Figure 3.20 shows the effect of loaded conditions in

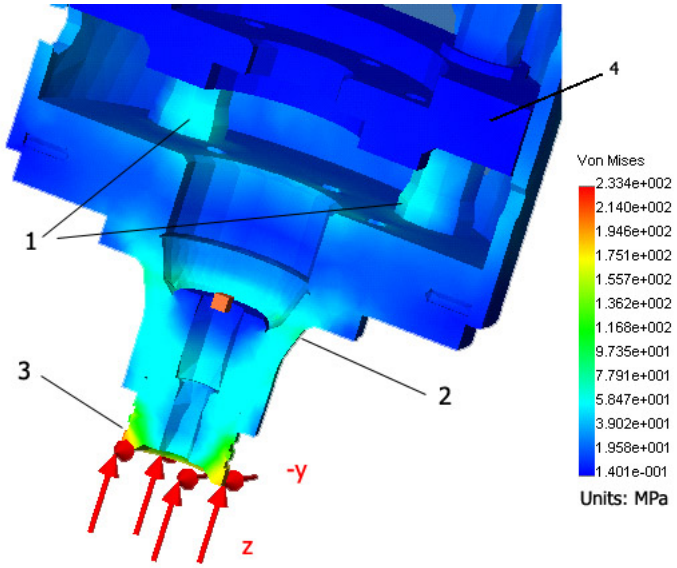

Figure 3.20: The FEA study on the shoulder and actuator support structure.

the y-axis, in the direction of the weld, and in the z-axis, as the load applied on the shoulder to generate some of the heat required for the weld.

From the Figure 3.20, the stress concentrations are shown, *(1)* shows the stress concentrated at the base of the columns, considering the the tool will be rotating the stresses, of approximately 60 MPa, at this point will be fluctuating and a possible fatigue failure area. The region at *(2)* shows the area where the stress concentrated on the shoulder flanged housing, this was approximately 60 MPa, and the region at *(3)* is where the shoulder face is in contact with the welded plate, here the stress was calculated to be approximately 200 MPa, and as it rotates this would be only concentrated at that point relative to the speed of rotation.

In Figure 3.21, the stress flow from the shoulder *(1)* to the columns

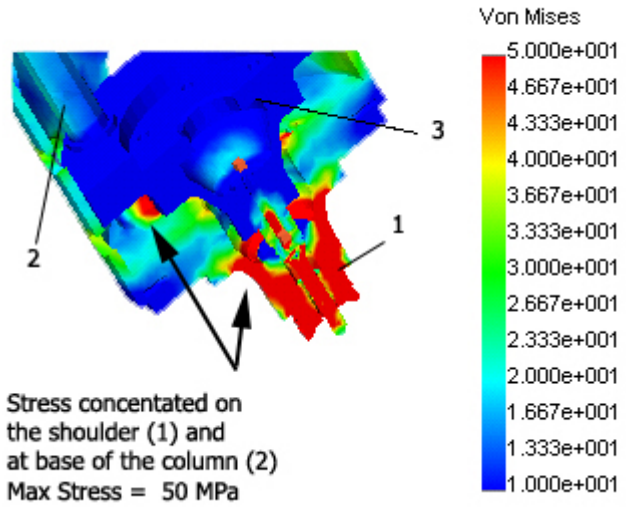

Figure 3.21: The FEA study on the assembly to see the stress flow from the shoulder to the columns.

supports *(2)*, here the stress is shown at 50 MPa, and it shows the equal distribution of stress around the pin and shoulder, with a region of lower stress between the shoulder and the column structure. The components where minimal stress was required as shown in Figures 3.20 and 3.21, *(3)* and *(4)* respectively, forming part of the actuator assembly, are not affected by the loads inflicted on the shoulder, and therefore do not hinder the actuator-pin assembly movement.

3.3 Prototype Tool

Once the tool manufacture was completed, all the components were checked to ensure that they met the design specifications, as per final drawings, which can be viewed in the Appendix A. Assembly of

the components was carried out in phases, to ensure to ensure that a working proof of concept was realized. The nature of the design, being modular also required a higher tolerance along the axial axis to prevent run out.

The rotary joint was tested initially, statically, that is not rotating and found to be working, no major leaks were encountered. After this first phase was completed, the Fluidic Muscle was tried to verify how it functioned together with the rotary joint configuration.

Final assembly of the actuator assembly, as shown in Figure 3.22 comprising of the following main components, **(1)** as the rotary joint, on the slip-ring inlets for air **(2a)** for the actuator and **(2b)** for the cooling. The upper adapter plate **(3)** forming the upper part of the support structure, had to be aligned precisely with the lower face of the rotary

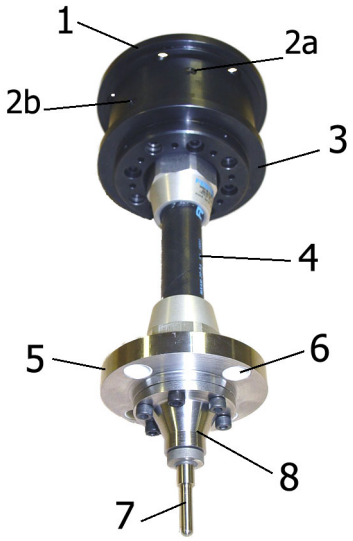

Figure 3.22: Assembly of the rotary joint, Fluidic Muscle actuator and the pin.

joint, as **(5)** had to parallel with **(3)**, to allow for the pin **(7)** to move freely in axial channel of the shoulder (not shown). The Fluidic Mus-

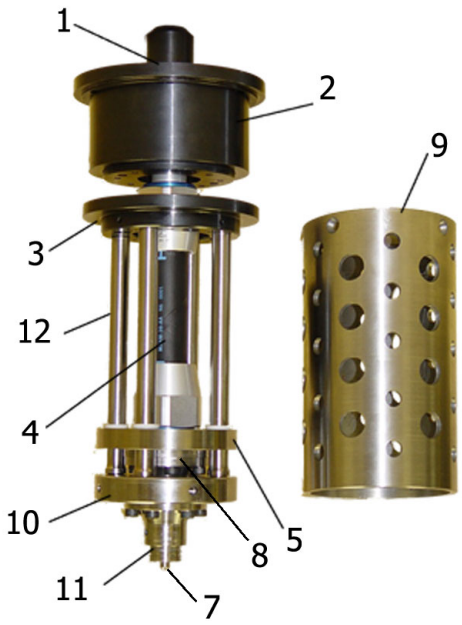

Figure 3.23: The prototype tool assembly.

cle **(4)** was attached to the rotary joint with a axial adapter (Festo) at one end, and the other end on the actuator plate **(5)**. The flanged pin bracket **(8)** is attached to the actuator plate and insulated from the Fluidic Muscle with two "Tufnol" washers (not shown). Since the insulating properties of this material are good and, the Fluidic Muscle was susceptible to failure from high temperature. The actuator plate had four rods (not shown, see Figure 3.23) through which movement was limited to one axis, as the Fluidic Muscle would fail in torsion. The "Teflon" bushes **(6)** were added to allow for a stiction free travel, and prevent metal to metal rubbing whilst in operation.

The completed assembly is shown in Figure 3.23 (where the numbering system corresponds to that of Figure 3.22), with the cover **(3)** removed from the actuator to show the details of the system. The rods **(12)** as discussed above form part of the support structure for the actuator system, and these are attached to the lower adapter plate **(10)**. The shoulder flanged bracket assembly **(11)** is also attached to the lower adapter plate and would have to take the torque applied to the shoulder during the welding process.

3.4 Summary

In this Chapter the material presented deals with the theory of design, namely axiomatic and the conceptual parametric design process and the final design calculations, to realize the prototype retractable pin tool. Furthermore the process of Friction Stir Welding in described and a survey of proposed retractable tools is discussed.

The tool once assembled was put through initial tests, these and any problems that occurred are dealt with in the next Chapter 4 Section 4.1. In Figure 3.24 the components designed for the experimental tool are shown in their relative positions.

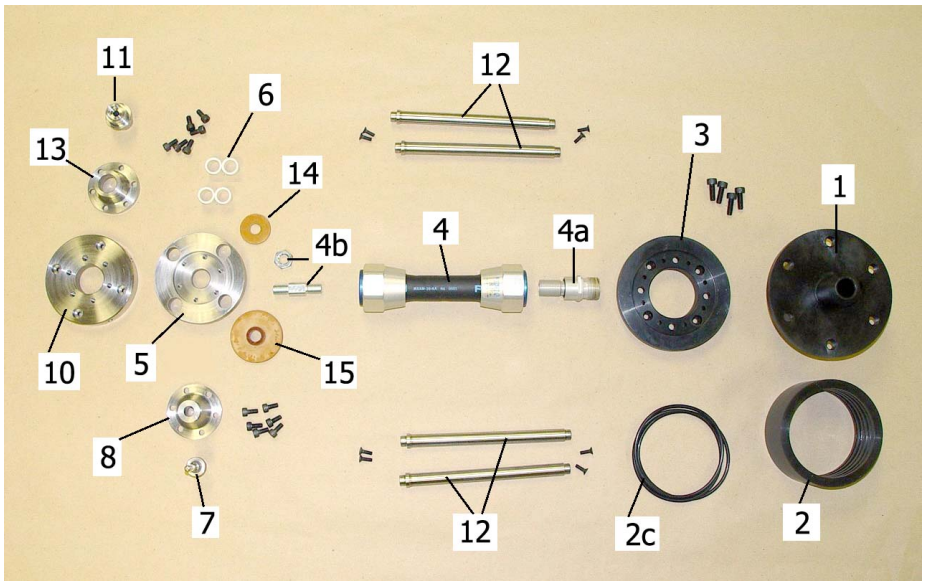

Figure 3.24: The components making up the experimental tool.

1. Rotary joint
2. Slip-ring
2c. 'O'-rings
3. Upper Adapter Plate
4. Festo Fluidic Muscle
4a. Festo Axial Adapter
4b. Festo Rod end with Nut
5. Actuator Plate
6. 'Teflon' bushes
7. Pin
8. Flanged bracket for pin
10. Lower Adapter plate
11. Shoulder
12. Rods for support structure
13. Flanged bracket for shoulder
14. Lower 'Tufnol' Washer
15. Upper 'Tufnol' Washer

4 EXPERIMENTAL METHODOLOGY

The experimental setup and procedure forms the basis of this chapter, with the tool testing and refinement forming one section. The second section deals with the preparation of the samples and preliminary tests that were done to facilitate and give a better understanding of the limitations and requirements of the experimental procedure proposed. The final section discusses the experimental procedure.

4.1 Tool Calibration

Once the tool was assembled and all the design constraints checked for their integrity, the tool was tested for proof of concept (details concerning assembly, see Appendix A). This involved a static test of the system to ensure that the tool functioned as required. The calibration of the tool was necessary to ensure that any discrepancies in the function of the tool were accounted for and recorded.

The tool calibration was carried out by first testing the rotary joint, statically, to ensure that the compressed air was not leaking from the system. Completed as shown in Figure 4.1, note the rotary joint was not rotating. After assembly, the O-rings were lubricated with

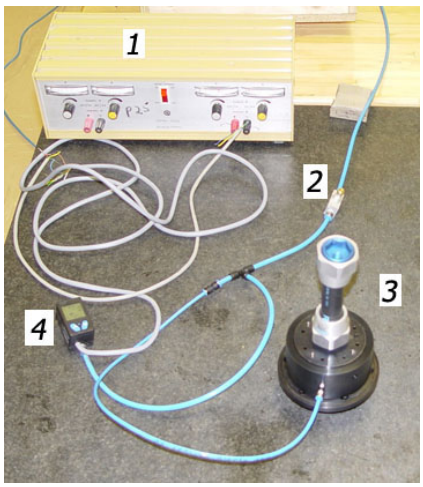

Figure 4.1: Static tool test setup, (1-Power Supply, 2-Regulator Valve, 3-Rotary Joint-Muscle Assembly, 4-Pressure Reader).

oil and then air pressure applied to the rotary joint assembly, to check that the system was not leaking. The Fluidic Muscle was then attached to the tool assembly and the movement of the pin tested. A one-way regulator **2** in Figure 4.1, was used to control the air pressure, for the initial trial of the Fluidic Muscle a pressure of approximately 2.0 bar was used. The pressure was then increased

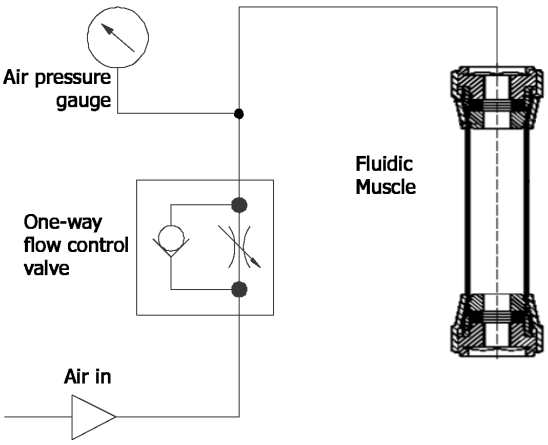

Figure 4.2: Schematic of the pneumatic layout for the tool calibration.

Figure 4.3: The tool static test with the Fluidic Muscle in operation.

gradually to a nominal value of 6.00 bar, the maximum limit as specified by the manufacturer and anticipated operating pressure. The complete assembly of the tool was then assembled together and the initial proof of concept, was done as shown in Figure 4.3.

The next step was to check the actuation system and attempt to obtain a relationship between pressure and pin movement, which would be essential to control the pin. The tool was placed on a measuring table as illustrated in Figure 4.3 (base support not shown). References from the datum surface (in this case the reference table surface) were taken to measure the pin length in an "unloaded" state, that is when the muscle is without any air pressure. As the pressure increases, the pin is retracted and with a pressure decrease, the pin extends. This was carried out to observe if any errors in the actuation positioning occurred, especially when the actuator was repositioned to a designated position.

Air was supplied in stages, ranging initially from 0.25 - 2.00 bar and increasing until 4.00 - 5.80 bar. Readings of pin displacement were recorded at specific pressures, during cycles; a cycle begins when the test starting pressure is increased till the designated pressure is reached and then the pressure is reduced until this pressure is reached again, to end the cycle.

The tool was tested initially without the Lower adapter Plate Assembly (referred to as LPA in this text), to provide reference data, and then the tests were repeated with the complete tool assembly. The reason being to establish if there was any interference between the components. This interference could then influence the actuation of the pin, especially on the shafts and with the pin in the shoulder opening, since the tolerance for both required a sliding fit.

First Test at 0.25 - 2.00 bar

The initial tests without the lower actuator plate or the shoulder, gave the resulting data as in Figure 4.4(a), which revealed a pressure/pin displacement relationship that was constant for the range 0.25 - 2.00 bar.

When the complete assembly was tested, Figure 4.4(b) shows the resulting pin movement with an offset in the pressure decrease phase. The extent of the offset for T2, at the turning point of the cycle (2.00 bar), had a displacement difference of 0.71 mm and increasing to 0.93 mm at 1.00 bar.

Comparing the difference between the values at the start of a cycle (1.00 bar), and again at the end of the same cycle (2.00 bar), shows

small variations between pin displacement values for those taken without the LPA, than the same tests undertaken with the LPA, as shown in Table 4.1.

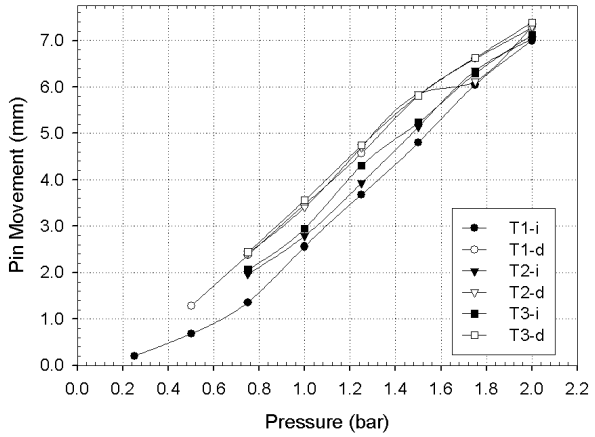

(a) Without the lower adapter plate.

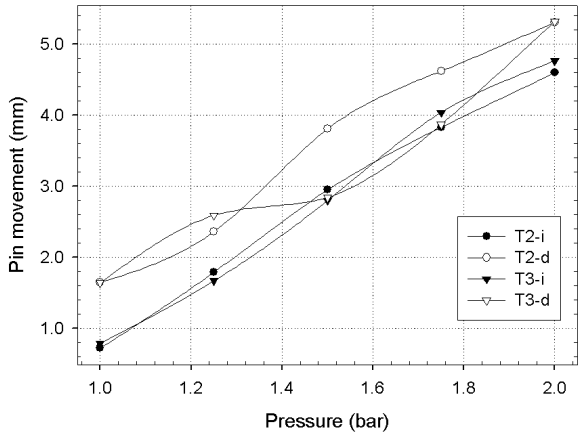

(b) With the lower adapter plate.

Figure 4.4: Pin displacement at 0.25 - 2.00 bar (T-Test, i-increasing pressure, d-decreasing pressure).

Table 4.1: Displacement difference of pin at 1.00 and 2.00 bar, without and with the LPA, (T represents test)

	With the LPA [a]			Without the LPA [a]		
Pressure	T1	T2	T3	-	T2	T3
bar	mm					
1.00	0.51	0.45	0.38	-	0.93	0.85
2.00	0.28	0.00	0.27	-	0.71	0.56

a- Lower adapter Plate Assembly

The tool was inspected to ensure that no interference existed between the components during movement. After which all the components were refitted and tightened to ensure that there was no interference or play between them.

Further tests were conducted, these were at higher pressures, again without and with the LPA. The tests were conducted in the same manner as all the previous tests.

Second Test at 2.00 - 4.00 bar

The results show that the tool without the LPA, as in Figure 4.5(a), the pin movement follows curves consistent with the relationship between the compressibility of air and the elasticity of the Fluidic Muscle as shown by Chou and Hannaford [1996]; Daerden [1999] and Lee *et al.* [2002].

In Table 4.2, a consistent data spread can be seen, when considering the difference between the values in a cycle. Any discrepancies in the data can be attributed to errors in recording the data, systematic

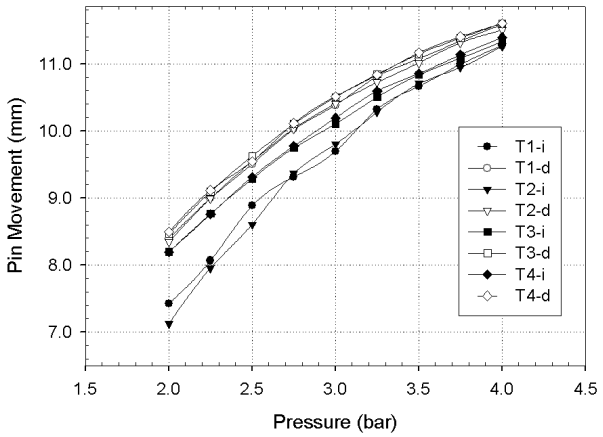

(a) Without the lower adapter plate.

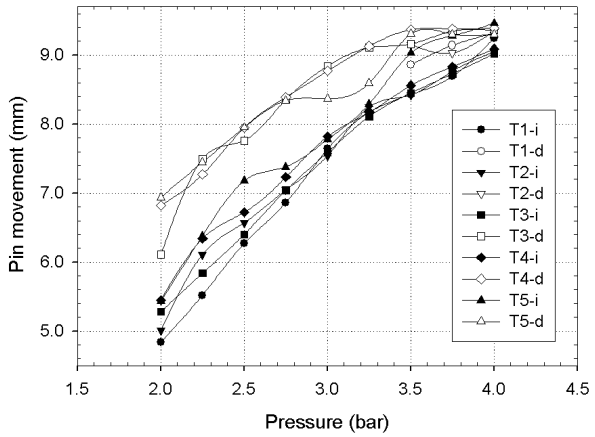

(b) With the lower adapter plate.

Figure 4.5: Pin displacement between 2.00 - 4.00 bar (T-Test, i-increasing pressure, d-decreasing pressure).

errors. The difference from the original position through the cycle gave readings that had a 0.01% change for every 0.25 bar pressure change.

Table 4.2: Percentage difference of the pin displacement during cycle 2.00-4.00-2.00 bar (without lower adapter plate), taking 2.00 bar at T()-i, as the reference datum, (T1-i represents test 1 during increasing pressure and T1-d represents decreasing pressure respectively)

Pressure	T1-i	T1-d	T2-i	T2-d	T3-i	T3-d	T4-i	T4-d
bar	%							
2.00	0.00	0.31	0.00	0.39	0.00	0.09	0.00	0.10
2.25	0.20	0.50	0.26	0.59	0.18	0.29	0.18	0.29
2.50	0.46	0.66	0.47	0.77	0.35	0.45	0.36	0.43
2.75	0.60	0.82	0.71	0.92	0.49	0.61	0.50	0.61
3.00	0.72	0.94	0.85	1.04	0.61	0.73	0.64	0.74
3.25	0.92	1.08	1.00	1.14	0.73	0.84	0.76	0.84
3.50	1.03	1.16	1.13	1.23	0.84	0.94	0.85	0.94
3.75	1.13	1.24	1.21	1.33	0.92	1.01	0.93	1.02
4.00	1.22	1.32	1.31	1.39	1.00	1.08	1.02	1.08

However, the actual pin displacement results for each cycle, as given in Table 4.3, shows that without the LPA, the pin travel remained

Table 4.3: Actual pin displacement between 2.00-4.00 bar (increasing pressure) and 4.00-2.00 bar (decreasing pressure), with the lower adapter assembly and without, (T represents test)

	Without the LPA [a]				With the LPA [a]		
Pressure	T1	T2	T3	T4	T3	T4	T5
bar	mm						
2-4	3.85	4.14	3.18	2.45	3.74	3.64	4.01
4-2	3.19	3.16	3.14	3.11	3.25	2.57	2.36

a- Lower adapter Plate Assembly

constant during the pressure decreasing phase, with T3 giving the best result.

Whereas the data in Figure 4.5(b) illustrates a similar graph to that in Figure 4.5(a), with the difference in the decreasing pressure data. When comparing this data, as a percentage difference, (Table 4.4), the increasing pressure phase of the cycles compares favorably with the data of increasing pressure, as given in the Table 4.2.

However, the decreasing pressure phases of these cycles tend to be offset between 0.4% to 0.5% at the lower pressures and between 0.2% at higher pressures. Considering the percentage difference in the decreasing pressure phase, and with the LPA in place, this difference

Table 4.4: Percentage difference of the pin displacement during cycle 2.00-4.00-2.00 bar (with lower adapter plate), taking 2.00 bar at T()-i, as the reference datum, (T1-i represents test 1 during increasing pressure and T1-d represents decreasing pressure respectively)

Pressure	T3-i	T3-d	T4-i	T4-d	T5-i	T5-d
bar	%					
2.00	0.00	0.26	0.00	0.43	0.00	0.48
2.25	0.18	0.70	0.28	0.58	0.30	0.64
2.50	0.36	0.79	0.40	0.79	0.56	0.80
2.75	0.56	0.98	0.56	0.93	0.62	0.92
3.00	0.73	1.13	0.75	1.05	0.75	0.93
3.25	0.90	1.21	0.86	1.17	0.91	1.00
3.50	1.01	1.23	0.99	1.24	1.14	1.23
3.75	1.09	1.29	1.07	1.25	1.22	1.23
4.00	1.19	1.29	1.15	1.25	1.28	1.23

is 0.1%. This implies that the actuator assembly was sticking during this phase.

Third Test at 4.00 - 5.80 bar

The tests at higher pressures, were measured using the same procedure as in previous tests. Here the results as in Figure 4.6, illustrate smaller variations in pin displacement data, due to the smaller movement of the pin.

The increasing pressure data again appears more consistent than the decreasing pressure values. Table 4.5 illustrates this pattern, slight variations in the percentage difference, of between 0.02 to 0.1% were seen.

Table 4.5: Percentage difference of the pin displacement during cycle 4.00-5.75-4.00 bar (without lower adapter plate), taking 4.00 bar at T()-i, as the reference datum, (T1-i represents test 1 during increasing pressure and T1-d represents decreasing pressure respectively)

Pressure	T1-i	T1-d	T2-i	T2-d	T3-i	T3-d
bar	%					
4.00	0.00	0.17	0.00	0.04	0.00	0.07
4.25	0.06	0.23	0.04	0.12	0.07	0.13
4.50	0.13	0.29	0.11	0.17	0.13	0.21
4.75	0.21	0.36	0.16	0.23	0.18	0.30
5.00	0.29	0.39	0.21	0.27	0.22	0.32
5.25	0.34	0.43	0.25	0.32	0.28	0.35
5.50	0.40	0.48	0.32	0.35	0.32	0.39
5.75	0.47	0.50	0.35	0.37	0.35	0.40

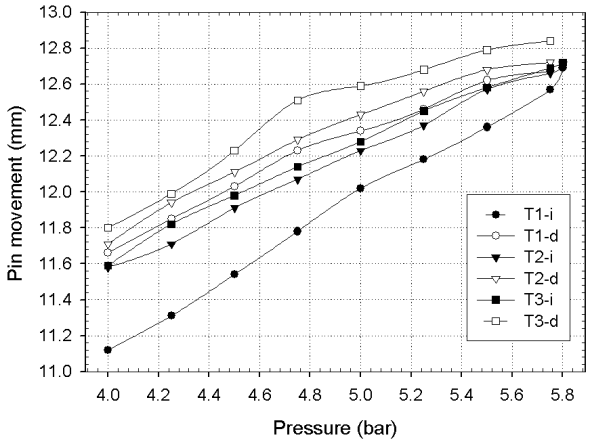

(a) Without the lower adapter plate.

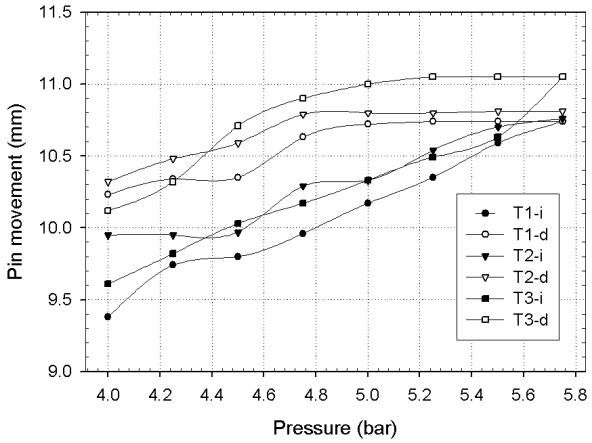

(b) With the lower adapter plate.

Figure 4.6: Pin displacement between 4.00 - 5.80 bar (T-Test, i-increasing pressure, d-decreasing pressure).

When comparing the same range of data, with the LPA in place, the data reflects a trend as seen in the previous tests, with the decreasing pressure phase having pin displacements of ≈0.0%. In Table 4.6

this is evident in the decreasing pressure phase at 5.75 to 4.75 bar, the readings change by 0.04%. When compared with Table 4.5 for the same pressure change, an average 0.13%, was observed. The possibility of stiction between the Teflon bushes in the actuator plate and the rods, together with the tolerance and alignment of the pin/shoulder assembly, was considered as a contributing factor to this phenomenon.

The actual pin displacement as given in Table 4.7, shows that the displacement is constant when the tool was tested without the LPA, compared to the 50% reduction in pin travel in the decreasing pressure phases with the addition of the LPA.

Whilst inspecting the tool to see if there was indeed any interference

Table 4.6: Percentage difference of the pin displacement during cycle 4.00-5.75-4.00 bar (with lower adapter plate), taking 4.00 bar at T()-i, as the reference datum, (T1-i represents test 1 during increasing pressure and T1-d represents decreasing pressure respectively)

Pressure	T1-i	T1-d	T2-i	T2-d	T3-i	T3-d
bar	%					
4.00	0.00	0.27	0.00	0.12	0.00	0.16
4.25	0.12	0.31	0.00	0.17	0.07	0.23
4.50	0.13	0.31	0.01	0.21	0.14	0.35
4.75	0.19	0.40	0.11	0.27	0.18	0.41
5.00	0.25	0.43	0.12	0.27	0.23	0.45
5.25	0.31	0.44	0.19	0.27	0.28	0.46
5.50	0.39	0.44	0.24	0.28	0.33	0.46
5.75	0.44	0.44	0.26	0.28	0.46	0.46

Table 4.7: Actual pin displacement between 4.00-5.75 bar (increasing pressure) and 5.75-4.00 bar (decreasing pressure), with the lower adapter assembly and without, (T represents test)

	Without the LPA [a]			With the LPA [a]		
Pressure	T1	T2	T3	T1	T2	T3
bar	mm					
4-5.75	1.45	1.08	1.10	1.36	0.81	0.44
5.75-4	1.01	1.01	1.04	0.51	0.49	0.38

a- Lower adapter Plate Assembly

on the pin movement, it was noticed that the actuator plate was not properly aligned. The misalignment caused the actuator plate to stick occasionally and this would partially account for the flattening of the curves during decreasing pressure phases.

By considering the principal of a pneumatic muscle actuator, when the system pressure is increased the resultant action is expansion

Table 4.8: Percentage difference of the pin displacement during cycle 2.00-5.80-2.00 bar, taking 2.00 bar at T()-i, as the reference datum, (T1-i represents test 1 during increasing pressure and T1-d represents decreasing pressure respectively)

Pressure	T1-i	T1-d	T2-i	T2-d	T3-i	T3-d
bar	%					
2.00	0.00	0.35	0.00	0.08	0.00	0.12
3.00	0.83	1.07	0.63	0.79	0.62	0.84
4.00	1.22	1.45	1.00	1.16	1.06	1.16
5.00	1.53	1.67	1.28	1.40	1.33	1.45
5.75	1.75	1.75	1.45	1.47	1.50	1.52

of the muscle body, which then pulls the end pieces together. The system therefore is in a state of tension and with potential energy. When the air pressure is decreased, the muscle body then relaxes. This relaxation causes the end pieces to move apart from each other, converting the potential energy to kinetic energy.

Thus a portion of the movement to return to an equilibrium state is the releasing of the tensile stress in the muscle body and the rest due to the pressure equalizing as the pressure drops. The instant the load pressure drops the pin will momentarily come to a halt or slow down, as the pressure difference equalizes. This in principle would also be a contributing factor to the difference recorded in the increasing and decreasing pressure results.

Final test at 2.00 - 5.80 bar

Together with the continuous sticking of the pin during pressure decrease phases, it was decided to inspect the tool to see if this could be improved. The alignment of the rods to the lower adapter plate were checked to ensure that they were perpendicular to the actuator plate. After having found the alignment to be out by +0.3 mm on one of the locating holes for the rods in the lower adapter plate. The Pitch Circular Diameter (PCD) on the lower adapter plate was checked and the hole in question was then modified to align it with the upper adapter plate PCD. This was not an ideal solution, but was deemed appropriate due to a lack of time. A possible reason for this was due to a manufacturing error in the tolerance due to two different workshops manufacturing the upper adapter and lower adapter plates respectively.

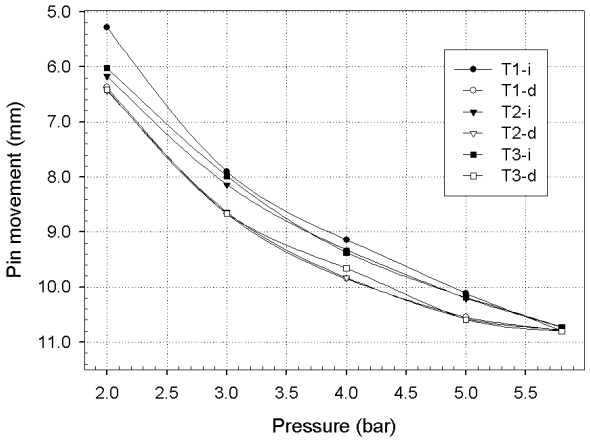

Figure 4.7: Pin displacement between 2.00 - 5.80 bar with the lower adapter plate, (T-Trail, i-increasing pressure, d-decreasing pressure).

Table 4.9: Actual pin displacement between 4.00-5.75 bar (increasing pressure) and 5.75-4.00 bar (decreasing pressure), with the lower adapter assembly, (T represents test)

	With the LPA [a]					
Pressure	T1-i	T2-i	T3-i	T1-d	T2-d	T3-d
bar	mm					
2-3	2.62	1.97	1.96	2.30	2.21	2.25
3-4	1.24	1.18	1.39	1.18	1.19	1.00
4-5	0.98	0.88	0.82	0.74	0.75	0.93
5-5.8	0.67	0.53	0.54	0.20	0.20	0.21
2-5.8	5.51	4.56	4.71	4.42	4.35	4.39

a- Lower adapter Plate Assembly

After which, a test was completed in same manner as the previous tests and the recorded data is illustrated in Figure 4.7 with the

corresponding pin displacement percentage difference in Table 4.8. Here again the data shows that the repeatability was consistent, especially comparing cycles T2 and T3.

By comparing the actual pin travel in Table 4.9, the data follows a regular pattern, however there remains a difference between the increasing and decreasing pressure phases, this could be due to the actuation system, and the property of compressed air. The tool once calibrated was prepared for installation on the host machine.

4.2 Experimental Setup

The experimental setup was divided into two parts, the preparation of the test workpieces and the host FSW machine. In order to gain

Table 4.10: Chemical compositions of aluminum alloys 2014-T3 and 5083-H321

2024-T3					
Comp.	%Wt.	Comp.	%Wt.	Comp.	%Wt.
Al	93.5	Fe	Max 0.5	Si	Max 0.5
Cr	Max 0.1	Mg	1.2-1.8	Ti	Max 0.15
Cu	3.8-4.9	Mn	0.3-0.9	Zn	Max 0.25
5038-H321					
Comp.	%Wt.	Comp.	%Wt.	Comp.	%Wt.
Al	94.8	Fe	Max 0.4	Si	Max 0.4
Cr	0.05-0.25	Mg	4-4.9	Ti	Max 0.15
Cu	Max 0.1	Mn	0.4-1	Zn	Max 0.25

Ref: ASM Metals Reference Book

an understanding of the effects that a retractable pin has in a FSW weld, sample welds were done. The workpieces were embedded with either, tracers for material flow and thermocouples for thermal flow purposes.

4.2.1 Material Preparation

The material chosen for the sample welds was Al2024-T3 and Al5083-H321, 6.1 mm thick aluminum plates, their material properties are as Table 4.10. For all the welds only plates of the same material were used. All the plates were machined along the abutted face to give a straight edge and ensure that these faces were aligned without any gaps.

Material Flow Preparation

The plates were prepared with tracers of copper rod with a diameter of 1.7 mm and 10 mm deep, in an Al5083 plate for the material flow visualization as illustrated in Figure 4.8. The tracers were placed in three different positions, similar to that of Reynolds and Siedel [2001]; Dunn [2002]. As shown in Figure 4.8, the holes were drilled into the advancing side plate. A sample weld was made using a standard fixed pin FSW tool with Al5083-H321 plate, to study the flow patterns as the tool was retracted. The samples were then cut into blocks measuring 26 mm long by 12 mm wide, then encased in a standard polymeric base. After polishing, they were etched with an Na OH + H_2O solution before being digitally photographed using a Olympus PMG-3 Microscope with a CCD camera, at 50x

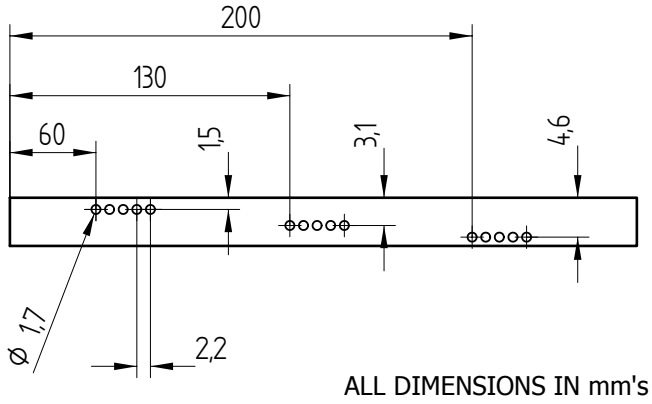

Figure 4.8: Schematic of tracer position in aluminum plate.

magnification and captured on Leica Material workstation software. These results are shown in detail in Chapter 5.

The tool was plunged at approximately 40 mm before the marker location and moved to approximately the center of the marker before being lifted out. This would effectively make a separate weld for each marker location, and ensure no residual marker tracer was being deposited into another sample area. As this would make it difficult to know the origin of the marker material and therefore making analysis impossible.

Thermal Flow Preparation

A similar procedure as used by Khandhar *et al.* [2003]; Lambrakos *et al.* [2003] to prepare the aluminum alloy plates for thermocouples was employed. The plates, 400 mm long and 120 mm wide and 6.1 mm thick were divided into three sections and a pattern of holes of diameter 2.0 mm, as shown in Figure 4.9 were drilled. The plates

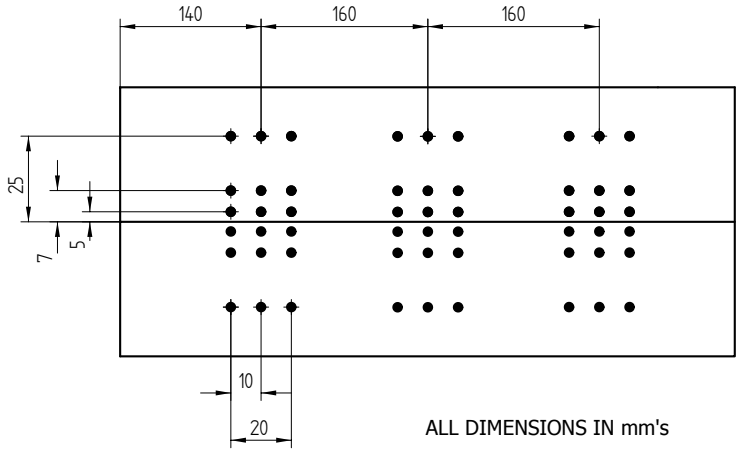

Figure 4.9: Schematic layout of thermocouples.

were squared off along their abutted faces to ensure a good alignment.

The holes were drilled from the bottom surface and at different depths of 3 and 5 mm, with those of 5 mm being closer to the welding surface. The holes were set, as Figure 4.9, with the different depths in the pattern shown in matrix form for clarity;

$$\mathbf{L_{i,j}} = \begin{bmatrix} x_{11} & x_{12} & x_{13} \\ x_{21} & x_{22} & x_{23} \\ x_{31} & x_{32} & x_{33} \end{bmatrix} \qquad \mathbf{R_{i,j}} = \begin{bmatrix} y_{11} & y_{12} & y_{13} \\ y_{21} & y_{22} & y_{23} \\ y_{31} & y_{32} & y_{33} \end{bmatrix}$$

The columns L=[x_{13} x_{23} x_{33}] and R=[y_{11} y_{21} y_{31}] representing the center of the weld, columns L=[x_{11} x_{21} x_{31}]and R=[y_{13} y_{23} y_{33}] the furthest from the weld center. Therefore the resulting matrices are, where zero represents no drilled hole;

$$\mathbf{L_1} = \begin{bmatrix} 5 & 3 & 5 \\ 3 & 3 & 5 \\ 0 & 5 & 3 \end{bmatrix} \qquad \mathbf{R_1} = \begin{bmatrix} 5 & 3 & 5 \\ 3 & 5 & 3 \\ 3 & 5 & 0 \end{bmatrix}$$

$$\mathbf{L_2} = \begin{bmatrix} 3 & 5 & 3 \\ 5 & 5 & 3 \\ 0 & 3 & 5 \end{bmatrix} \qquad \mathbf{R_2} = \begin{bmatrix} 3 & 5 & 5 \\ 5 & 3 & 5 \\ 5 & 3 & 0 \end{bmatrix}$$

$$\mathbf{L_3} = \begin{bmatrix} 5 & 3 & 5 \\ 3 & 3 & 3 \\ 0 & 3 & 5 \end{bmatrix} \qquad \mathbf{R_3} = \begin{bmatrix} 3 & 5 & 3 \\ 5 & 3 & 5 \\ 5 & 3 & 0 \end{bmatrix}$$

Thermocouples of, 36 Gauge (diameter of 0.25 mm), type K , fiber-glass coated, were first calibrated and then embedded at the different locations and depths. The temperatures were recorded with a data acquisition PCI-730 PnP Analogue board, with a sampling rate between 0.4 and 1.0 s.

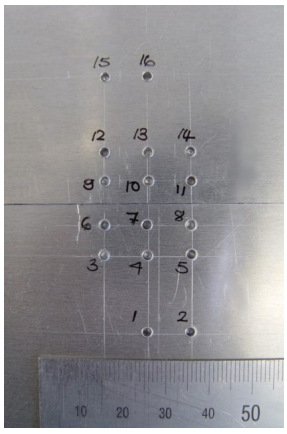

Figure 4.10: Thermocouple placement example on the bottom of an aluminum alloy plate.

4.2.2 Tool Setup

Prior to setting up the tool on the host machine, the tool was tested to ensure it was running concentrically about its axial axis. As the tool

was assembled from various interlocking components, this alignment would be crucial to prevent the tool from having a eccentric motion at the pin.

The tool was setup in a lathe, and squared up with the upper surface of the rotary joint as shown in Figure 4.11. The axial offset was, initially found to be 0.15 mm at the upper adapter plate and 0.4 mm on the shoulder, by adjusting the tool, 0.25 mm was measured at the shoulder . No change was measured at the upper adapter plate. The tool was then fitted to the FSW host machine. The test was repeated on the host machine and measuring only the shoulder. A difference of 0.8 mm was measured compared to the tests on the lathe. This measured result lead to the assumption that the host machine possibly had a misaligned spindle. This was not pursued further as it would have required a machine overhaul.

The FSW machine used for the FSW welding tests was a refurbished milling machine. By inserting the rotary joint into an existing modified spindle, the experimental tool was fitted to the host machine. The need to secure the slip ring was accomplished by making modi-

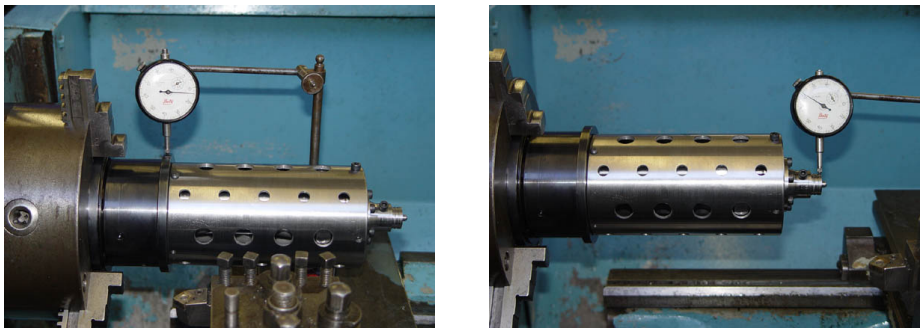

(a) Checking the tool upper. (b) Checking the tool lower.

Figure 4.11: Checking tool for eccentricity.

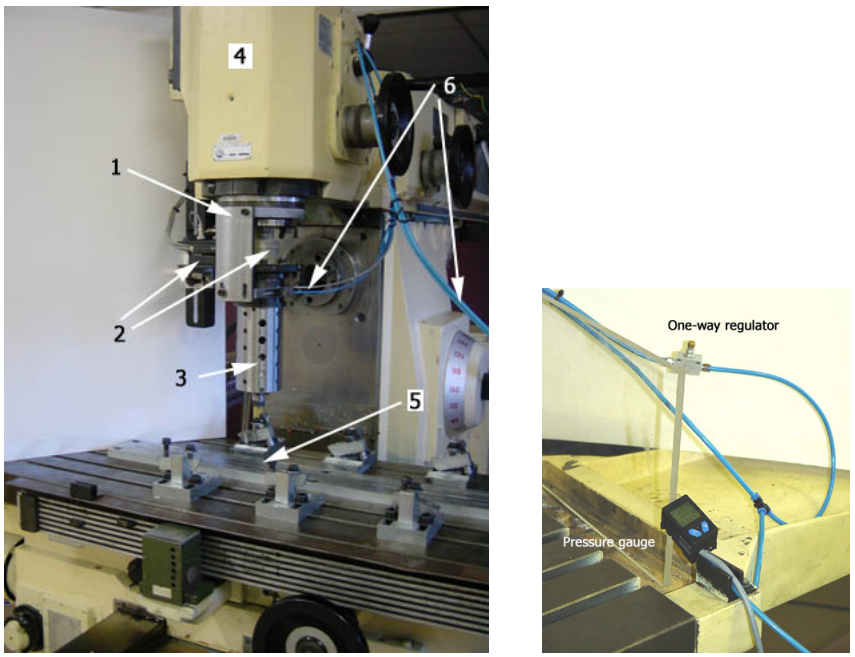

(a) Tool setup (1-Mounting bracket, 2-Data acquisition, 3-Experimental tool, 4-Host machine, 5-Backing plate, 6-Pneumatic lines).

(b) The pneumatics control and pressure gauge for the tool setup.

Figure 4.12: Tool setup on host machine.

fications to the machine and designing a bracket to keep the slip ring from rotating. The Figure 4.12 illustrates the setup used for the FSW sample welds.

The data acquisition system was included on the spindle head. The system was limited in its data recording capabilities, by not allowing for extra recording channels to be added. This proved unfortunate as the required displacement sensor to measure the position of the pin accurately could not be used.

As the control of pneumatic muscle actuators, tends to be nonlinear [Carbonell *et al.*, 2001], the implementation of pin control was

considered necessary. This however, was not pursued due to other commitments by the software developer for the FSW machine. Thus the control of the pin was done manually by using a one-way regulator, as used in the calibration tests. A schematic of the pneumatic setup is shown in Figure 4.13.

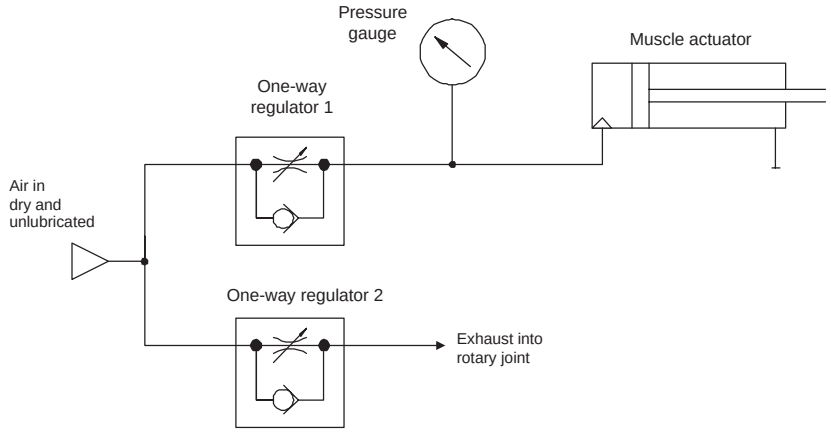

Figure 4.13: Schematic of the experimental pneumatic control setup.

4.3 Experimental Procedure

As previously stated the goals of this research, was to investigate the actions of a retractable pin on the material in a FSW weld. Once the setup was completed, the limitations of both the tool and the experimental environment were assessed. The following procedures were decided upon, the welds were divided into two types, static and dynamic.

Static welds were to test the workings of the tool, especially the pin movement. A limitation of the research was to investigate the pin action in the retraction phase of a weld. Thus in a static weld the pin would be retracted from its extended position in the weld and

no transverse motion of the tool along the weld face was carried out. Weld samples would be for both material and thermal flow respectively.

The dynamic welds were to be carried out, in the same manner as the static welds, with the difference being that the tool would be transversed along the weld face before retracting the pin. The pin was to be retracted when the tool was in a stationary position or whilst the tool was transversed back along the weld. The tool would be transversed manually along the weld, as there was no control from the host machine. Weld samples would be for both material and thermal flow respectively.

The experimental parameters, results and problems encountered in the welding trails are left for discussion in the Chapter 5.

5 EXPERIMENTAL RESULTS

The chapter begins with the visual study of the material during pin retraction in a standard FSW weld, similar to work done by Colligan [1999]; Reynolds and Siedel [2001], with the exception of concentrating on the flow in the *keyhole* area of a FSW weld. This is followed by the initial tests of the experimental retractable pin tool, using thermal techniques, and detailing the problems encountered.

5.1 Material Flow around a Keyhole

The effects on the material during pin retraction are complex and an investigation was conducted to verify and test certain techniques of flow visualization.

The main purpose was to see the effects a pin has on the flow of material during retraction. As this would give a better understanding to the flow patterns the around a pin. However the shoulder would be moving away from the surface, therefore would not present an ideal situation, and its effects would not be truly measured.

The material was prepared as in Chapter 4, where the copper was embedded into an Al5083-H321 aluminum alloy plate. The markers were placed in the same positions as shown in Figure 4.8. Then the

plate was securely fixed to the backing plate on the FSW machine. A standard tool was used, and plunged about 40 mm from the center of the embedded markers. Then transversed at a speed of 80 mm per minute, with the tool rotating at 500 rpm and at angle of zero degrees, toward the markers. Upon reaching the center position of the markers, the tool was extracted whilst still rotating. The samples were processed as discussed in Section 4.2.1 for digital imaging and then a photo montage as shown in Figure 5.1 was completed.

In Figures 5.2(a) and 5.2(b), details of the material flow in the region of the shoulder are shown, where (**C**) indicates the infused copper marker in both figures. In both Figures 5.2(a) and 5.2(b) the numbers (**1**) and (**2**), represent the material deposited under the shoulder and the material dislocated and driven upwards by the action of heat from the pin, respectively.

The material movement can be seen, denoted by (**2**) in the Figure 5.2(b), where copper forms a boundary between the regions (**1**) and (**2**). In Figure 5.2(b), the region (**4**) shows the start of the

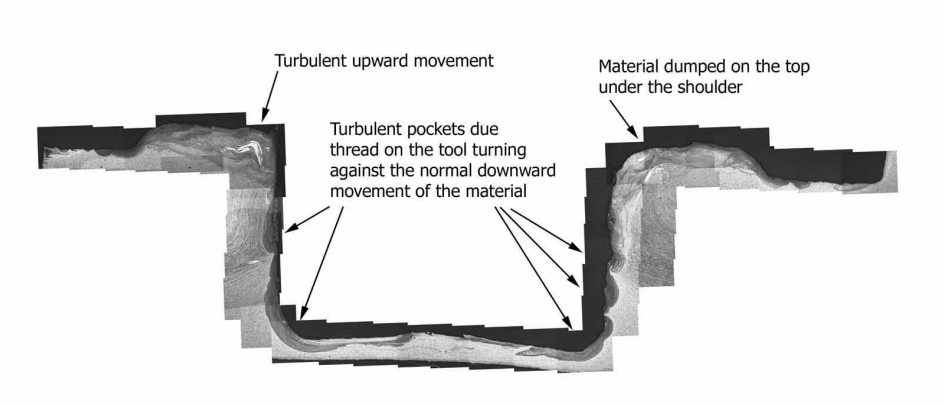

Figure 5.1: Detail material flow in a keyhole cross section.

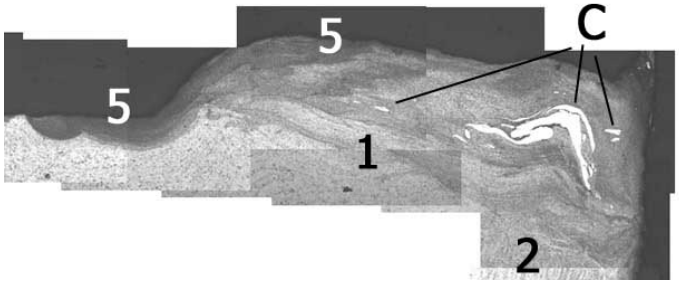

(a) Advancing side shoulder detail.

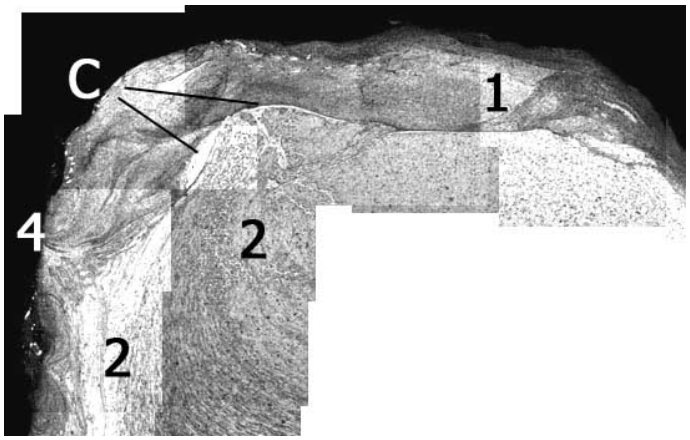

(b) Retreating side shoulder detail.

Figure 5.2: Detail of material around the shoulder, (Marker positioned in the center of the Al5083-H321 plate.

interface action between the pin and the shoulder into the regions (**1**) and (**2**). The areas denoted by (**5**) in Figure 5.2(a), represents the effect of the shoulder edges on the material during welding. Where the darker shade represents a larger percentage of copper infused into the aluminum.

In Figure 5.3, copper is deposited on the upper surface, here the marker position was in the upper part of an Al5083-H321 plate. This action is contrary to the norm as stated and shown by Colligan [1999]; Reynolds and Siedel [2001] in their work. It was noticed

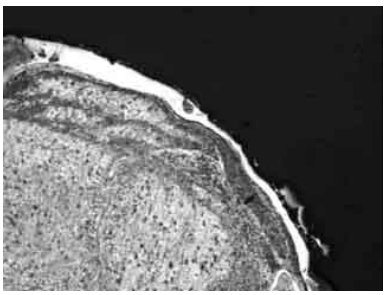

Figure 5.3: Copper deposited on the shoulder surface.

that the threaded pin was rotating opposite to the thread lead angle and therefore would explain the material being driven upward. It should be noted that the tool was the standard, as used by the Port Elizabeth Technikon.

The turbulent and complex mixing that occurs in a FSW weld is clearly shown in the following Figures 5.4 and 5.5. The copper tracer, in white, resembles the turbulence as discussed in Chapter 2, on page 14, which consists of vortex-like, non-linear fluid dynamic flow [Murr *et al.*, 1998]. The Figures 5.4 illustrate this chaotic mixing, at a profile interface on the shoulder face.

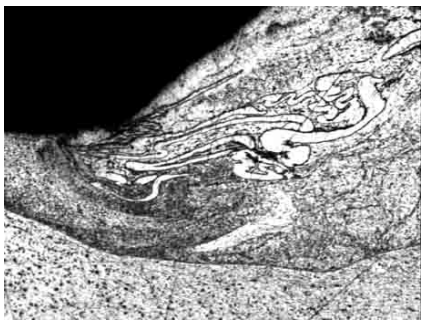

(a) Copper flow on the advancing side.

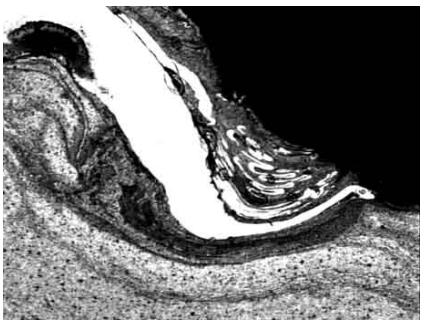

(b) Copper flow on retreating side.

Figure 5.4: Detail of turbulent material flow around the shoulder, (Marker positioned in the center of the 5083-H321 plate.

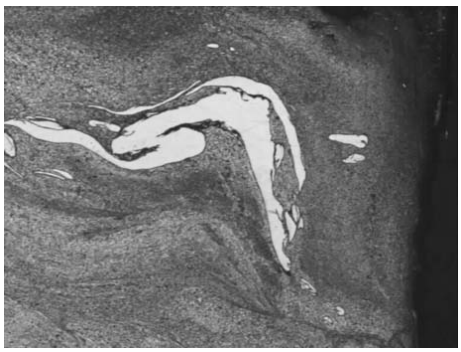

Figure 5.5: Detail of material flow of copper marker in shoulder region with reference to Figure 5.2(a).

The threaded profile of the pin, shows similar vortex-like chaotic turbulence, as in the Figures 5.6, where (**C**) denotes the copper tracer, amidst the dislocation of the material (**2**) around them. This area close to the pin shows a shear flow, and deformation of the material due to the action of the pin. In this case in an upward direction due to the reverse action of the pin profile. The area around the pin shows up as a darker shade, due to the copper infused into the aluminum.

A closer look at these dark areas reveals the effects of the pin threads on the material, as in Figure 5.6(b) the traces of copper shows flow patterns as a result of this action. These are also bear a resemblance to the turbulent patterns in Figures 5.4 , 5.5 and 5.7, therefore the threads can seen to be vortex generators [Shindo *et al.*, 2002].

As the dark area around the pin illustrates, in Figure 5.1 and in more detail in Figures 5.6, that the flow near the pin, for this type of tool, is not uniform around the pin as shown by Reynolds and Siedel [2001]; Dunn [2002]; Guerra *et al.* [2003]. This turbulence around the pin and the transverse motion of the tool may have a part in the

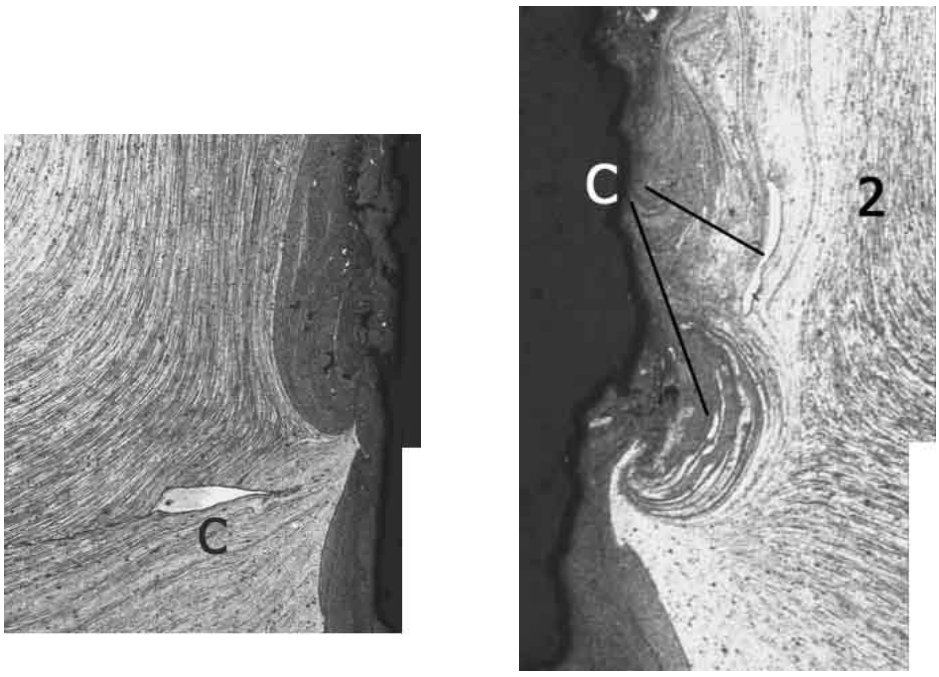

(a) Advancing side. (b) Retreating side.

Figure 5.6: Detail of material flow around the pin and the deformation of the material, (Marker positioned in the center of the 5083-H321 plate).

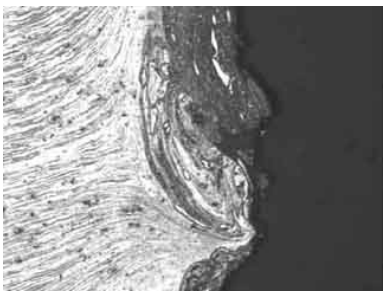

Figure 5.7: Detail of pin profile induced turbulence, (Marker positioned in the center of the 5083-H321 plate).

formation of the so-called "onion-rings" pattern in the weld.

The flow patterns revealed that the mixing in a FSW weld can be chaotic and non-linear in nature around the pin. The pin's influence and shape plays an important role in both the structure of material

flow and as a fundamental parameter of a FSW weld.

5.2 Preliminary Trial welds

The aim of the trial welds were to ensure that the tool functioned as designed. A trial run of the experimental weld tool was carried out, initial tests were concerned with the concept verification.

Tests with only static runs, as discussed in Chapter 4, proved successful, here the tool and actuation performed as anticipated. After assembling the tool onto the host machine, a check of the rotary joint function was carried out, to ensure that air would be delivered to the actuator, this proved successful.

Test procedure

The tests were all conducted in the same manner, with the tool controlled manually. The pressure was set manually and adjusted as necessary but this proved difficult to control. Before each run the thermocouples were calibrated, by inserting them in controlled conditions, such as iced water (4°C) and boiling water (100°C). Upon insertion into the plates they were again calibrated and recorded, to allow for correcting of the test data.

Thermal measurement in FSW is usually difficult to achieve repeatable accuracy of the data, as Colegrove and Shercliff [2003] states the various problems that may affect the measurement are due to electrical noise, the rubbing of the thermocouple against the tool, imprecise thermocouple positioning, thermal gradients and thermal

Table 5.1: Parameters used in the preliminary trail weld tests

No.	Speed	Air Pressure	Tool Angle
	rpm	bar	°
1	300	3.70	0
2	300	2.00	0
3	300	2.00	0

lag.

This delay in response has been studied in the fluid medium, however solid-embedded thermocouples require different analysis techniques as described by Rabin and Rittel [1999, 2000] and these were considered when performing the thermal work and during the analysis of the data. The deviation from the surrounding bulk temperature is 36.8% for the first time constant (a value of e^{-1}) and 13.5% and 5% after two and three time constants, respectively. Previous experiments have shown a standard deviation of approximately 10°C per time unit.

Each test consisted of plunging into the material surface, having a dwell period of 12 seconds and if a static weld, at this point the pressure was increased in the actuator to retract the pin, otherwise the tool was transversed for a distance of 15-20 mm before the pressure was increased. After this the tool was extracted from the material surface.

5.2.1 Static welds

Two Al2024-T3 plates were prepared to accommodate three sets of 16 thermocouples, type K, which were embedded through the

back end of the plates. These were at random depths to reduce the permutations required to analyze the thermal effects throughout the material thickness during welding, see Chapter 4, Section 4.2.1 for details on the layout and preparation.

Trail 1

The first static weld, was completed, and the resulting weld (Figure 5.8). The tool speed was set to 300 rpm, and manually plunged till the temperature on the centrally placed thermocouples rose to +400 °C, at this point the air pressure was at ≈3.70 bar. The temperature remained constant and then began to drop, at which point more load was applied, that is, the plunge depth was increased, till the temperature stabilized again. At this point the pressure in the pin actuator was reduced to allow the pin to extend into the weld. However after a period of 10 seconds, no change in temperature was noticed and the pressure increased to 5.00 bar, to simulate pin retraction. Thereafter the tool was extracted from the plate.

Figure 5.9 compares the a cross section through the welds from

Figure 5.8: First Static weld.

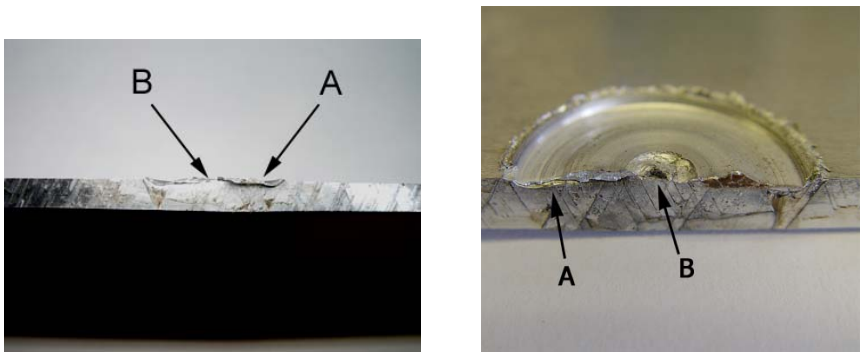

(a) Test 1, Advancing side. (b) Test 1, Retreating side.

Figure 5.9: Detail views of the welds, comparing the the advancing and retreating side of the first weld.

the first static test. In Figure 5.9(a) and 5.9(b), the following was observed, at (**A**), minimal influence of the shoulder can be seen, and where (**B**) represents the pin indentation or the remnants of the capillary action.

As Figure 5.8 illustrates, the pin did not penetrate the material. The pin having been pushed up into the shoulder opening, and becoming stuck in place. It was assumed that the pin was pushed up into place as the heated material was forced into the opening on the shoulder surface, by the action of plunging a second time. Another possibility was that the heated aluminum formed in the shoulder opening by capillary action and thus preventing the pin from extending.

After the test, the tool was stripped to check for problems with the components, it was noticed indeed that aluminum had formed a column in the shoulder opening for the pin. Including the problems encountered with the pin, no data was recorded from the host machine nor from the thermocouples, due to a software crash on the host machine.

Trial 2

A further test was conducted, and ensuring that the thermal data would be recorded. The test was to proceed in the same manner as the previous test. The parameters were left unchanged, except for

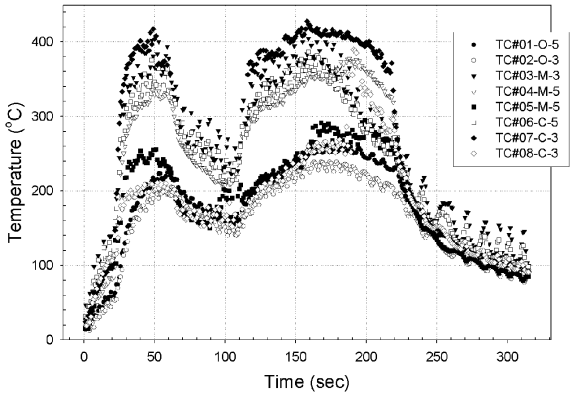

(a) Advancing side.

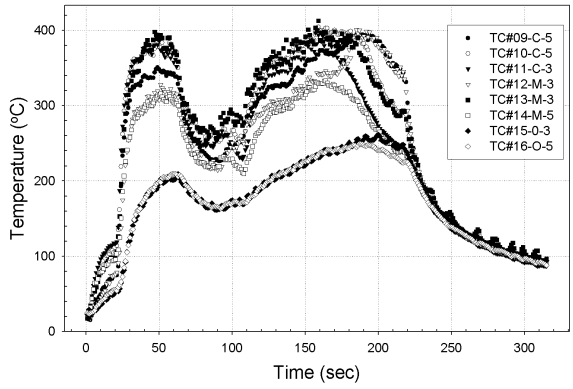

(b) Retreating side.

Figure 5.10: Thermocouple data of trial test 2, the initial plunge is shown and the following transverse motion of the tool. (Thermocouple pattern L_1-R_1)

the pressure was reduced to 2.00 bar at the initial starting point. This would ensure that more of the pin protruded from the shoulder surface. The tool was plunged manually until the temperature recorded rose to ≈420°C. After allowing for a 10 second dwell time, it was noticed as in the test prior to this, that the temperature started to drop, at a rate of ≈4.2°C s^{-1}. This could be attributed to the shoulder frictional heat generation becoming saturated, and thus the value of μ=0, would result in no further heat being generated. The tool was manually plunged deeper into the material, until a temperature of 420° was attained. After which the tool was transversed for 20 mm.

If one considers the relationship,

$$q_i = 2\pi\mu F_z R_i N \tag{5.1}$$

Where q_i is the heat flux, W/m^2 and μ the coefficient of friction, F_z the normal force, R_i is the distance from the calculated point to the rotating axis of the tool, and N is the rotational speed. Then it could be shown that μ tends to zero and the influence of the rotational speed would not increase the heat input from the shoulder. Then an increase in the F_z would in turn change the μ and therefore produce more heat until equilibrium was attained. This presumption for the rate of temperature decreasing as shown in Figure 5.10 was used, however this calculation has been left for future work since not all the data is available.

The thermal data (Figure 5.10), this has been summarized in Table 5.2, showing the peak temperatures of the advancing side and the corresponding retreating side at 49 seconds. Which represents the first peak of the test, the second at time 158 seconds shows a

Table 5.2: Temperature peaks of second test weld at certain time intervals, comparing advancing and retreating sides

Side	Time	Outer	Middle	Center
	sec		°C	
Advancing	49	201	336	417
Retreating	49	198	378	389
Advancing	158	231	352	428
Retreating	158	233	400	403

temperature of 428°C on the advancing and 403°C on the retreating side. Taking into consideration the response time and the difference in the position of the thermocouples resulted in this difference between the temperature.

The data from the outer thermocouple points show a lag of 12 seconds before reaching their peak temperature on the advancing side, however the outer points TC15 and TC16 on the retreating side lag by a further 10 seconds with respect to the advancing side.

The action of the pin in the second test, were again similar to the first with the pin being stuck in the retracted position after plunging into the material and in the case of the second with the tool transversing along the surface. This is clearly shown in the Figure 5.11, with the pneumatic muscle actuator being deformed due to the pin being pressed into the shoulder opening.

A column of semi-molten material was extracted from the opening. No mechanical problems with the tool were encountered, apart from the bolts near the heat source, becoming difficult to loosen, therefore

Figure 5.11: Tool after static weld test.

heat resistant copper-slip was applied, to allow for easier removal. This also applied to the inside upper section of the shoulder opening, to prevent the pin becoming stuck due to heat.

The plan view in Figure 5.13 shows the effect of the shoulder on the material from a different perspective. Here the twisting of the material as described in tests by Colligan [1999] is clearly seen,

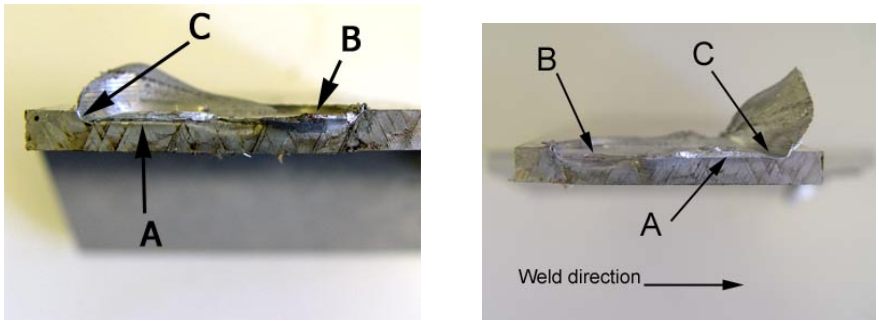

(a) Test 2, Retreating side. (b) Test 2, Advancing side.

Figure 5.12: Sectional views of the test 2.

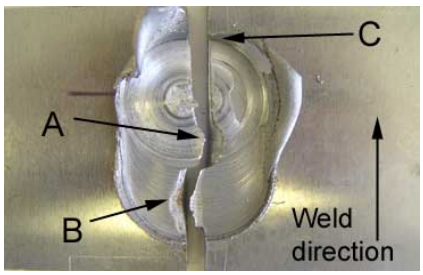

Figure 5.13: Plan view of the test 2.

refer to Figure 2.3 and 2.4 in Chapter 2, however the heat input is marginal and only surface deformation occurs. The results from the second weld test in cross-section (Figure 5.12) and in plan view (Figure 5.13), shows patterns in the weld that represent little heat generation. Here **A** represents the effect of the shoulder on the material, which can be seen to be very slight, more of a plating effect. At **B** this similar effect of surface deformation is noticeable. **C** shows that the material had reached a temperature of solidus (±420°C) and formed a fan-like wave of material due the shoulder gouging in the material, due to a tool angle of 0°.

Trial 3

On the final test, a pilot hole was drilled to allow the pin to remain extended, during plunging. The parameters remained as in the previous weld, with the pressure in the actuator at 2.00 bar, resulting in the pin being extended. The tool was held in place for a period of 10 seconds before manually transversing it along the weld line for ≈10 mm. No machine data was recorded due to the recurring software problem on the host machine, and thermal data was also not recorded.

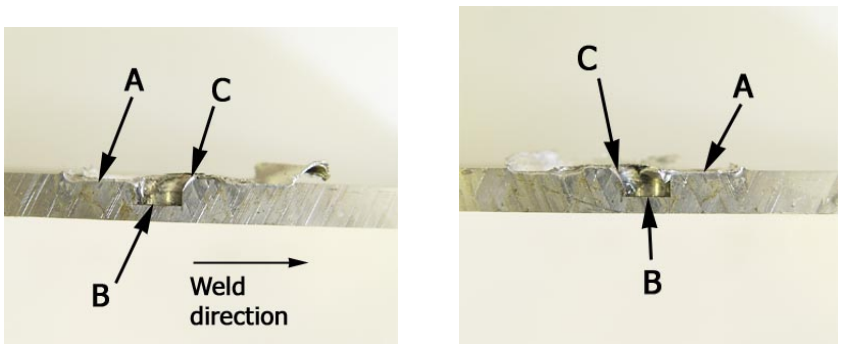

(a) Test 3, Advancing side. (b) Test 3, Retreating side.

Figure 5.14: Sectional views of the test 3.

The third trail test, with the pilot hole for the pin, showed similarities between the two previous welds. The previous assumption that the material was pushed into pin opening on the shoulder welding face was confirmed. In Figure 5.14, (**B**) represents the pilot hole and (**A**) the trailing side, and (**C**) the affect of the pin. The influence heat generated by the shoulder is shown by (**A**), and represents a small percentage of heat input in the process. In Figure 5.14, the tool is moving away from (**A**), and face on pilot hole on which the pin is forced against as can be viewed in Figure 5.15, during the transverse

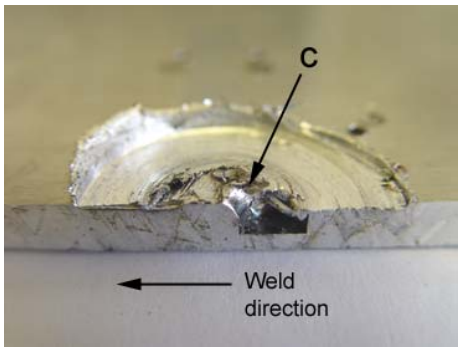

Figure 5.15: Test 3 showing the effect of the pin on the pilot hole during a weld.

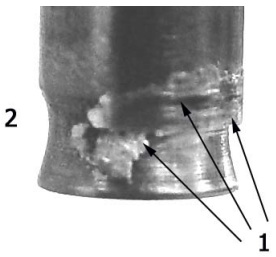

Figure 5.16: The shape of the modified pin (**2**) and the material deposits after welding (**1**).

phase of the weld, shows slight deformation in the weld direction.

As transverse motion begins, the pin is pushed further into the shoulder opening, and this is then filled with material due to capillary action, thus restricting the pin movement. The shape of the pin base, being spherical would also influence this action.

A modification to the pin was carried out, where a flat base and a slight necking was ground out, as the profile (**2**), in Figure 5.16. The shoulder was modified, by increasing the surface, with the assumption that it was not producing enough frictional heat. This modification increased the surface by 33 %.

5.3 Dynamic trial welds

The welds in this section represent an attempt to weld using the tool and configuration as designed. The welds were not very different to the previous section, in execution and the same procedure was used. The aim was to test the tool with modifications carried out, resulting from the preliminary welds.

Table 5.3: Weld parameters trial welds

No.	Speed	Air Pressure	Tool Angle
	rpm	bar	°
1	350	3.30	0
2	300	3.20	0
3	300	3.30	0

Test procedure

Once the pin and shoulder were modified and the material prepared for the thermocouples, a following three trial welds were done. For these welds the material used was Al5083-H321, due its lower solidus temperature and less shear resistance at these temperatures compared to the Al2024-T3 used in the previous tests.

The tool was plunged manually onto the surface, ensuring that the pin entered the pre-drilled pilot hole. The tool was held in dwell for 10-12 seconds and then transversed manually along the weld joint for 15-20 mm. Upon reaching the prescribed distance the pin was retracted by increasing the pressure and then the tool was retracted manually.

Dynamic trial 1

The first trial weld with the new pin showed some improvement in the weld cross-section compared to those previously described. The welding parameters are given in Table 5.3, with an adjustment to the pin fitting, to allow the pin to protrude by 5 mm from the shoulder at a pressure of 3.30 bar.

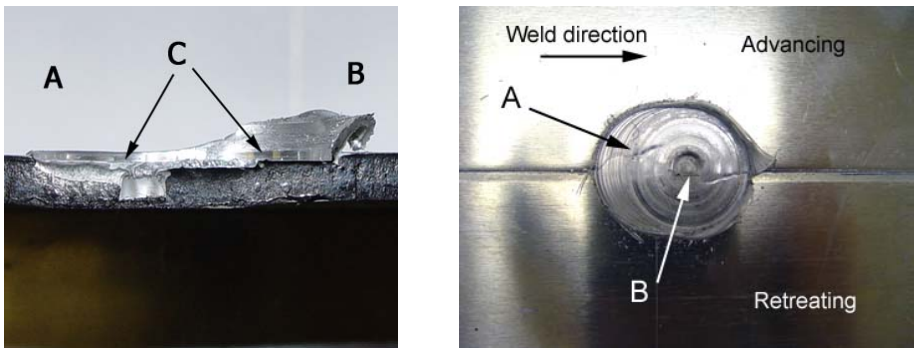

(a) Test 4, Advancing side. (b) Test 4, Plan view.

Figure 5.17: Sectional and plan view of the test 4 (First dynamic weld).

The weld cross-section is given in Figure 5.17, where in the weld direction is from (**A**) to (**B**). On the advancing side, (**C**) shows that the pin moved through the material at a depth of 2-3 mm, and the heat input is greater when the cross-section in Figure 5.14 is compared. The influence of the shoulder can be seen in Figure 5.17(a) denoted by (**C**), which appears to be deeper in this weld. Side flash is visible around the point (**B**), indicating that the parameters for welding were not optimal. In Figure 5.17(b), the movement of material on the surface is shown at point (**A**) and this confirms the movement of material around the pin (**B**) due to the shoulder.

The thermal data shows the temperature peaking around the 100 second point, and reaching a temperature around 460°C, Table 5.4 shows the comparison of the peaks during the weld. The temperatures follow a consistent pattern as shown in studies from Khandhar *et al.* [2003]; Song and Kovacevic [2003*b*]; Colegrove and Shercliff [2003]. The drop in temperature at the 160 second point would indicate that the pin had been retracted into the shoulder opening. By comparing this with the weld cross-section, the influence of the

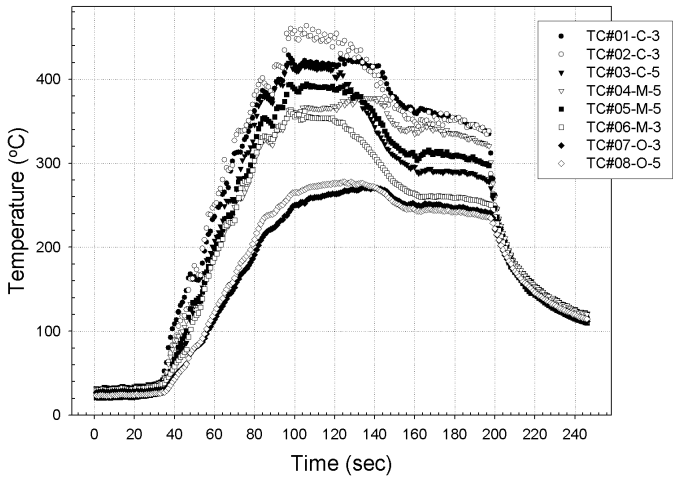

(a) Advancing side

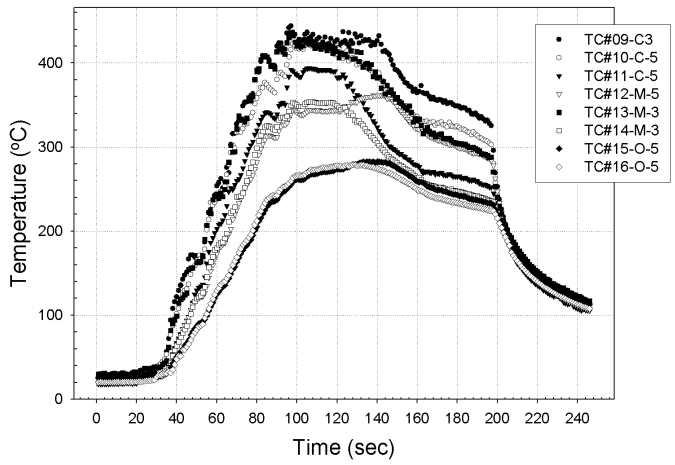

(b) Retreating side

Figure 5.18: Thermocouple data of the first test weld with the modified pin and shoulder.(Thermocouple pattern L_2-R_2)

pin is not visible in Figure 5.17(b).

The average temperature spread in the weld after the position and response was considered, reveals that the advancing side is on average at a higher temperature than the retreating side by 0.72% at

Table 5.4: Temperature peaks of dynamic test 1 at certain time intervals, comparing advancing and retreating sides

Side	Time	Outer	Middle	Center
	sec	°C		
Advancing	98	263	394	460
Retreating	98	260	392.09	444
Advancing	125	231	352	428
Retreating	125	233	400	403

the center and 3.5% at the middle regions. The outer positions have an average of only 0.26%, which is due to heat soak. By comparing the average data recorded at 125 seconds the following was noticed, 0.13% for the center and 3.5% for the middle and 1.6% in the outer regions. Therefore the pattern was presumed constant.

A further test was carried out after the shoulder assembly was removed and all traces of material removed from the opening and from the pin. An example of these deposits is shown in Figure 5.16, where the deposited material on the pin surface is denoted by (**1**).

Table 5.5: Temperature measurement of dynamic test 1 at 98 seconds, comparing advancing and retreating sides (Error ±10°C)

Advancing			Retreating		
O	M	C	C	M	O
°C					
254	364	425	436	349	255
263	394	460	444	392	260
-	362	419	416	340	-

Dynamic trial 2

The second dynamic test was completed in the same way as the previous tests and the results were consistent, as can be seen in the following Figure 5.19.

The weld again showed that the pin was being pushed up into shoulder and looking at Figure 5.19(a) the amount of heat generated was greater as the pilot hole at (**E**) shows deformation and the area around (**D**) has evidence of this deformation. At (**C**) the indentation caused by the pin is visible , a pin depth of 2 mm transversing through the weld is also shown.

In Figure 5.19(b) the deformation of the material on the surface, being translated from the advancing to the retreating side, is illustrated by the position of (**A**) as shown.

The thermal data shows a constant temperature for a larger period of time, but the temperature range is lower the previous test,

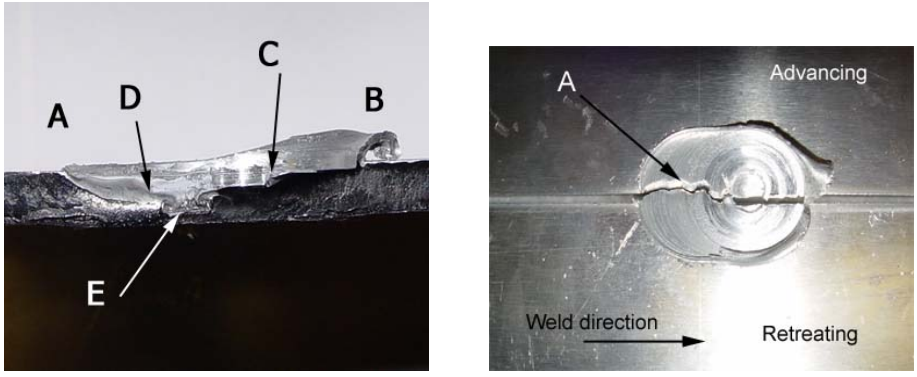

(a) Dynamic trial 2, Advancing side. (b) Dynamic trial 2, Plan view.

Figure 5.19: Sectional and plan views of the dynamic trial 2.

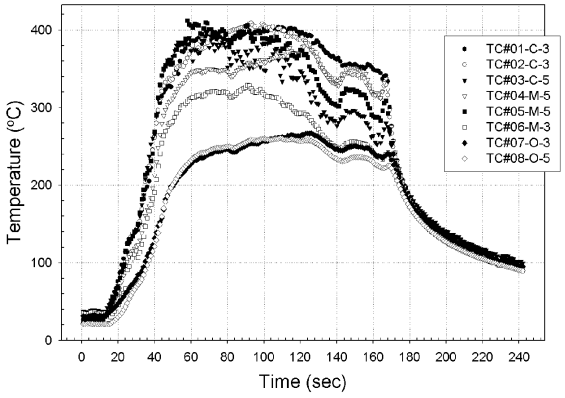

(a) Advancing.

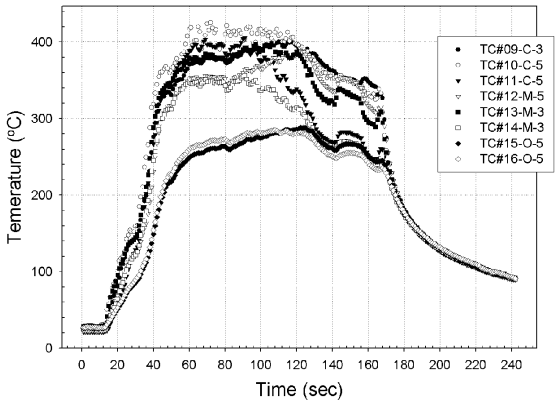

(b) Retreating.

Figure 5.20: Thermocouple data from dynamic test 2.(Thermocouple pattern L_2-R_2)

ranging at a maximum of 420°C after 60 seconds. The force in the z-direction was recorded at +10kN. A noticeable difference is that the temperature does not fall off sharply as seen in Figure 5.18. The peak temperature at the 60 second point are given in Table 5.6

Table 5.6: Temperature measurement of dynamic test 2 at 60 seconds, comparing advancing and retreating sides (Error ±10°C)

Advancing			Retreating		
O	M	C	C	M	O
°C					
223	339	381	371	352	249
227	364	421	417	379	260
-	308	387	389	347	-

Dynamic weld 3

The final dynamic weld was completed and no successful pin penetration was seen, the data revealed that the pin would initially start in the pilot hole and slowly would be pushed into the shoulder.

at the thermal data (Figure 5.22) and the sectional view (Figure 5.21), no change to the previous tests was seen.

The thermal data revealed a drop in the temperature after the peak

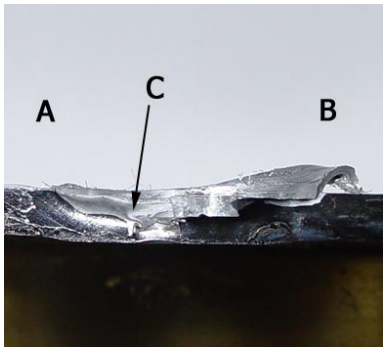

(a) Dynamic trial 3, Advancing side.

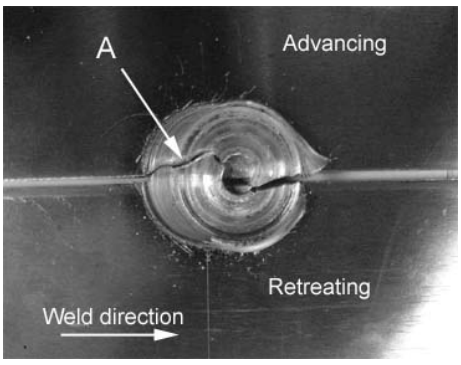

(b) Dynamic trial 3, Plan view.

Figure 5.21: Sectional and plan view of the dynamic trial 3.

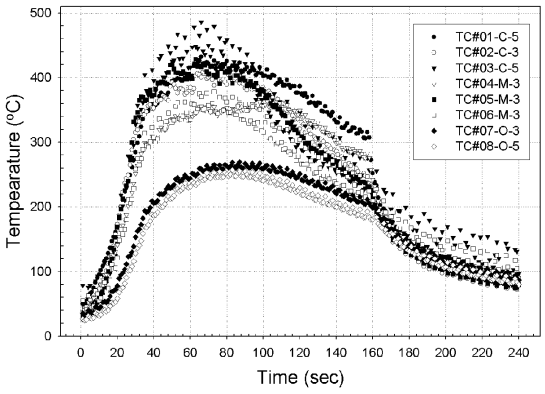

(a) Advancing.

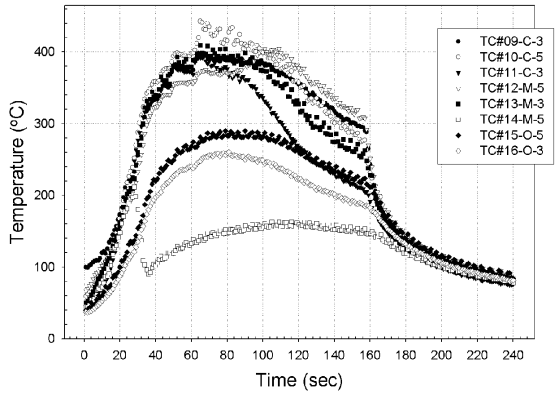

(b) Retreating.

Figure 5.22: Thermocouple data from dynamic trial 3.(Thermocouple pattern L_3-R_3)

was reached at 460°C, this is influenced by the transverse speed along the weld. As this was done manually there is no data to verify this assumption. In tests conducted by Colegrove and Shercliff [2003]; Song and Kovacevic [2003*a*], the drop in weld temperature is attributed to the speed of the weld, but in this case as there is no

major pin influence to be able to compare these results.

5.3.1 Plastic trials

There were still may unanswered questions, so it was decided to attempt to see what was happening to the pin during a weld. Since the density and thermal properties of a plastic material are lower than aluminum, and the need to apply large z-force would be reduced, a trial run was attempted.

A trial run with an ABS plastic sheet of thickness 5 mm was attempted. The tool was placed in front of the joint line of the two plates, and with the pin extended, to start a weld. There was no attempt to plunge into the material.

For the first trial, the rotational speed was set at 300 rpm and the pressure on the actuator set to 3.30 bar. Again manual transverse speed along the weld was carried out.

Trial two was conducted in the same way as the first, with the exception that the rotational speed was increased to 400 rpm. All the other parameters were kept constant. However in the second test, the pin was jogged up and down, during the final stages of the weld. This was done by increasing and decreasing the pressure to

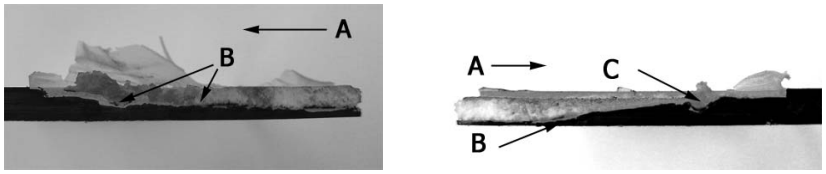

(a) Test Plastic 1. (b) Test Plastic 2.

Figure 5.23: Sectional views of the plastic welds.

see if the pin would leave a trace in the weld.

Both views, in Figure 5.23 show the movement of the pin being slowly retracted into the shoulder, where (**A**) denotes the weld direction, and (**B**) the point where the pin beings to move into the shoulder. In Figure 5.23(b) at point (**C**) there is a slight indentation left by the pin as the pressure was increased and decreased during the point prior to extraction. The welding parameters were not optimized and as a result the welds are of poor quality. After the welds, material was found in the shoulder opening and on the pin, the second weld, did have less build up on the pin.

The tool was removed and inspected after the final welds, and no problems were uncovered. It was noted that the tool would require some modifications to improve its welding capabilities, these and the conclusions are left for discussion in Chapter 6.

6 Conclusions and Future Work

6.1 Conclusions

The purpose of this study, and its relevance to FSW, should be seen as attempting to gain a better understanding into the complexities of material flow caused by a retractable pin tool during welding.

An experimental modular retractable pin tool was successfully designed using a Pneumatic Muscle Actuator. The novel use of this actuator however, proved problematic when the repeatability of the pin position was concerned. Even though compressed air as a actuating medium, is simpler to use, cheaper and environmentally friendlier, the compressibility of air proved to be the limiting factor. Together with the nonlinearity due to elasticity in the pneumatic actuator and the compressibility of air, contributed to the calibration difficulties. Furthermore not having adaptive control of the pin, and not knowing its actual position also proved to be a disadvantage.

The trail welds in Al2024 and Al5083 aluminum plate, with the retractable pin tool, were not successful. This was partly due to the misconception that the shoulder generates enough heat to allow for pin penetration during the dwell period in a FSW weld cycle. However, it was noticed, that the heat generated by the shoulder,

tended to decrease after a period of 12-20 seconds, even though all the parameters remained constant. This would indicate that equilibrium was reached concerning the heat produced by the effect of friction. The influence of μ (coefficient of friction) on the heat input at the shoulder, is given by the relationship, $q = 2\pi\mu F_z RN$ from prior work. Thus when considering the difference resulting from changes in μ from 1 to 0.4, a 60% decrease in the heat flux at the shoulder is calculated, and a further 50% when the value of μ decreases from 0.4 to 0.2. This however, would not have been noticed in welds with the standard FSW tools (fixed pin type), as the fixed pin generates most of the heat during plunging. Therefore it appears that the shoulder is only responsible for the heat generated at the surface and as shown in the welds performed, this influence is to a depth of 2-3 mm in a 6.3 mm Al5083 plate.

Considering the tests where the pin was not protruding from the shoulder face, temperatures of 420°C were recorded, but when similar tests were conducted with a pilot hole, to allow the pin to protrude into the fayed joint before welding, this resulted in higher temperatures of 485°C. As the tool transversed along the weld, it was shown that the pin would retract into the shoulder and the temperature would decrease. Welds using plastic samples emphasized this phenomenon of pin movement during a weld, due to the compressibility of the air in the pneumatic actuator. Thus confirming the importance of the pin for heat generation in a FSW weld.

When the tool was inspected after each weld, material found in the shoulder pin opening, and on the pin itself. This material through

capillary action had solidified during welding in the shoulder opening. This caused the pin to remain stuck in the shoulder opening for all the weld tests, even though temperatures of 420-485°C in the weld were recorded. Heat dissipation through the tool may have been a contributing factor or that the pin was not hot enough, due to it not generating any heat during the test welds with this tool. No pin temperature was taken to verify this.

The tests of material flow, using a standard tool,confirmed the material flow around the pin to be chaotic and turbulent. The influence of a threaded pin's, pitch angle and the direction of rotation confirmed previous results that the material flow could affect the quality of a weld. The turbulent action around the threads together with the the welding speed, could possibly influence the formation the "onion-rings" in a weld.

6.2 Future Work

This section is divided into two parts , firstly the changes recommended to improve the tool followed by the work required to better understand the FSW process.

Considering the conclusions resulting from this work, it is necessary to rethink, the design of the tool. The possible use of another medium of actuation to reduce the effects of compressibility, such as hydraulics would needs consideration. Furthermore by improving the muscle actuation system, by allowing for a double actuator, to improve the control the pin movement in extension and retraction phases. The need for a system to allow the pin to remain extended

especially during plunging to produce more heat during welding. By ensuring a stiction free actuator movement, to improve pin movement, during the pressure decreasing phase needs to be investigated.

Since this research did not take the problems encountered in the FSW welds further, more tests are necessary to quantify the effect of the shoulder and the effects due to variations in μ, which affect heat generation during welding. Developing a model to formulate the rate of change in viscosity and density, during welding using nonlinear continuum mechanics techniques, when changes in surface friction coefficient and temperature are known.

Finally, as proposed in this research, the analysis into material flow around a pin during retraction, needs to be continued.

REFERENCES

Aramayo G, Radhakrishnan B, David S A, Sarma G and Babu S S [2002]. Modeling of Friction Stir Welding Process for Fusion Energy Applications, *in Fusion Materials*, Vol. 32, Oak Ridge National Laboratory, Oak Ridge, TN, USA, Semiannual Progress Report for Period Ending June 30, 2002 1.1, pp. 2–5.
URL: *http://www.ms.ornl.gov/programs/fusionmatls/pdf/june2002/1.1-pg.2-5/Aramayo.pdf*

Askari A, Silling S, London B and Mahoney M [2001]. Modeling and Analysis of Friction Stir Welding Processes, *in* K Jata, M Mahoney, R Mishra, S Semiatin and D Field, eds, *Friction Stir Welding and Processing*, TMS, pp. 43–54.

Carbonell P, Jiang Z P and Repperger D W [2001]. Nonlinear Control of a muscle actuator system, 5th IFAC Symposium, "NONLINEAR CONTROL SYSTEMS"(NOLCOS 2001), St. Petersburg, Russia.

Chen C and Kovacevic R [2003]. Finite element modeling of friction stir welding - thermal and thermomechanical analysis, *Int. Journal of Machine Tools and Manufacture* **43**, 1319–1326.

Chou C P and Hannaford B [1996]. Measurement and modeling of McKibben pneumatic artificial muscles, *in IEEE Transactions on*

Robotics and Automation,, Vol. 121, IEEE, pp. 90–102.
URL: *citeseer.nj.nec.com/chou96measurement.html*

Colegrove P and Shercliff H [2003]. Experimental and numerical analysis of aluminum alloy 7075-T7351 friction stir welds, *Science and Technology of Welding & Joining* **8**(5), 360–369.

Colligan K [1998], 'Friction Stir Welding Tool for Welding Variable Thickness Workpieces'. US Patent No. 5,718,366.

Colligan K [1999]. Material Flow Behavior during Friction Stir Welding of Aluminum, *Welding Journal Research Supplement* **78**(7), 229s–237s. Sponsored by the American Welding Society and Welding Research Council.

Czernik D E and Hopkins R [1986]. *Gaskets and Seals*, McGraw-Hill, New York, NY, USA.

Daerden F [1999], Conception and Realization of Pleated Pneumatic Artificial Muscles and their Use as Compliant Actuation Elements, PhD thesis, Vrije Universiteit Brussel.

Ding R J [2000]. Force Characterization on the Welding Pin of a Friction Stir Welding Retractable Tool using Aluminum-Lithium 2195, Second International Friction Stir Welding Symposium, Gothenburg, Sweden.

Ding R J and Oelgoetz P A [1999], 'Auto-Adjustable Pin Tool for Friction Stir Welding'. US Patent No. 5,893,507.

Dong P, Lu F, Hong J and Cao Z [2001]. Coupled thermo-mechanical

analysis of friction stir welding process using simplified models, *Science and Technology of Welding & Joining* **6**(5), 281–287.

Dorodnitsyn V and Kozlov R [2003]. A Heat Transfer with a Source: the Complete Set of Invariant Difference Schemes, *Journal of Nonlinear Mathematical Physics* **10**(1), 16–50.

Dunn Z P [2002], Material flow patterns in aluminum Friction Stir Welding, Master's thesis, Brigham Young University.

Festo AG. [2003]. *Fluidic Muscle MAS, Info 501*, Festo AG & Co. KG.
URL: *http:/www.festo.com/Info_501_en.pdf*

Frigaard O, Grong O and Midling O [1999]. Modelling of heat flow phenomena in Friction Stir Welding of Aluminuim alloys, *Joints in aluminium: INALCO'98* pp. 208–218.

Guerra M, Schmidt C, McClure J, Murr L and Nunes A [2003]. Flow paterns during friction stir welding, *Material Characterization* **49**, 95–100.

Hansen M [2003]. A cooler weld, *Mechanical Engineering Design* . Taken from Web 19/08/2003.
URL: *http://www.memagazine.org/medes03/coolweld/cwsidebar.html*

Heinz R [1996]. *Actuators*, 4th edn, Robert Bosch GmbH, Stuttgart, Germany.

Heston T [2002]. Taking Off with Friction Stir Welding, *Fabrication and Metalworking Magazine* .
URL: *http://www.ndx.com/article.asp?article_id=392&channel_id=4*

Holt E S and Lang L J [1998], 'Programmable Friction Stir Welding Process'. US Patent No. 5,713,507.

Johnson R [2001]. Forces in Friction Stir Welding of Aluminium Alloys, Third International Friction Stir Welding Symposium, Kobe, Japan.

Kawasaki T, Makino T, Todori S, Takai H, Ezumi M and Ina Y [2001]. Application of Friction Stir Welding to the Manufacture of Next Generation "A-train" type Rolling Stock, Third International Friction Stir Welding Symposium, Kobe, Japan.

Khandhar M, Khan J and Reynolds A [2003]. Prediction of temperature distribution and thermal history during friction stir welding: input torque based model, *Science and Technology of Welding & Joining* **8**(3), 165–174.

Kreuzer E J [1991]. *Introduction into the concepts of chaos and some numerical methods*, Vol. 391 of *International Center for Mechanical Science, Courses and Lectures*, Springer-Verlag, New York, NY, USA.

Kroll E, Condoor S S and Jansson D G [2001]. *Innovative Conceptual Design*, Cambridge University Press, Cambridge, UK.

Lambrakos S, Fonda R, Milewski J and Mitchell J [2003]. Analysis of friction stir welds using thermocouple measurements, *Science and Technology of Welding & Joining* **8**(5), 385–390.

Lee H K, Choi G S and Choi G H [2002]. A study on tracking position control of pneumatic actuators, *Mechatronics* **12**, 813–831.

Lesieur M [1997]. *Turbulence in Fluids*, 3rd rev. edn, Kluwer Academic Publishers, Dordrecht, Netherlands.

Mase G T and Mase G E [1999]. *Continuum Mechanics for Engineers*, 2nd edn, CRC Press, Boca Raton, FL, USA.

Melvin J W [2003], Axiomatic System Design:Chemical Mechanical Polishing Machine Case Study, PhD thesis, Massachusetts Institute of Technology.

Messler R W [1999]. *Principles of Welding: Processes, Physics, Chemistry, and Metallurgy*, John Wiley & Sons, New York, NY, USA.

MTS Systems Corporation [2002], 'FSW Process Experience at MTS'. **URL:** *http://www.mts.com/aesd/friction_stir2.htm*

Munson B R, Young D F and Okiishi T H [1998]. *Fundamentals of Fluid Mechanics*, 3rd edn, John Wiley & Sons, New York, NY, USA.

Murr L, Li Y, Flores R, Trillo E A and McClure J [1998]. Intercalation vortices and related micro, **2**, 150–163.

Murr L, Trillo E, Li Y, Flores R, Nowak B and McClure J [1999]. solid-state flow associated with the friction-stir welding of dissimilar metals, *in* N El-Kaddah, D Robertson, S Johnson and V Voller, eds, *Fluid flow phenomena in metals processing*, Warrendale, PA.

Nakamura N, Seikiguchi M, Kawashima K, Fujita T and Kagawa T [2002]. Developing a Robot Arm using Pneumatic Artificial Rubber Muscles, Power Transmission and Motion Control Workshop, Bath, UK.
URL: *http://www.k-k.pi.titech.ac.jp/pam/PTMC2002Final.pdf*

North T, Bendzsak G and Smith C [2000]. Material Properties Relevant to 3-D FSW Modeling, Second International Friction Stir Welding Symposium, Gothenburg, Sweden.

Oberg E, Horton H L and Ryffel H H [1996]. *Machinery's Handbook*, 25th edn, Industrial Press, New York, NY, USA.

Parker O-Ring Division [2003]. *Parker O-Ring Handbook, 5700*, Parker Hannifin Corporation.
URL: *http:/www.parker.com/o-ring*

Rabin Y and Rittel D [1999]. A Model for the Time Response of Solid-embedded Thermocouples, *Experimental Mechanics* **39**(2), 1–5.

Rabin Y and Rittel D [2000]. Infrared Temperature Sensing of Mechanically Loaded Specimens: Thermal Analysis, *Experimental Mechanics* **40**(2), 197–202.

Reynolds A P [2003]. FSW BASICS, International Workshop on Friction Stir Welding, Port Elizabeth, South Africa.

Reynolds A and Siedel T [2001]. Visualization of Material Flow in AA2195 Friction Stir Welds Using a Marker Insert Technique, *Metallurgical and Materials Transactions A* **32A**, 2879–2884.

Rohner P and Smith G [1989]. *Pneumatic Control for Industrial Automation*, rev. edn, John Wiley & Sons, Brisbane, Australia.

Russell M and Shercliff H [1999]. Analytical modelling of friction stir welding, *in Joints in Aluminium*, INALCO '98, 7th International Conference, Woodhead Publishing, Cambridge, UK, pp. 197–207.

Sakano R, Murakami K, Yamashita K, Hyoe T, Fujimoto M, Inuzuka M, Nagao Y and Kashiki H [2001]. Development of Spot FSW Robot System for Automobile Body Members, Third International Friction Stir Welding Symposium, Kobe, Japan.

Shigley J E [1986]. *Mechanical Engineering Design*, 1st metric edn, McGraw-Hill, Singapore.

Shindo D, Rivera A and Murr L [2002]. Shape optimization for tool wear in the friction-stir welding of cast Al395-20% SiC MMC, *Journal of Materials Science* **37**, 4999–5005.

Smith C, Bendzsak G, Hinrichs J, Noruk J and Heideman R [1999]. Heat and Material Flow Modeling of the Friction Stir Welding Process, *in International Conference on Computer Technology in Welding*, International Conference on Computer Technology in Welding, Detroit, MI, USA, pp. 475–486.

Song M and Kovacevic R [2003*a*]. Numerical and Experimental study of the heat transfer process in friction stir welding, *in Proc. Instn Mech. Engrs., Part B: J. Engineering Manufacture*, Vol. 217, IMechE, pp. 73–85.

Song M and Kovacevic R [2003*b*]. Thermal modeling of friction stir welding in a moving coordinate system and its validation, *Int. Journal of Machine Tools and Manufacture* **43**, 605–615.

Suh N P [1998]. Axiomatic Design theory for Systems, *Research in Engineering Design* **10**, 189–209.

Suh N P [1999]. A Theory of Complexity, Periodicity and the Design Axioms, *Research in Engineering Design* **11**, 116–131.

Technology Transfer Dept. [2001]. Friction Stir Welding, Web Page - Techtans Report, NASA MSFC Space Flight Center.
URL: *http://techtrans.msfc.nasa.gov/pdf/FSW11.20.01.pdf*

Thomas W M, Nicolas E D *et al.* [1995], 'Friction Welding'. GB Patent No. 9,125,978 (1991) and US Patent No. 5,460,317.

Thompson D E [1999]. *Design Analysis: Mathematical Modeling of Nonlinear Systems*, 1st edn, Cambridge University Press, New York, NY, USA.

Truesdell C and Rajagopal K [2000]. *An Introduction to the Mechanics of Fluids*, Birhäuser Boston, New York, NY, USA.

von Strombeck A and Dos Santos J [2002], 'Device for Joining Workpieces by Friction Stir Welding'. US Patent Application: US 2002/0179673 A1.

Wykes D H [1997], 'Adjustable Pin for Friction Stir Welding Tool'. US Patent No. 5,697,544.

Young W C [1989]. *Roark's Formulas for stress and strain*, 6th edn, McGraw-Hill, New York, NY, USA.

A Design Drawings

Detailed design drawings of the experimental FSW tool.
Note: The number enclosed in brackets represents the figure number.

List of components:

1. Rotary joint (A.3)
2. Slip-ring (A.1)
3. 4 x M8 Cap-head bolts
4. 2 x Festo M3 Push-in fitting
5. 3 x 2.62xID 82 mm O-rings
6. PTFE washer (A.2)
7. Festo M16 Axial adapter
8. Upper adapter plate (A.4)
9. 8 x Countersunk M4 screws
10. 4 Rods (A.5)
11. Festo Fluidic Muscle
12. Festo M10 Threaded-rod
13. Flanged (Tufnol) bush (A.11)
14. Actuator plate (A.13)
15. Washer (Tufnol) (A.12)
16. M10 SW17 Nut
17. 4 x PTFE Bushes (A.10)
18. Pin holder bracket (A.14)
19. Pin A.15
20. 2 x M5 Grub screws
21. 16 x M5 Cap-head bolts
22. Lower adapter plate (A.6)
23. Shoulder bracket (A.8)
24. Shoulder (A.9)
25. Outer sleeve (A.7)
26. 4 x M4 Cap-head bolts

Tool Assembly Procedure

The tool is assembled as follows, however certain procedures are relevant to the host FSW machine used. The number references enclosed in brackets are taken from the list in this Appendix.

Firstly assemble the rotary joint, by placing the three O-rings (**5**) into the slip-ring (**2**) and lightly oiled with lubricant (Wynns Number Five). Then place the slip-ring over the lower end of the rotary joint (**1**). Screw on the axial adapter (**7**) into the rotary joint base, and ensure a tight fit to prevent air leakage (plumber tape if necessary). The Fluidic Muscle (**11**) is fastened onto the axial adapter, also ensure that there is no leakage. At the opposite end of the Fluidic Muscle attach the threaded rod-end (**12**), this completes the rotary joint and Fluidic Muscle assembly.

The next stage is to assemble the actuator system. Teflon bushes (**17**) are inserted into the actuator plate (**14**), and the rods (**10**) pushed through, with the flanged shoulder side on the lower side toward the the pin. Locate the upper adapter plate (**8**) on the four rods and bolt together with the counter sunk screws (**9**).

The upper adapter plate and the rods are then attached to the base of the rotary joint with the PTFE washer (**6**) in between, using the M8 cap head bolts (**3**). The Tufnol flanged bush (**13**) is placed in the actuator plate facing the rotary joint and the threaded rod-end located through it. The Tufnol washer (**15**) is placed on the other side of the actuator plate, in the direction of the pin, and with the threaded nut (**16**) tightened to secure the Fluidic Muscle to the actuator plate.

The pin holder bracket (**18**) is fastened to the actuator plate with the M5 cap-head bolts (**21**) and the pin (**19**) is located and secured using a grub screw (**20**).

Assemble the lower adapter plate (**22**), on which the shoulder

bracket (**23**) is attached using the M5 cap-head bolts. The shoulder is located in the shoulder bracket and secured with a grub screw . The lower adapter plate assembly is located on the rods using the counter-sunk screws.

Once the tool is assembled, the outer sleeve (**25**) is put over the tool assembly and finally the air fittings (**4**) are attached. Loctite 222, is used for added security on all the bolts and screw not affected by heat, those near or in direct contact with heat (that is the bolts in region of the shoulder and pin) were tightened with Copperslip ((SPANJAARD) High Temperature Copper Compound).

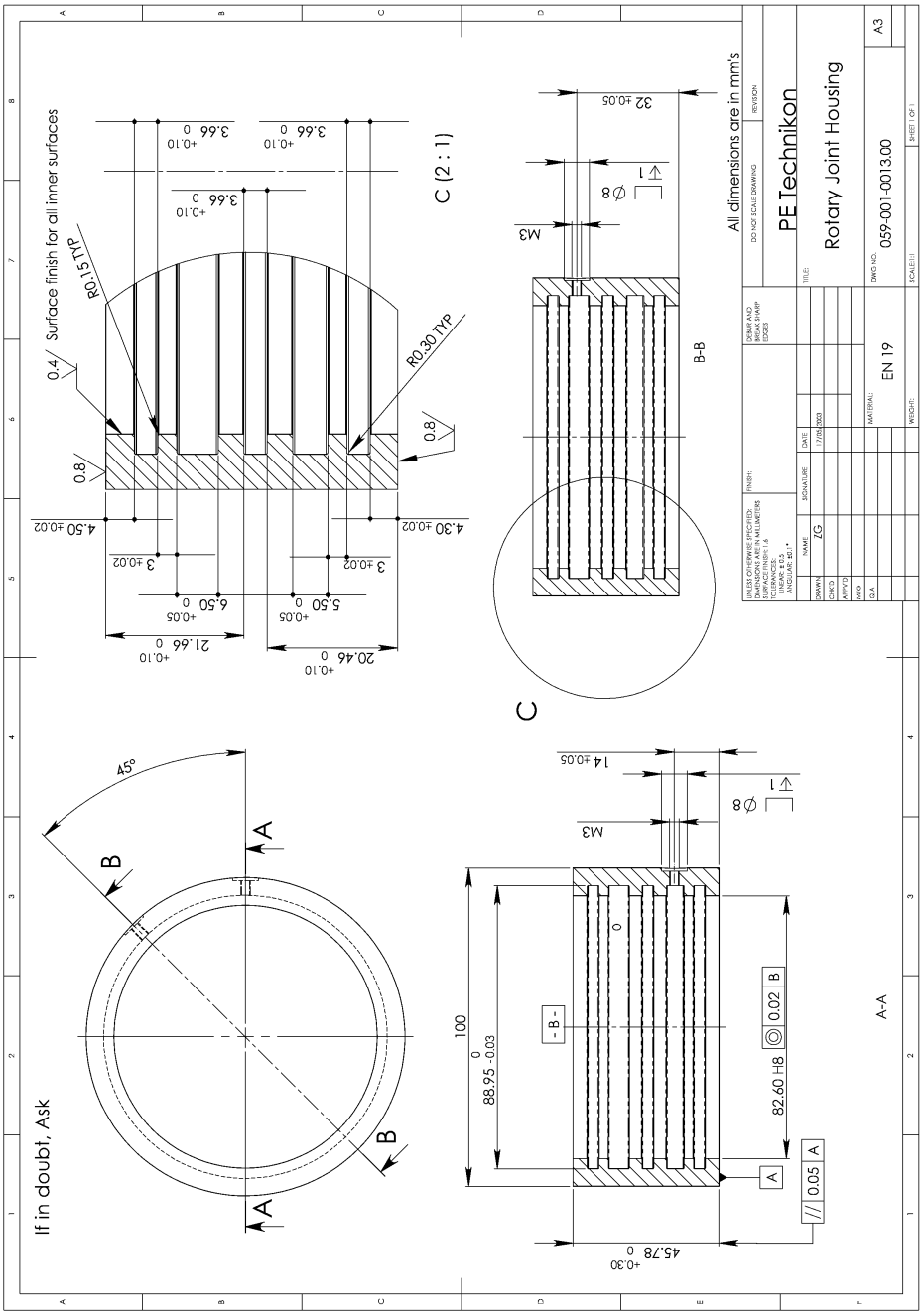

Figure A.1: Slip-ring.

Figure A.2: PTFE (Teflon) Washer.

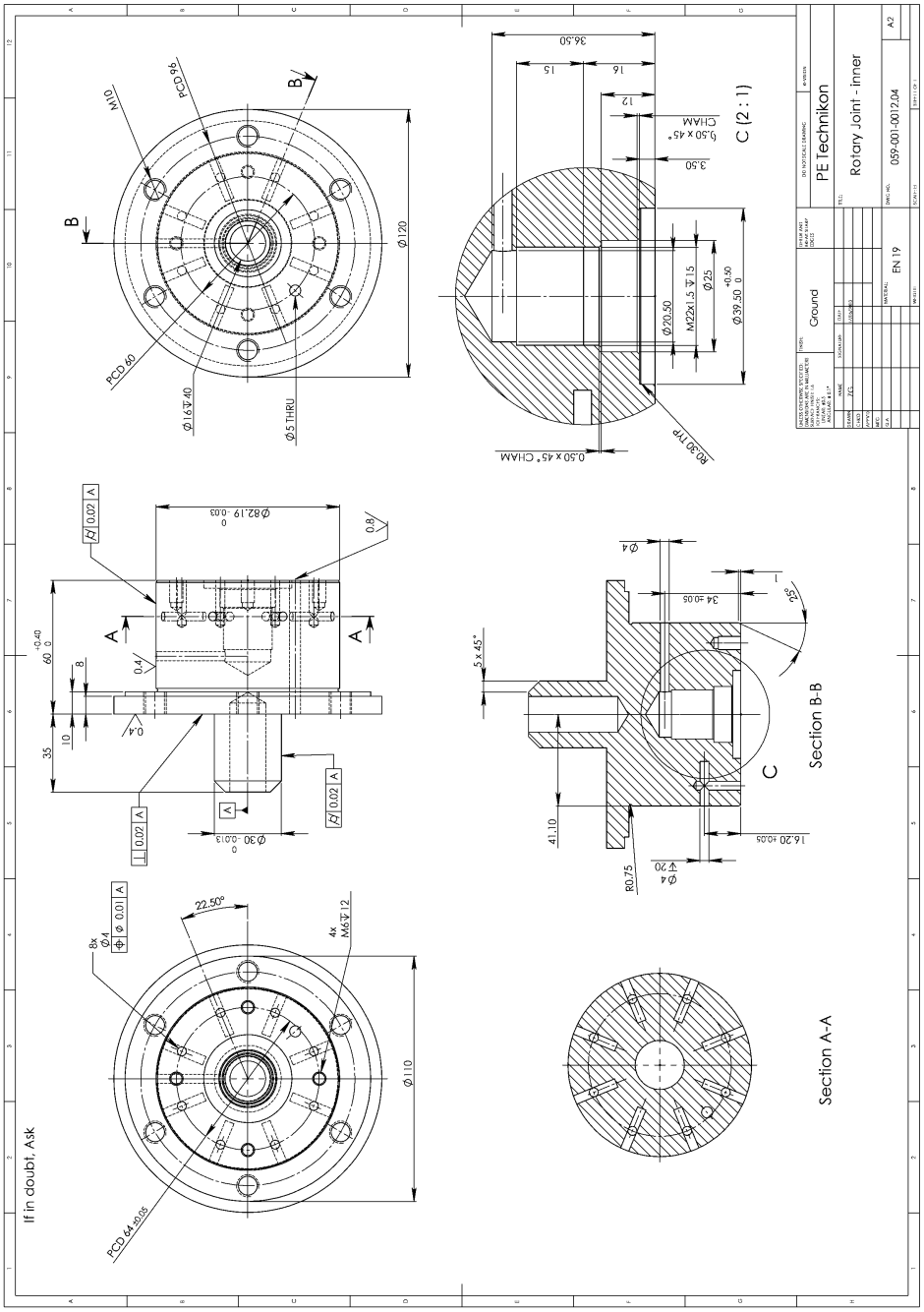

Figure A.3: Rotary joint.

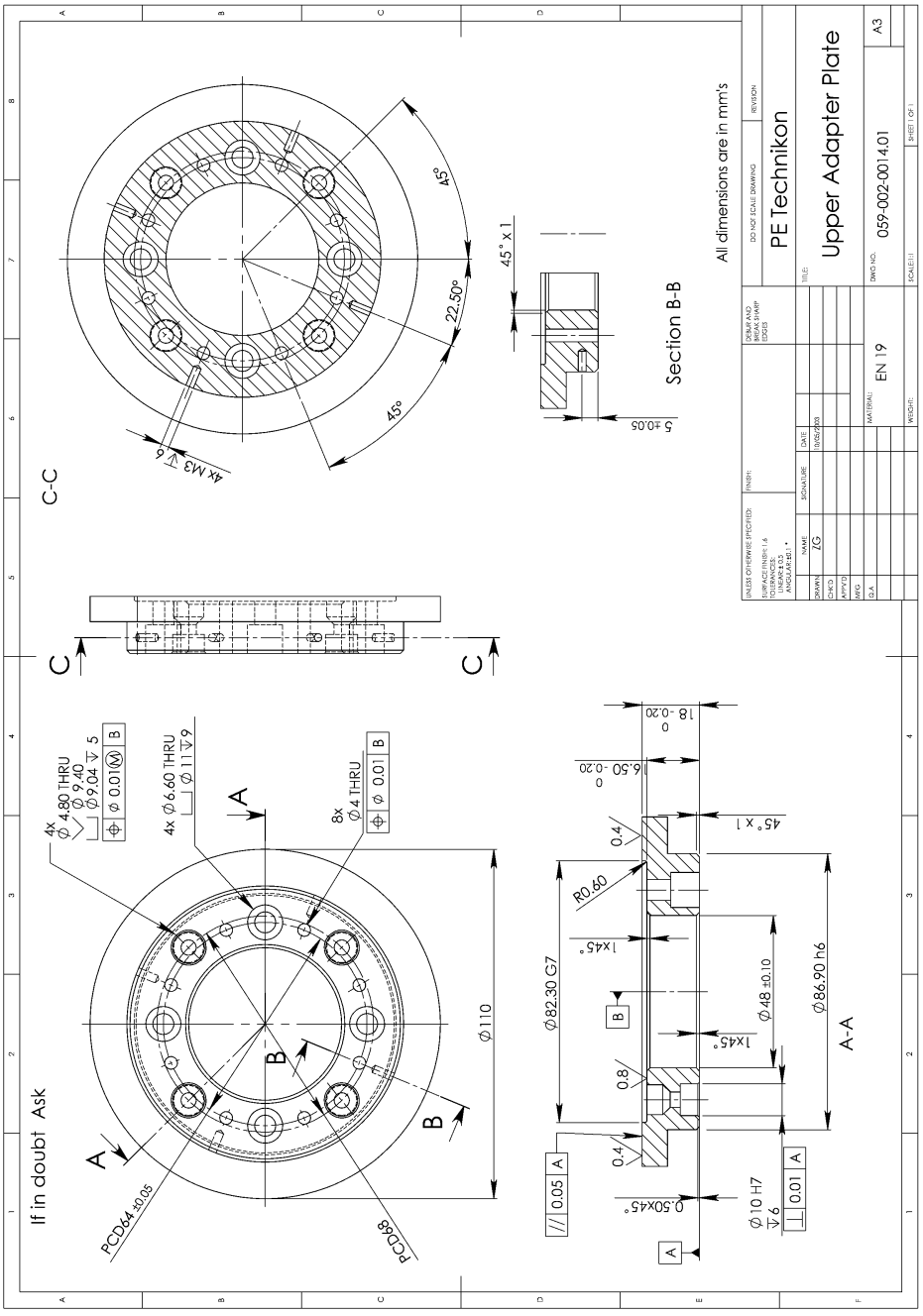

Figure A.4: Upper adapter plate.

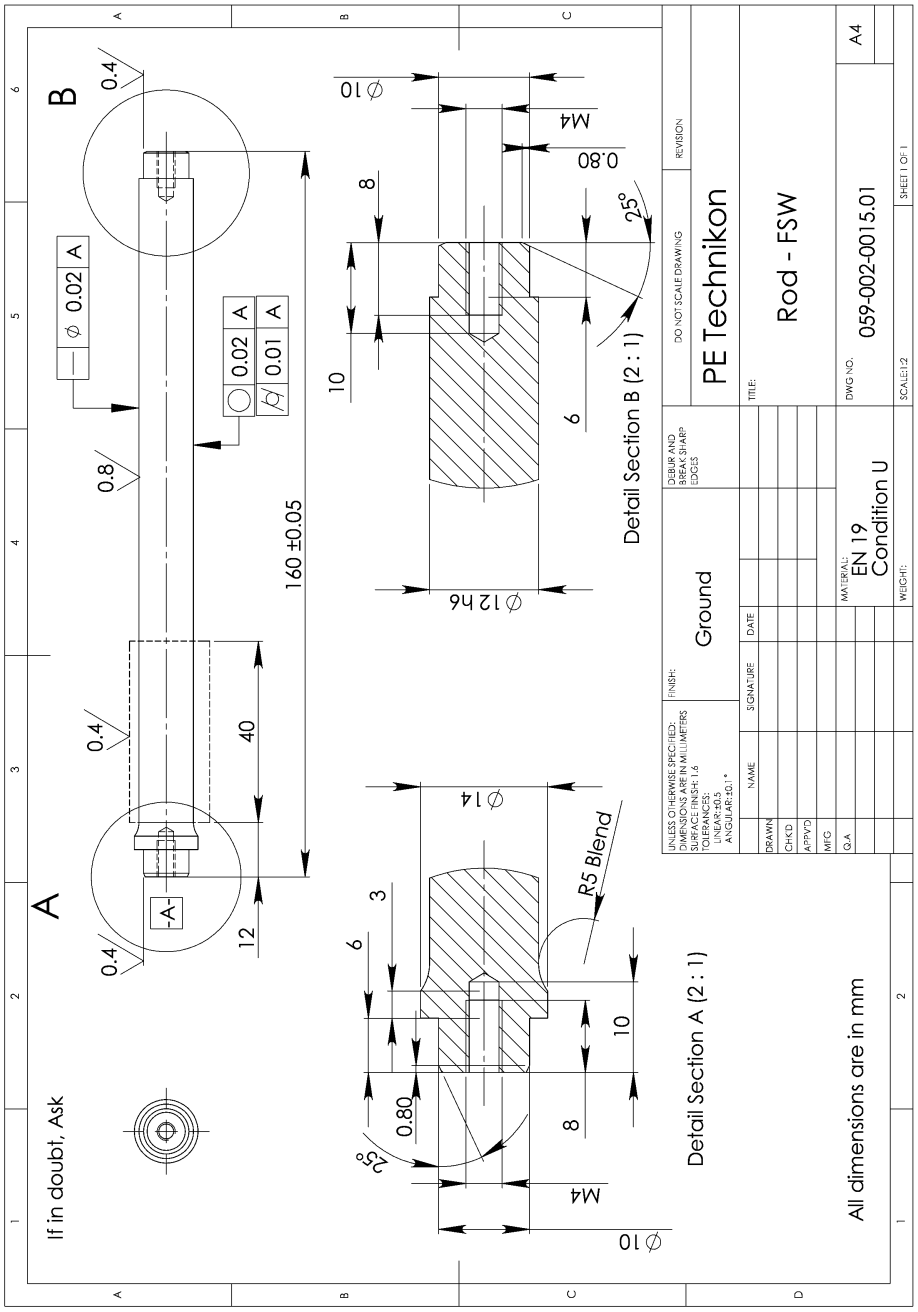

Figure A.5: Rod.

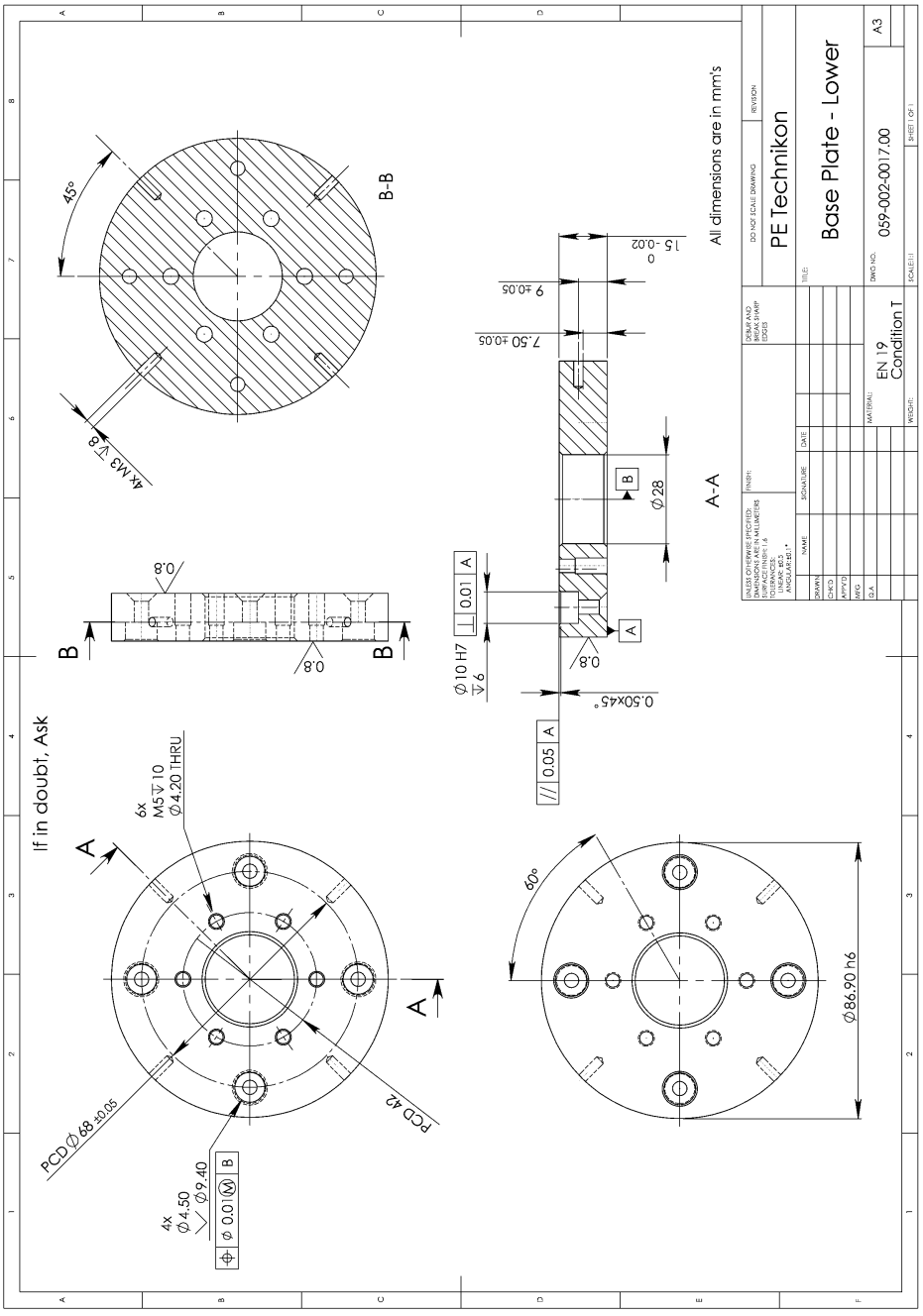

Figure A.6: Lower adapter plate.

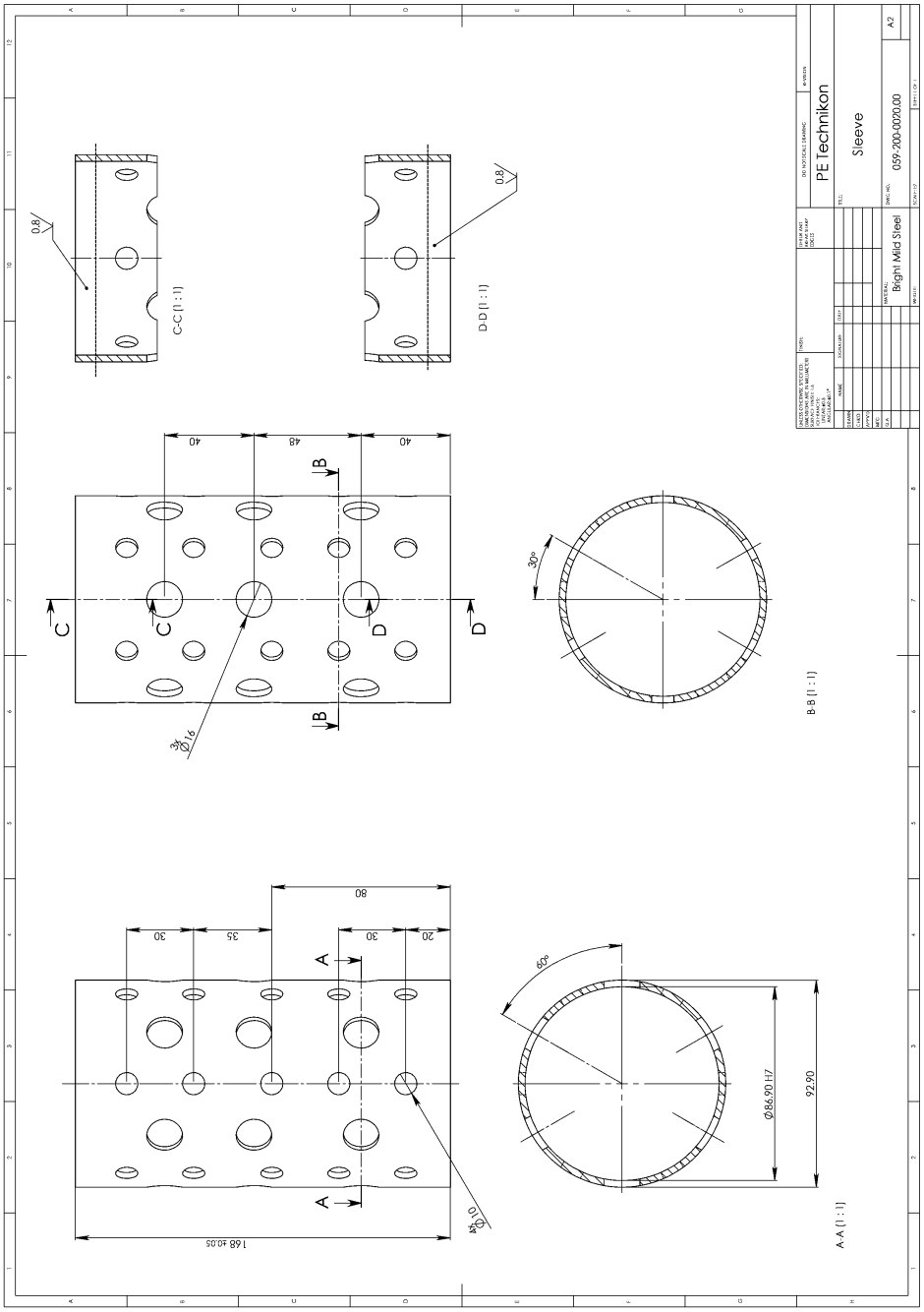

Figure A.7: Outer sleeve.

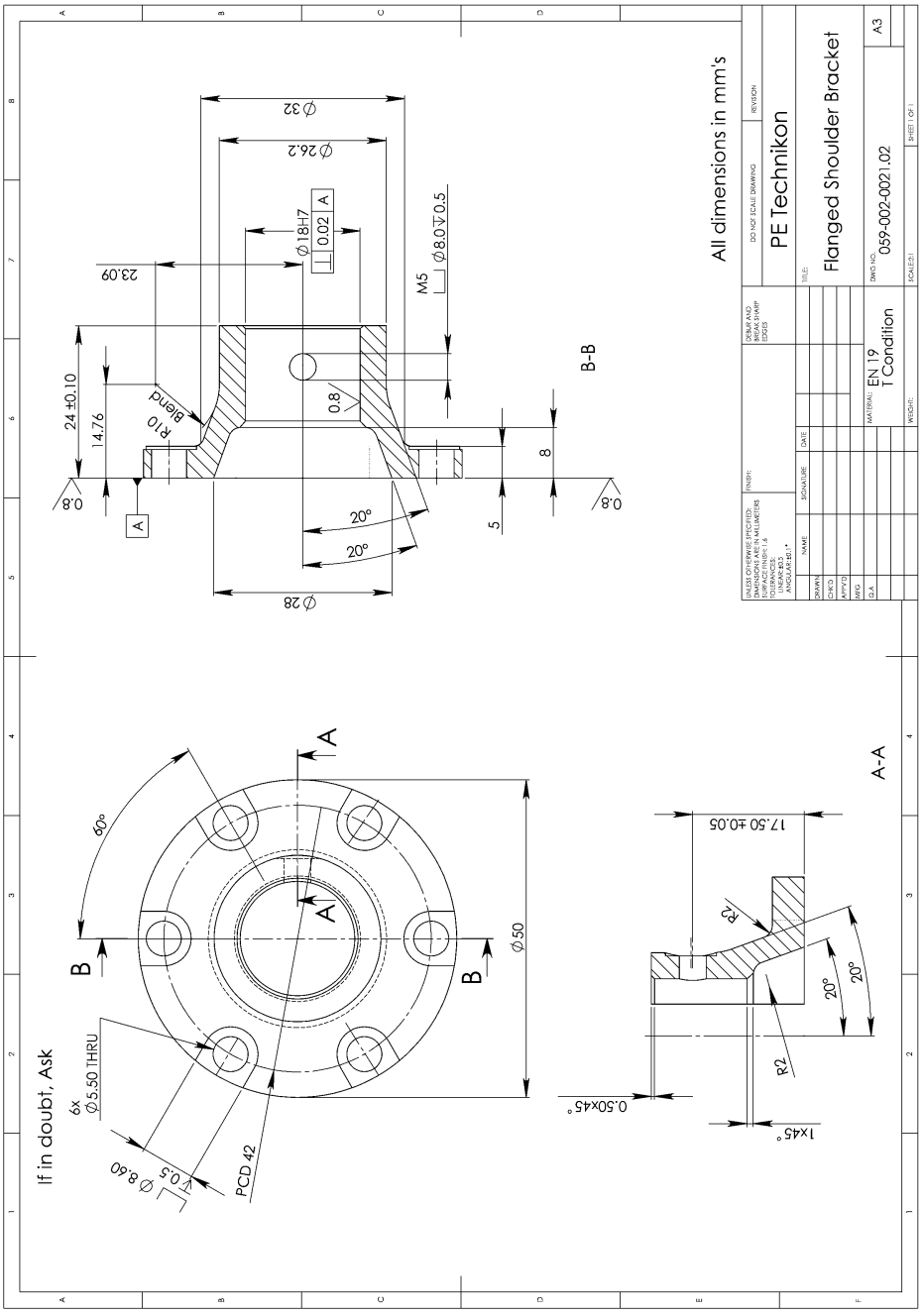

Figure A.8: Shoulder bracket.

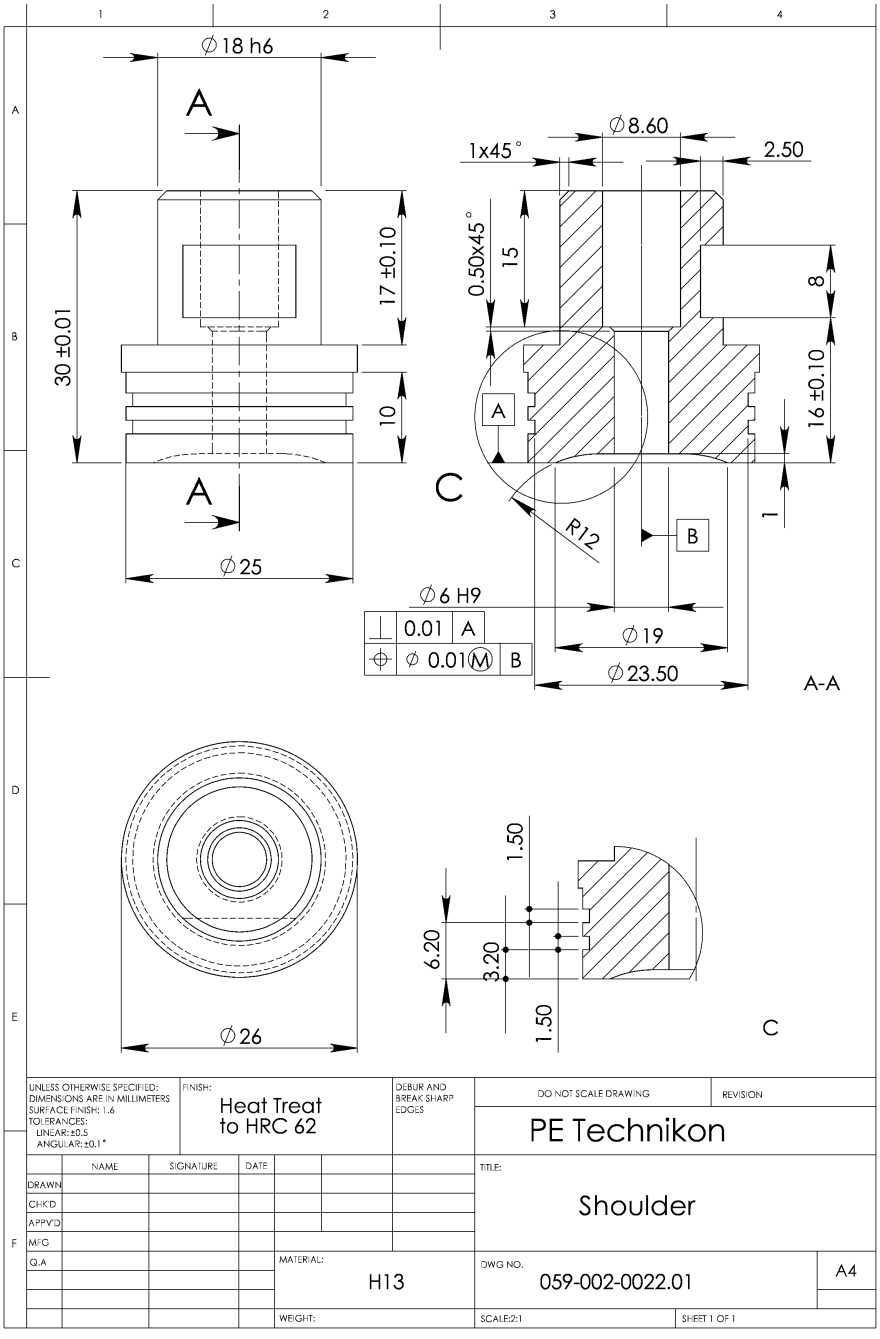

Figure A.9: Shoulder.

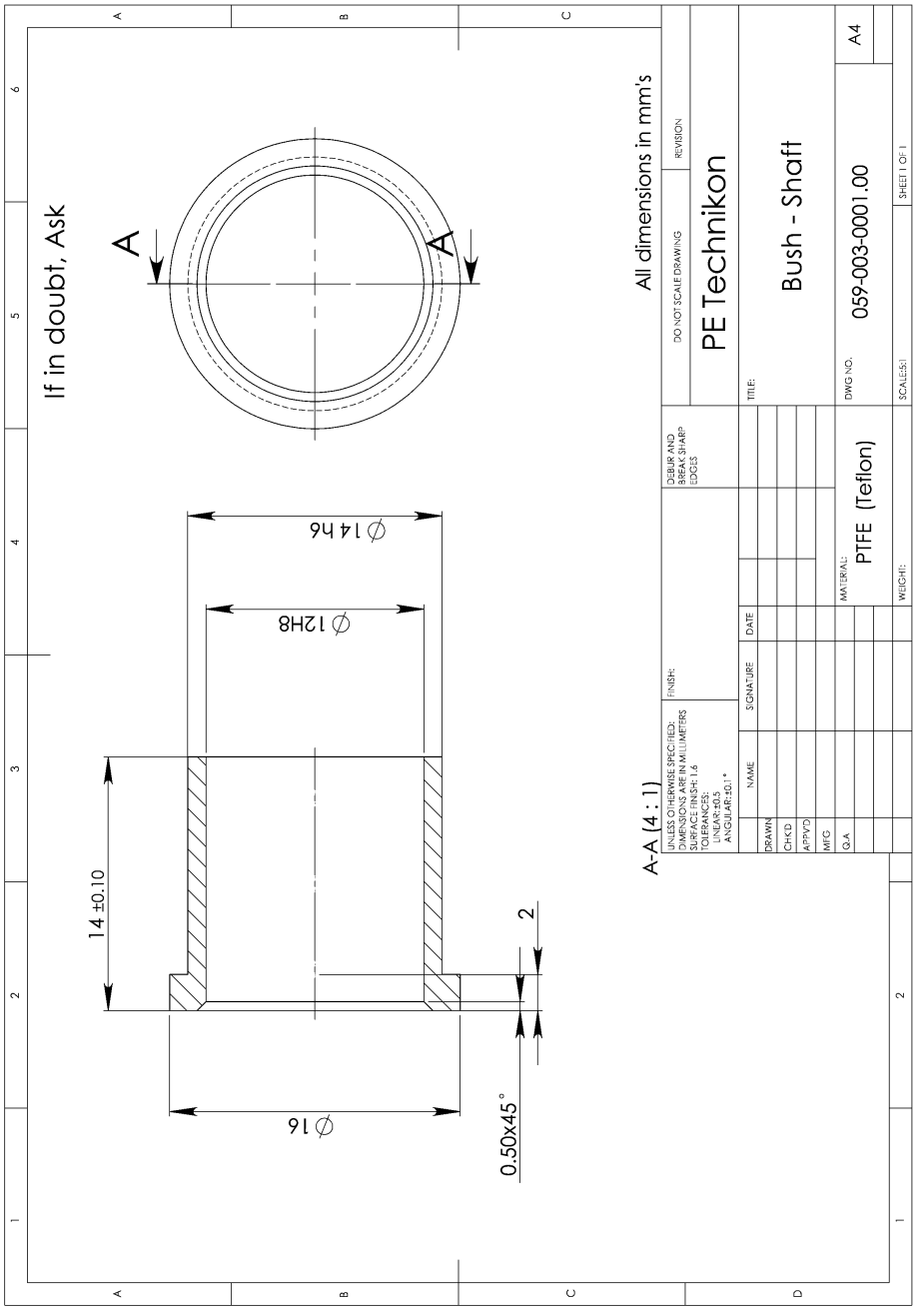

Figure A.10: PTFE Bush.

Figure A.11: Washer (Tufnol).

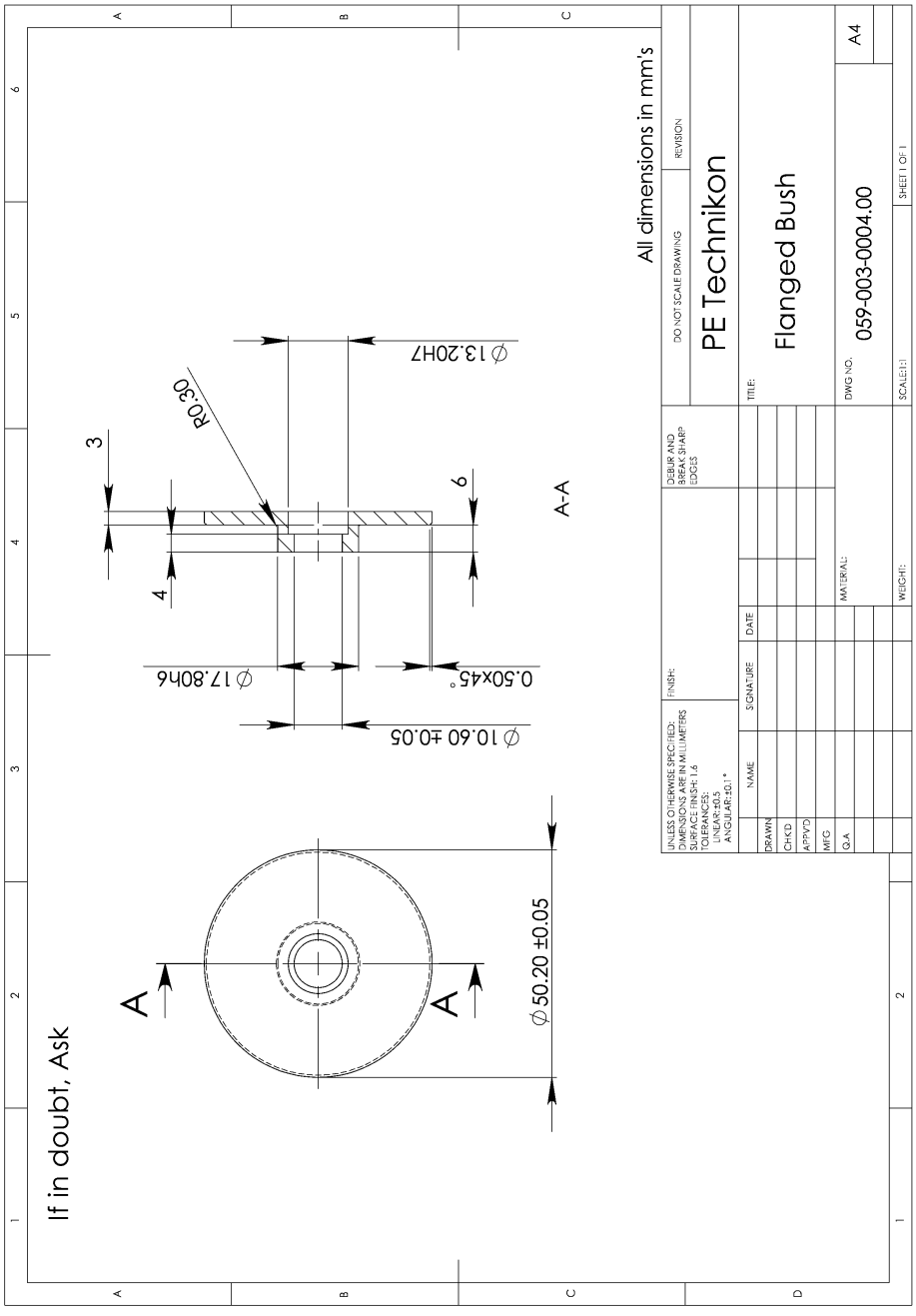

Figure A.12: Flanged (Tufnol) bush.

Figure A.13: Actuator plate.

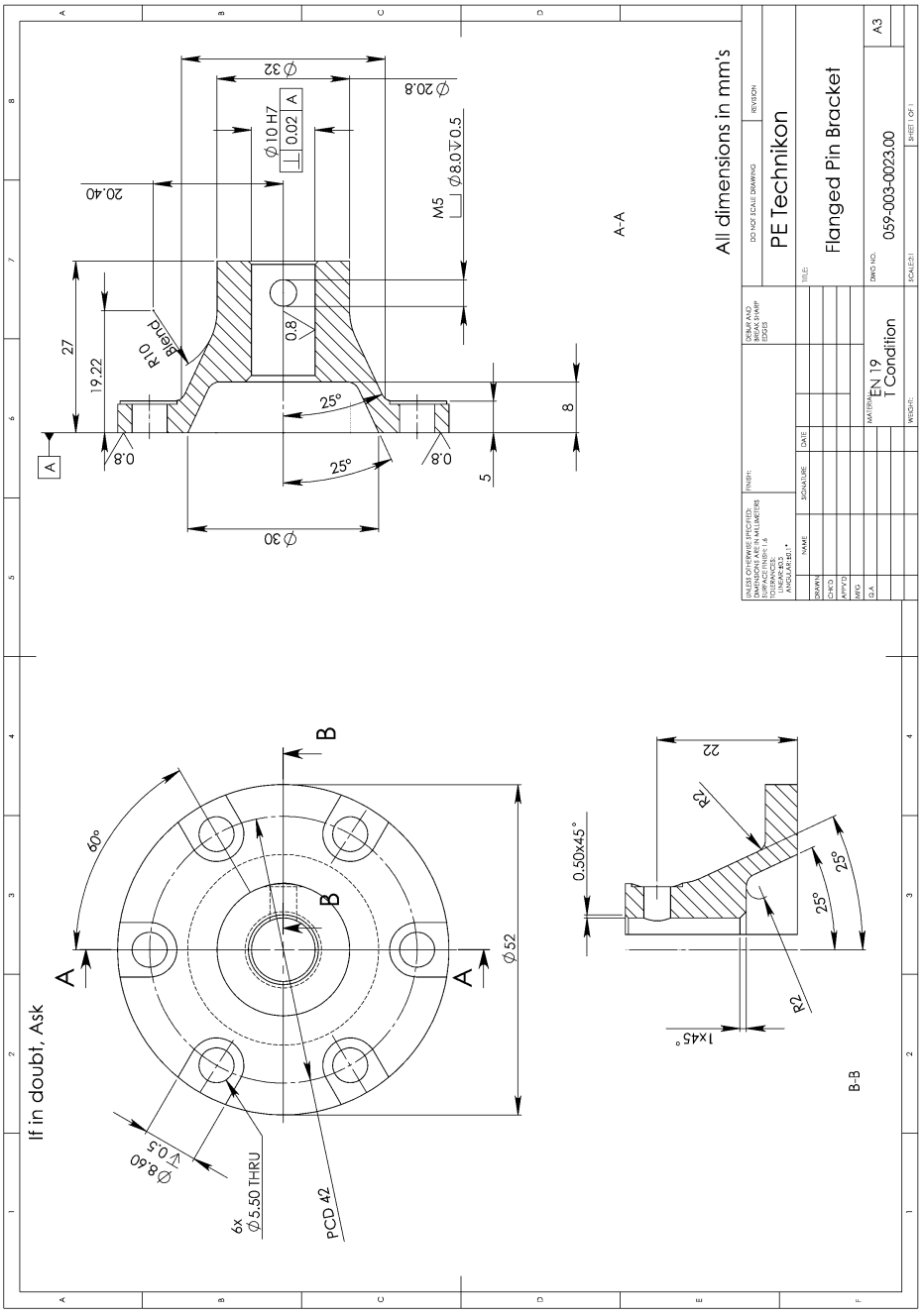

Figure A.14: Pin bracket.

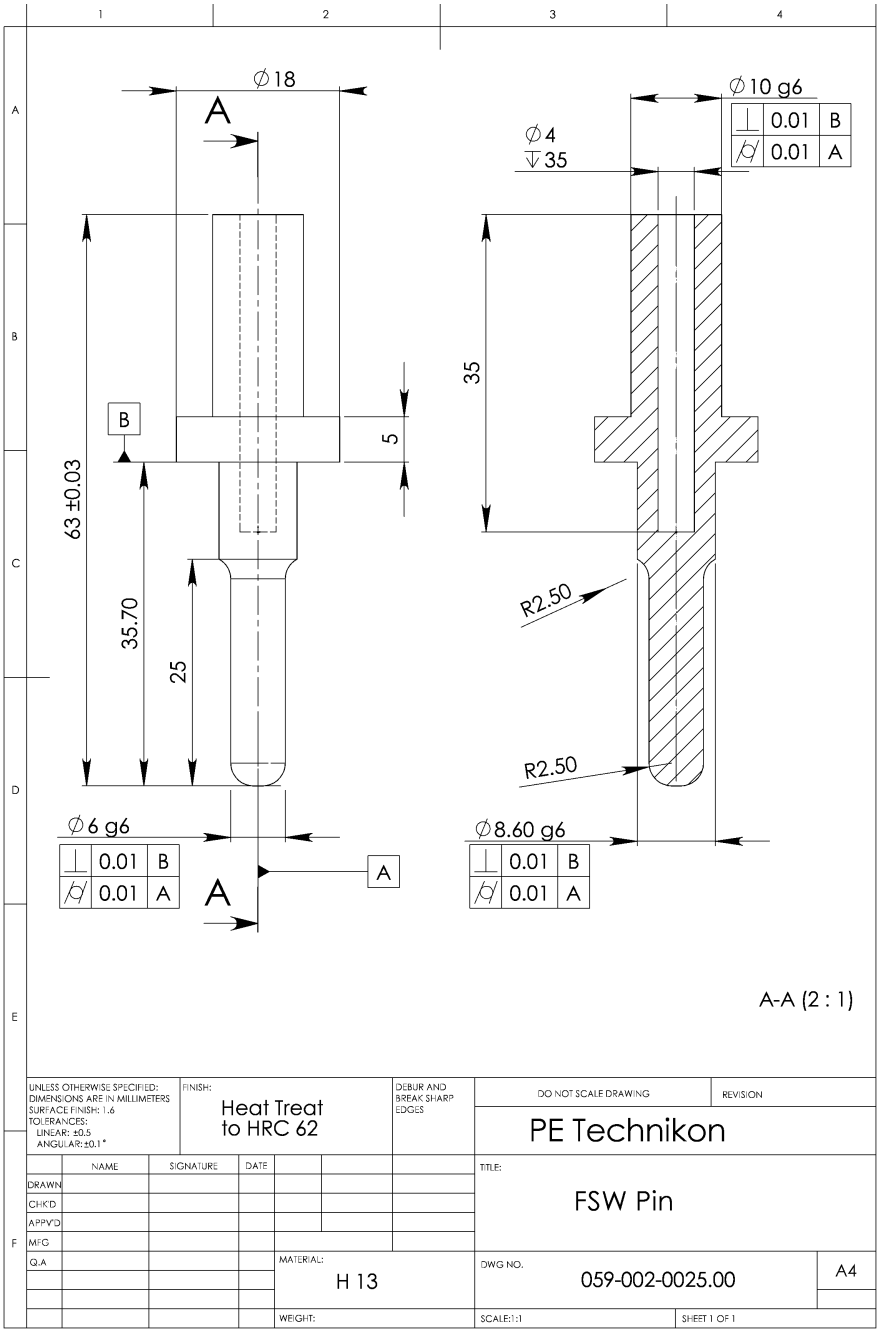

Figure A.15: Pin.

B O-RINGS

O-ring is a one piece torus shaped, molded elastomer seal having circular cross-section that seals by distortion of its resilient elastic compound [Oberg *et al.*, 1996]. O-ring seals can be used in both static and dynamic applications.

The rotary joint/slip-ring for the experimental tool required sealing of the compressed air used in the actuator. The following design specifications where used for the design of the slip-ring and the rotary joint. Since the functional requirement of the rotary joint and slip-ring was a dynamic application, the requirements for this application were only considered.

O-rings for rotary motion are used on rotating shafts to retain working fluids, retain lubricants, and exclude dirt. Selection of an O-ring depends on fluid pressure, shaft speed and whether any leakage can be permitted. Since O-rings perform their sealing action by deforming, to take the shape of the cavity in which they are inserted, and being over-sized in a predetermined interference fit. These cavities are also known as glands.

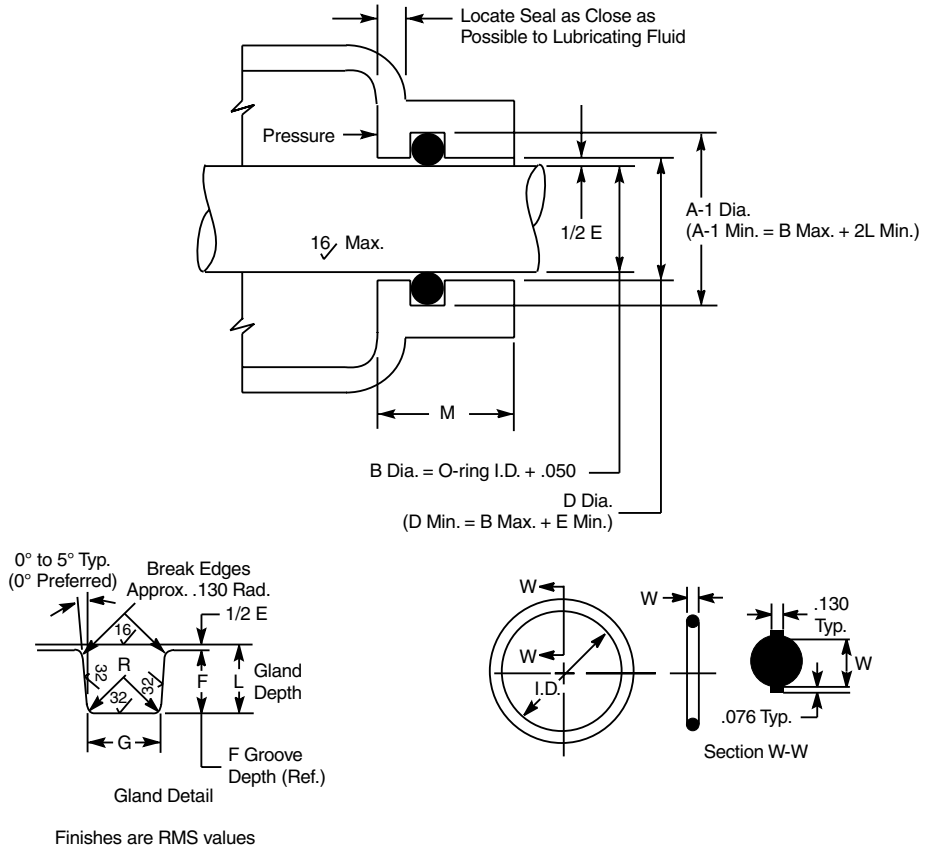

Figure B.1: Rotary O-ring design guide (Parker O-Ring Division, 2003).

Rotary Dynamic Sealing

Using O-ring seals on rotary shafts is a practical solution but unlike static applications, dynamic sealing requires that several considerations be dealt with during the conceptual design phase. Design conditions for rotary seals are critical and the need for relatively high durometer compounds, close tolerances, and minimum cross sections are important.

The surface finish of the shaft has to be sufficiently smooth and yet

include microfine "pockets" to hold lubricant. When using O-rings with pneumatics, the sealing has to overcome extreme conditions as the lubrication is poor, especially when non-lubricated air is used. Consideration for added lubrication is needed to alleviate the problem.

As dynamic applications place the O-rings under undesirable conditions, due to the motion acting against the O-ring seal interface. The metal or surface over which the O-ring moves becomes critical. It has to be hard and wear resistant, and sufficiently smooth so that the O-ring will not abrade. Hardened steel shafts are recommended, in the range of HRC 55 (Rockwell C).

For dynamic applications seal manufacturers recommend a roughness $R_t \leq 2.5\mu$mm for sealing surface (R_a=0.25 to 0.5 mm) or ($\bar{\nabla}\bar{\nabla}\bar{\nabla}$ roughness DIN 3141) when the load area is over 50%, or when the surface finish roughness R_p is under 50% Where R_t represents the vertical distance between the highest point and the lowest, R_p indicates the depth of roughness and R_a is the arithmetic mean roughness value.

Provision for heat dissipation should be considered, by having the seal interface running closer to room temperature, this results in improved sealing. There are two methods recommended by Parker O-Ring Division [2003] to achieve this:

Preferred Providing a clearance of 0.203 mm on a side between the rotating shaft and the O-ring housing. Ensuring that the shaft does not rub the housing.

Alternate The bearing length should be at least ten times the "W"

dimension of the O-ring used. This provides for a greater area for heat transfer. If clearance has to be kept to a minimum to prevent high pressure extrusion, the ten times "W" rule still applies.

Friction in dynamic applications is divided into, break-out and running friction. The amount of break-out friction a system will generate, depends on the length of time the surfaces of the metal and the seal element have been in physical contact at rest. Therefore with the rotary dynamic seal, this will occur at the start of running, also known as start-up friction. As the movement is established, the frictional forces decease and gliding begins. Running friction depends on many factors, making mathematical analysis practically impossible, to point exactly at which factors are contributing.

An O-ring should be inserted into a gland, where the tensional stress is at a minimum. Since most elastomers contract when subjected to a heated stressed, or stretched condition, this increases the chances for a rotary seal seizure at high speed. This effect is known as the Gow-Joule effect and occurs only if the O-ring is under tensile stress. As the heat causes more contraction, thereby increasing friction and a self perpetuating increase in heat and friction, eventually leads to failure of the O-ring.

Ideally the design should incorporate bearings to allow for the O-ring to operate under the lowest possible load. This limited interference should be used to avoid additional frictional heat, as the O-ring will not compensate for shafts that are not running true, or rotating eccentrically. Therefore shafts should remain concentric within 0.013 mm.

Further design considerations are that the O-ring not be placed in groove in the shaft, as due to centrifugal action this causes the O-ring to rotate and rub on all surfaces, preempting failure.

Design Calculations

For a design application an O-ring, is specified by its "inner diameter", its "cross-section", its hardness and, composition.

Design procedure

For the design of a rotary seal gland where the desired shaft diameter B_d and the maximum running speed of N (rpm) are known, the follow steps are used as suggested by Parker O-Ring Division [2003];
Firstly the shaft speed is converted to m/s to give the surface speed,

$$V_{surf} = \frac{\pi}{1000} N \cdot B_d \tag{B.1}$$

Determine from the Table B.2 the cross section of the O-ring relative to the speed of the shaft. Since the ID corresponds to the shaft diameter B, and according to Table B.2, with size of the O-ring cross section known, the O-ring specification can now be checked against the manufacturers tables (These have not been included).
To determine the maximum actual shaft diameter,

$$B_d = ID + 0.05 \tag{B.2}$$

Then determine L, the gland depth from Table B.1, and calculate the gland groove diameter, A_d,

$$A_{min} = B_{max} + 2L_{min} \tag{B.3}$$

$$A_{max} = B_{min} + 2L_{max} \tag{B.4}$$

Determine the diametral clearance E, also known as the extrusion gap, from the Table B.3, with the diametral clearance, calculate the shaft bore D_d,

$$D_{min} = B_{max} + E_{min} \tag{B.5}$$

$$D_{max} = B_{min} + E_{max} \tag{B.6}$$

Determine the groove width, Gw from Table B.1.

O-ring Rotary Seal Design Calculations

The following are the design calculations using the data from the previous section, for the O-rings used in the rotary joint and slip-ring. Design criteria:

Maximum shaft speed (rpm) = 600

Desired shaft diameter (mm) = 82

Maximum pressure (bar) = 6

Once the initial constraints have been decided the procedure of design follows as laid out in the previous section. As the O-rings from Parker O-Ring Division are dimensioned the Imperial system, these then had to be converted to SI units, the conversion factor will be

given where needed.

Converting the surface speed form rpm to m/s using Eq. (B.1),

$$V_{surf} = \frac{\pi}{1000} 60082 \;=\; 2.5584 \text{ m/s}$$

This gives a O-ring cross section of, 2.62 mm
Selecting an O-ring from the manufacturers tables, in this case from Parker O-Ring Division catalog, an O-ring of diameter 82.14 mm which corresponds to the desired shaft Outer Diameter (OD), and then calculate the maximum actual shaft OD, B_{max}, using Eq. (B.2),

$$B_{max} = 82.14 + 0.05 \;=\; 82.19 \text{ mm}$$

the recommended shaft tolerance given as, +0.00 to -0.025 mm giving;

$$\begin{aligned} B_{max} &= 82.19 \text{ mm} \quad \text{and} \\ B_{min} &= 82.19 - 0.025 \;=\; 82.17 \text{ mm} \end{aligned}$$

The gland depth L is found from Table B.1, given as 2.464 to 2.515, where L_{min} = 2.464 mm and L_{max} = 2.515 mm respectively. By substituting into Eq. (B.3) and Eq. (B.4), to calculate the minimum A_{min} and maximum A_{max} gland groove diameters.

$$\begin{aligned} A_{min} &= 82.19 + 2(2.464) \;=\; 87.12 \text{ mm} \\ A_{max} &= 82.17 + 2(2.515) \;=\; 87.20 \text{ mm} \end{aligned}$$

The diametral clearance E is now determined by referring to Table B.3 for the specified cross section W, this gives a E value of E_{min} = 0.305 mm and an E_{max} = 0.406 mm. The value of E with the calculated

shaft OD, B_d determines the shaft bore, D_d, using Eqs. (B.5) and (B.6) as follows;

$$D_{min} = 82.19 + 0.305 = 82.50 \text{ mm}$$
$$D_{max} = 82.17 + 0.406 = 82.58 \text{ mm}$$

The groove width is then determined from the Table B.1, giving Gw a value with a maximum at 2.743 mm to a minimum of 2.845 mm.

Once the calculations have completed, the relevant values for the design are listed, with reference to Figure B.1, these are:

$$ID \text{ Inner Diameter (Dia.)} = 82.14 \pm 0.61 \text{ mm}$$
$$W_{max} \text{ Maximum Cross Section Dia.} = 2.692 \text{ mm}$$
$$W_{min} \text{ Minimum Cross Section Dia.} = 2.540 \text{ mm}$$
$$W_{tol} \text{ Cross Section Tolerance} = \pm 0.076 \text{ mm}$$
$$C_{max} \text{ Maximum Compression} = 0.30$$
$$V_{surf} \text{ Surface speed} = 2.56 \text{ m/s}$$
$$A_d \text{ Gland Groove Dia.} = 87.12 \text{ mm}$$
$$A_{max} \text{ Max. Gland Groove Dia.} = 87.20 \text{ mm}$$
$$A_{min} \text{ Min. Gland Groove Dia.} = 87.12 \text{ mm}$$
$$A_{tol} \text{ Gland Groove Dia. Tolerance} = +.076 \text{ to } -0.00 \text{ mm}$$

$$B_d \text{ Shaft Dia.} = 82.19 \text{ mm}$$
$$B_{max} \text{ Max. Shaft Dia.} = 82.19 \text{ mm}$$
$$B_{min} \text{ Min. Shaft Dia.} = 82.17 \text{ mm}$$
$$B_{tol} \text{ Shaft Tolerance} = 0.00 to - 0.025 \text{ mm}$$

D_d Bore Dia. = 82.60 mm

D_{tol} Bore Dia. Tolerance = $+.076 to -0.00$ mm

E_{max} Max. Diametral Clearance = 0.406 mm

E_{min} Min. Diametral Clearance = 0.305 mm

Gw Groove Width = 2.743 to 2.845 mm

L Gland Depth = 2.464 to 2.515 mm

M Minimum Bearing Length = 26.16 mm

Maximum Allowable Eccentricity = 0.508 mm

Design Charts

Table B.1: Design Chart 1 for Rotary O-ring seals glands, (Parker O-Ring Division, 2003)

W Cross Section		Maximum Speed	Squeeze	L Gland	Gw Groove
Nominal	Actual	(m/s)	%	Depth	Width
1.6	1.778 ±.076	1.02-7.60	0-11	1.651 to 1.702	1.905 to 2.007
2.38	2.616 ±.076	1.02-3.05	1-8.5	2.464 to 2.515	2.743 to 2.845
3.175	3.531 ±.101	1.02-2.03	0-7	3.378 to 3.429	3.658 to 3.759

Where not indicated dimensions are in mm's

Table B.2: O-ring sections for Rotary seals (Parker O-Ring Division, 2003) and (Czernik and Hopkins, 1986)

Speed (m/s)	Maximum Recommended "W" Dimension(mm)
<1.02	Usually not critical
1.02 to 2.03	3.53
1.02 to 3.05	2.62
≥7.60	1.78

Table B.3: Design Chart 2 for Rotary O-ring seals glands, (Parker O-Ring Division, 2003)

W Cross Section		E Diametral	Eccentricity	M Bearing Length	R Groove
Nominal	Actual	Clearance	Max	Min.	Radius
1.6	1.778 ±.076	0.305 to 0.406	0.508	17.78	0.127 to 0.381
2.38	2.616 ±.076	0.305 to 0.406	0.508	26.16	0.127 to 0.381
3.175	3.531 ±.101	0.406 to 0.508	0.076	35.31	0.254 to 0.635

Where not indicated dimensions are in mm's

C Friction Stir Welding Tool Patent

The development of new concepts and ideas requires the procurement of a patent to protect one's intellectual property. Therefore the experimental tool patent has been included, as this patent is still pending the claims have been omitted.

Retractable pin tool for the use with the Friction Stir Welding Process

Technical field

The present invention relates to a welding tool design, comprising of mechanical component parts or assemblies and the like, relating to a novel welding tool apparatus, wherein a movable pin is used to create a weld between two workpieces and where low cost and modular tool functions are desired, as for example, in applications with the friction stir welding process.

Background

The Friction Stir Welding process has been known for several years now and has been continuously developed. The process is an off-shoot of friction welding, is performed when the two workpieces to be joined are moved together relative to each other in the area to where they are to be joined while they are pressed together with an adjustable force. As a result of heat generated by friction, the material of the workpieces is plasticized in the area of the joint. After sufficient plastic deformation occurs, the materials of the two workpieces intermix so that upon cooling a solid-state bond between them is formed.

In the method and apparatus of the present invention the use of a profiled pin shaft is used to form the weld. A detailed descrip-

tion, reference to the process can be found in Patent Publication WO93/10935; U.S. Patent No. 5,460,317; and WO95/26254. Friction Stir Welding uses the principle of the force of friction to generate heat, this results in the material, to be joined, to be transformed into a plasticized state and with the action of the pin, extending from a profiled shoulder, to stir the two materials into each other to form a solid-state bond without needing to add fillers.

The tool of prior art as referred to in the above reference, consists of a shaft, in which one end is a free-end and the other driven. The driven-end is that which rotates the tool, the free-end consists of a shouldered pin, which is lowered onto the surfaces between the two fayed workpieces which are to be joined. The shouldered pin on the free-end of the shaft-tool being of fixed length, generates the frictional heat to plasticize the material around the pin. The shaft-tool is then moved transversely along the fayed join line, whereby the stirring action of the pin, moves material from the front to the rear of the pin, thereby mixing the materials and forming a solid-state bond.

Present friction stir welding tools, in which the pin is of fixed length, have the disadvantage of being able only to weld materials of same thickness and leaving a crater or "keyhole" in the welded workpiece upon tool retraction. The "keyhole" effect has limited the friction stir welding process from more complex joining applications , such as those used in the aerospace and automotive industries. Both industries require the joining of materials, especially aluminum and aluminum alloys, to be of a high quality and strength. The need to weld various material thicknesses as in the Taylor blanks, used

extensively in the automotive industry has been a problem with a fixed pin tool of prior art. In the aerospace industry the use of rivets is widespread and the ability to reduce, and or replace, their use would result in large savings in weight and therefore resulting in cost savings.

Furthermore as robots play a greater role in the manufacturing processes, friction stir welding tools will need to become more adaptable, simple and cost effective, for extending the use into existing manufacturing setups.

Summary of the Invention

The present invention relates to an apparatus with which the joining of two materials is performed with a low cost modular tool. This relates to a friction stir welding tool in which a pin is accurately adjustable in length relative to the shoulder of the tool. The pin is extended and retracted relative to the cylindrical shoulder tool. The method of welding adjoining material faces is carried out with a rotating assembly, which consists of the actuator assembly and at opposite end a tool is attached. This tool consists of a cylindrical shoulder and a pin, which are attached to the actuator apparatus. The profile of the pin is ideally cylindrical in cross-section, however other suitable cross-section profiles can be used, the corresponding profile of sleeve in the shoulder would have to be the same as that of the pin. The shoulder is plunged slowly into the join between the fayed faces of the material. The influence of frictional heat slowly plasticizes the material beneath the shoulder. The pin is slowly

lowered into the plasticized material, where stirring of the material takes place and further plasticizing the material around the pin. The tool can be then transversed along the join line to form a weld or left in place to form a spot-weld. The pin's distance from the backing plate can be controlled and the tool can therefore be able to weld materials of differing thicknesses. Once the weld has reached the end, the tool is stopped in position but continuously rotating and the pin is slowly retracted into the shoulder. As the pin has fully retracted, the tool apparatus can be removed from material surface. This leads to a elimination of the "keyhole" effect.

Object of the Invention

An object of the present invention, accordingly, is to provide a simple cost-effective friction stir welding tool with a adjustable pin extension and enable the above mentioned tool to be adapted for use with existing converted milling machines, and or, with use on existing robotic systems.

A further object is to eliminate the keyhole or crater at the point of tool extraction, due to the movement of the pin independently to the shoulder.

Another object is to allow for the use of the tool to produce a friction stir weld with materials of differing thickness without the need to change tools.

It is also an object of the present invention to use the tool to repair defective welds.

Other objects and novel features of the present invention will be explained in the following detailed description of the invention when considered in conjunction with the accompanying drawings.

Brief Description of the Drawings

The aforementioned invention will be now described with reference to accompanying drawings, not to scale and schematic in the sense of illustrating features of the invention (or prior art in the case of FIG. 1)in which:
FIG. 1 is a schematic diagram of the prior art friction stir welding apparatus;
FIG. 2 is a partial exploded view showing some of the components of the friction stir welding apparatus of the invention;
FIG. 3 is another exploded view in which the method of actuation is shown as part of the friction stir welding apparatus of the invention.
FIG. 4 is a schematic cross-sectional view of the friction stir welding apparatus as part of the present invention.

Preferred Embodiment(s) of the Invention

The FIG. 1 shows prior art and use of a friction stir welding tool **12**. As shown in FIG. 1 the two workpieces **11**a' and **11**b' are aligned so that their edges are in contact to form a join line where they are to be welded **17**. The plates are held in place on a backing plate **13**, the friction stir welding tool **12** with a shoulder **14** at its free-end and the pin **16** placed centrally and extending downward from the

shoulder. The tool **12** rotates about its axis, as shown by **19** and is brought into contact at the join line between the plates **11**a' and **11**b', the pin **16** is forced into contact with both plates as shown. As the rotating shoulder **14** comes in contact with the material, a large amount of frictional heat is generated and this heats the material at the plate interface **17** and around the pin **16** into a plasticized state. The stirring action of the pin and the tool moving longitudinally **18** along the joint line which causes the material from the two plates to intermix and thus forming a weld **15** along the joint line of the two plates.

The present invention forms a weld or bond between two material workpieces using the process in principle as described above, the tool **10** of the invention is shown in detail in FIGS. 2, 3 and 4.

The tool **10** in FIG. 2 can be attached to converted milling machines or robotic platforms, which are used in the friction stir welding process, using a rotatory joint **20**. This consists of a slip ring **21** that is held stationary during the welding process whilst the tool **10** is rotated. The slip ring **21** as shown in FIG. 4, is used to deliver compressed gaseous or liquid medium to the actuator assembly as shown in FIG. 4 (**30**), this medium applied at the opening **34** and prevented from leaking by seals **51** and **52** on either side of the annular passageway **35**, the medium follows a path along **34**a' into an axial adapter **30**a' which is attached to **30**b' a "Fluidic Muscle"® Festo AG, the increase in pressure causes **30**b' to expand, the principle has been extensively documented and forms no part of this patent, this in turn causes the threaded rod **30**c', which is connected to **30**b' to move in the direction **X**, as indicated on FIG. 4. The plate **24** is attached to **30**c',

on to which the pin assembly, consisting of a housing **40** and the pin **41** is part thereof, moves accordingly and proportionally to the amount that **30**b' moves, thereby moving the pin **41** relative to the shoulder **42**.

As the tool rotates **10**, the pin **41** is allowed to slide through a centrally placed hole in the shoulder **42**, this when abutted with the upper face of the shoulder **42** is at the maximum extension, and the pin can be adjusted in the housing **40** to allow for different pin travel. The pin **41** is in the retracted position on the initial plunging of the tool **10** into the joint interference **17**, there is no protrusion of the pin form the lower face of the shoulder **42**, that is the face that will be in contact with the material workpieces **11**a' and **11**b'. When the shoulder is in contact with the material surfaces, the tool **10** a load is applied and this causes the frictional heat required to plasticize the material, at this point the pin is still retracted, due to the pressure in the pneumatic actuator **30**b'. The load bearing structure of the tool **10** consists of the four shafts **26** and the outer housing **27**.

The heat generated by the shoulder is directed away from the pin **41** by having the pin insulated from the shoulder **42**. This achieved by having the shoulder attached to the an adapter plate **25** which has no interference with plate **24** on which the pin is attached. The plate **24** is allowed to slide on the four shafts **23** by using high temperature resistant plastic bushes **26** these having the added function of reducing friction that maybe present due to the movement of the pin. Further insulation of the tool between the plate **24** and the actuator assembly **30**, is the use of temperature resistant material in the form of a bush **47** and washer **46**. In addition a method of

cooling has been included in order to keep the actuator assembly cooled, and further use of this air to cool the pin if required. This is carried out with the use of the rotatory joint housing **20** and the slip ring **21** through the opening **33** where a compressed gaseous medium to be applied using the annular passage **37** which is sealed using seals **52** and **53**, this leads through **33**a' in housing **20** and **33**b' in adapter plate **22**. The air is then circulated in the area between plate **22**, **24** and bounded by the outer housing **27**. Direct application of cooling air is possible through pipes connected to one of the eight openings that lead out from passage **33**b', these can be attached cool the cavity **38** between the housing **40** and plate **24**. Further, cooling of the workpieces **11**a' and **11**b' after welding is possible by directing air from **43** onto the welded plates, this would improve the surface finish of the welded materials.

What is claimed:

The claims have been omitted, as the patent is still pending

Abstract

The invention of a welding tool design for use with the friction stir welding process, relating to a novel welding tool apparatus. The use of a variable pin length, with which to create a weld between two workpieces and where low cost and modular tool functions are desired.

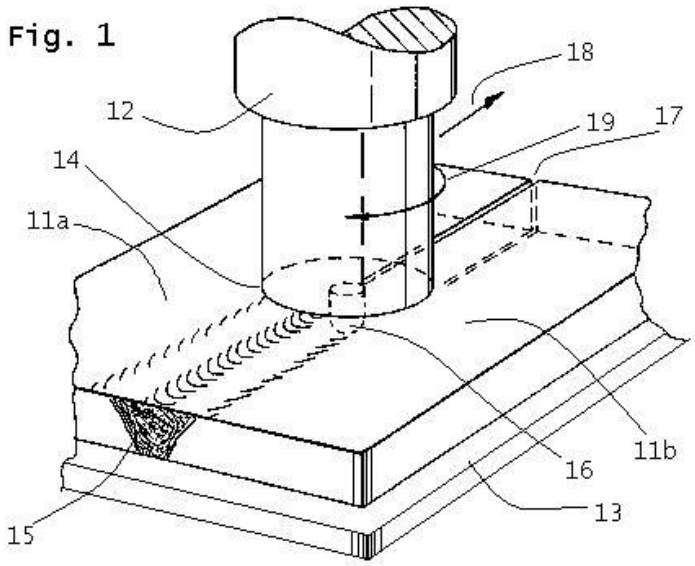

Figure C.1: Patent Figure 1.

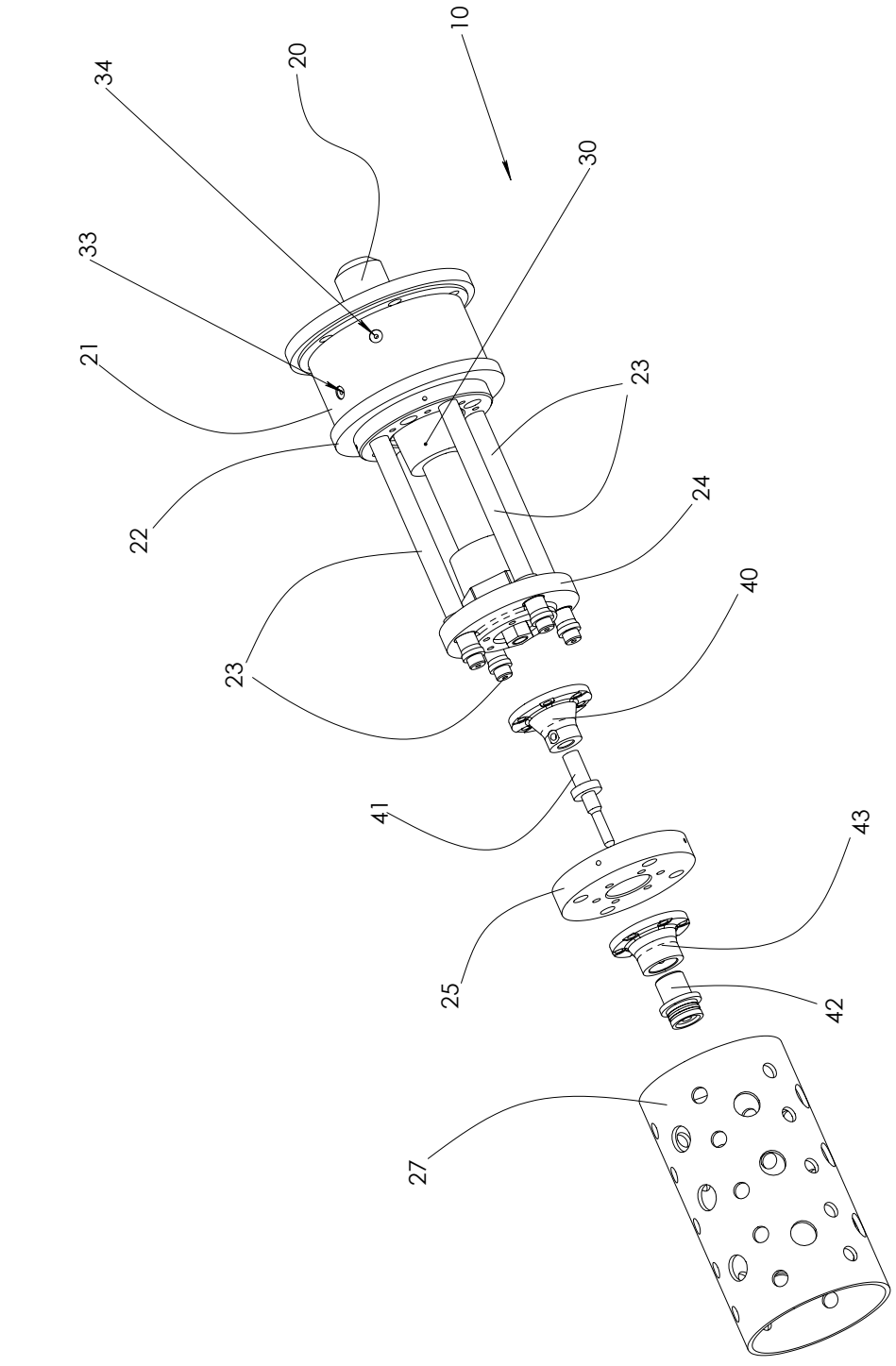

Fig. 2

Figure C.2: Patent Figure 2.

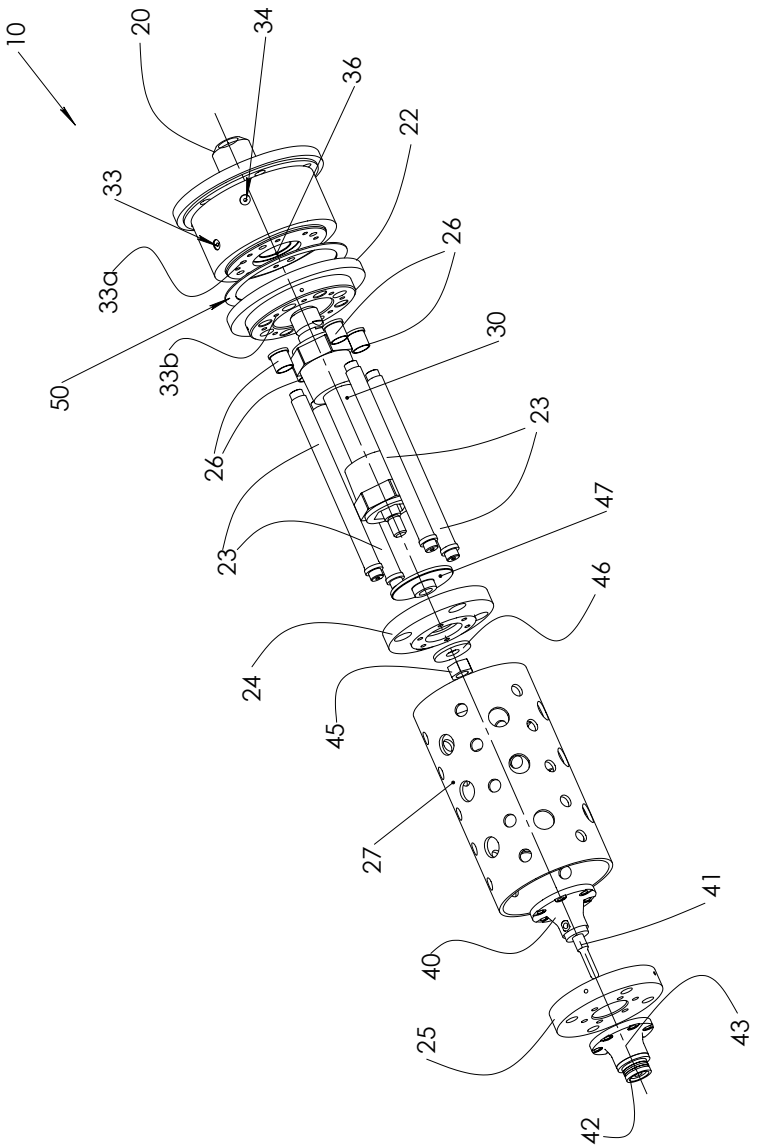

Fig. 3

Figure C.3: Patent Figure 3.

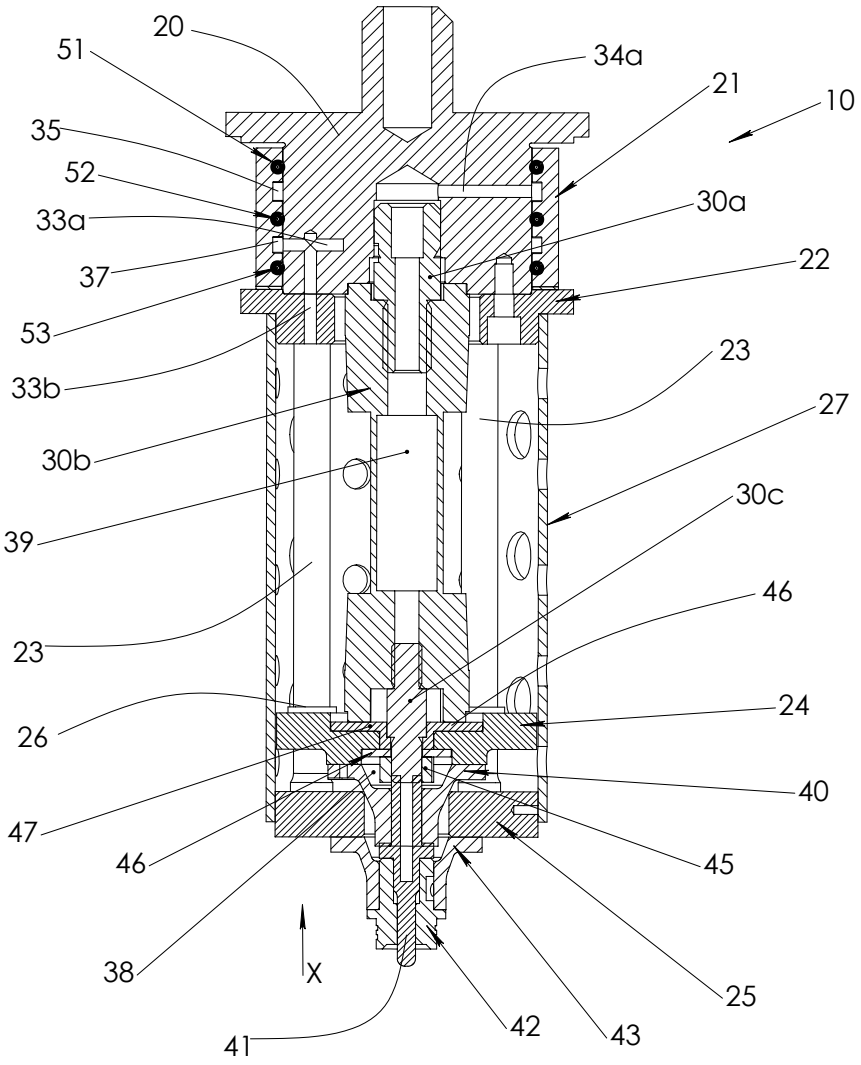

Fig. 4

Figure C.4: Patent Figure 4.